ERDC TR-06-5

Engineer Research and Development Center

US Army Corps of Engineers®
Engineer Research and Development Center

Evaluation of Ground Vibrations Induced by Military Noise Sources

Final Report for SERDP SEED Project SI-1410

Donald G. Albert, Patrice Boulanger, Keith Attenborough and Michael J. White

August 2006

Approved for public release; distribution is unlimited.

Cover Photo: A predictive model for ground vibrations induced by military explosions, which have properties different from larger mining blasts, has been developed in this project.

This report was prepared under contract to the Department of Defense Strategic Environmental Research and Development Program (SERDP). The publication of this report does not indicate endorsement by the Department of Defense, nor should the contents be construed as reflecting the official policy or position of the Department of Defense. Reference herein to any specific commercial product, process, or service by trade name, trademark, manufacturer, or otherwise, does not necessarily constitute or imply its endorsement, recommendation, or favoring by the Department of Defense.

ERDC TR-06-5
August 2006

Evaluation of Ground Vibrations Induced by Military Noise Sources

Final Report for SERDP SEED Project SI-1410

Donald G. Albert

Cold Regions Research and Engineering Laboratory
U.S. Army Engineer Research and Development Center
72 Lyme Road
Hanover, NH 03755-1290

Patrice Boulanger, and Keith Attenborough

University of Hull
Hull
United Kingdom
HU6 7RX

Michael J. White

Construction Engineering Research Laboratory
U.S. Army Engineer Research and Development Center
2902 Newmark Dr., Interstate Research Park
Champaign, IL 61826-9005

Final report

Approved for public release; distribution is unlimited.

Prepared for U.S. Army Corps of Engineers

Under Strategic Environmental Research and Development Program

Abstract: Measurements from locations with a variety of ground types were analyzed to determine the mechanisms and levels of the ground vibrations produced by airborne detonations of C4. The measurements show that an early seismic arrival from an underground path is always much smaller than the vibration induced by the air blast arrival. The acoustic-to-seismic coupling ratio for the atmospheric wave is a constant with respect to distance and peak pressure at a given location, but varies from site to site, and is usually between 1 and 13 (μm/s)/Pa. A numerically intense computational method to predict the air pressure spectrum above ground and the waveform shape of the vertical component of solid particle velocity near the ground surface compares tolerably well with measurements at short range (60 m) in grass and snow covered ground. A conservative empirical equation to predicts that the commonly used vibrational damage criteria of 12 or 25 mm/s will be exceeded when the peak positive pressure exceeds 480 Pa or 1 kPa, respectively. Either of these levels is much higher than the Army overpressure damage criterion of 159 Pa (138 dB). Thus in most situations damage from blast overpressure will occur long before damaging levels of ground vibration are reached.

DISCLAIMER: The contents of this report are not to be used for advertising, publication, or promotional purposes. Citation of trade names does not constitute an official endorsement or approval of the use of such commercial products. All product names and trademarks cited are the property of their respective owners. The findings of this report are not to be construed as an official Department of the Army position unless so designated by other authorized documents.

DESTROY THIS REPORT WHEN NO LONGER NEEDED. DO NOT RETURN IT TO THE ORIGINATOR.

Contents

Figures and Tables iv

Preface vi

Executive Summary ix

1 Objectives 1

Task 1—Construct an accurate but simple model of induced ground motion from military activities 1

Task 2—Determine the acoustic-to-seismic coupling coefficients *C1* and *C2* 1

Task 3—Computational modeling of acoustically induced ground motion 1

2 Background 2

3 Materials and Methods 5

Overview of the measurements 7

C4 Charge heights and sizes 9

Charge scaling 9

4 Results and Accomplishments 12

Data Analysis of C4 airblast measurements 12

Test 1—Propagation over concrete 12

Test 2—Propagation over soil with light vegetation 18

Test 3—Propagation over soil with light vegetation, with a gravel pile 23

Test 4—Propagation through heavy tropical vegetation 27

Test 5—Propagation at a site with a low density snow cover over frozen ground 30

Test 6—Propagation over a high density snow cover 33

Test 7—Propagation through a conifer forest 37

Combination of Tests 1–5 and 7—Propagation in various environments 40

Prediction method 41

Detailed modeling of ground vibrations produced by explosions 43

5 Conclusions 45

Task 1—Construct an accurate but simple model of induced ground motion from military activities 46

Task 2—Determine the acoustic-to-seismic coupling coefficients *C1* and *C2* 46

Task 3—Computational modeling of acoustically induced ground motion 47

References 48

Appendix A: Supporting Data 50

Appendix B: List of Technical Publications 61

Report Documentation Page 58

Figures and Tables

Figures

Figure 1. Ground vibration model 5

Figure 2. Example of cube root scaling of the charge size. 11

Figure 3. Photo of some of the sensors used during Test 1, propagation measurements over concrete. 12

Figure 4. Geometry of the measurements over concrete 13

Figure 5. Waveforms measured during Test 1, for a single block of C4 (0.57 kg) detonated at a height of 1.5 m above a concrete pad 14

Figure 6. Measurement results for Test 1, propagation over concrete 15

Figure 7. Photo taken during Test 2 propagation over soil with grass/weed vegetative cover. 19

Figure 8. Waveforms measured during Test 2, for a single block (0.57 kg) of C4 detonated at 1.5 m above soil 21

Figure 9. Waveforms measured during Test 2, for 32 blocks (18.2 kg) of C4 detonated at 1.5 m above soil. 22

Figure 10. Measurement results for Test 2, propagation over soil 23

Figure 11. Photo from Test 3, soil and a gravel pile. 24

Figure 12. Waveforms measured during Test 3, for a single block of C4 (0.57 kg) detonated at 1.5 m above soil approximately 30 m to the side of a large gravel pile 26

Figure 13. Measurement results for Test 1, propagation over concrete 27

Figure 14. Photos of Test 4, tropical vegetation (Eglin AFB, Florida, 2002). 28

Figure 15. Waveforms measured during Test 4, for a single block of C4 (0.57 kg) detonated at a height of 1.5 m through tropical vegetation 29

Figure 16. Measurement results for Test 4, propagation through tropical vegetation 30

Figure 17. Photographs of Test 5 experiment, with a low density snow cover over frozen ground present (Camp Ripley, MN, 2002). 31

Figure 18. Waveforms measured during Test 5, for a single block of C4 (0.57 kg) detonated at 1.5 m above a low density snow cover over frozen ground. 32

Figure 19. Measurement results from Test 5, propagation over a low density snow cover 10 to 15 cm thick over frozen ground 33

Figure 20. Photo of Test 6 experiment, measurements for propagation with a sintered snow cover present (Fort Drum, NY, 2004)....34

Figure 21. Waveforms measured during Test 6, for a single block of C4 (0.57 kg) detonated at a height of 1.5 m over a snow cover. 35

Figure 22. Measurement results from Test 6, a sintered snow cover 8 to 25 cm deep....36

Figure 23. Photo of Test 7 experiment, propagation through a conifer forest (Lone Star Army Ammunition Plant, Texas, 2002). 38

Figure 24. Waveforms measured during Test 7, produced by a 2.3-kg charge of C4 detonated 1.9 m above the ground level, after propagation through a conifer forest. 39

Figure 25. Measurement results for Test 7, propagation through a conifer forest. 40

Figure 26. Combined measurement results from Tests 1–5 and Test 7, propagation in a variety of environments, including concrete, frozen and unfrozen soil, forest, and tropical vegetation 41

Figure 27. P_{max} vs. V_{max} for Tests 1–5 and Test 7, propagation in a variety of environments 42

Figure 28. Acoustical power spectral magnitude and pulse shapes predicted and measured in experiment 8 of Albert (2001)....43

Figure 29. Seismic power spectral magnitude and pulse shapes predicted and measured in experiment 8 of Albert (2001)....44

Figure 30. Acoustical power spectral magnitude and pulse shapes predicted and measured in experiment 4 of Albert (2001)....44

Figure 31. Seismic power spectral magnitude and pulse shapes predicted and measured in experiment 4 of Albert (2001). 44

Tables

Table 1. Coefficients (in English units) for equation (1) used to estimate peak particle velocity. 3

Table 2. Test environments, charge sizes, and propagation distances. 8

Table 3. Attenuation rates and coupling ratios determined from the measured data). 17

Table 4. Peak acoustic pressure levels needed to exceed vibration damage criteria....18

Preface

This is the final report for SERDP SEED Project SI-1410, *Evaluation of Ground Vibrations Induced by Military Noise Sources*. The research in this report was conducted by Dr. Donald G. Albert, ERDC-CRREL, Dr. Patrice Boulanger, University of Hull, Dr. Keith Attenborough, University of Hull, and Dr. Michael J. White, ERDC-CERL. The authors gratefully acknowledge SERDP funding for this research. Dr. Robert Holst is the Sustainable Infrastructure Program Manager and Bradley Smith is the Executive Director.

The measurements analyzed in this report came from a variety of sources. The authors thank Richard Andrejkovics and Andre Edwin, U.S. Army PM-CCS (Project Manager, Close Combat Systems) for funding Tests 1, 2, 4, 5, and 6 as part of the Sympathetic Detonator (SYDET) project, and all of the many individuals from various government agencies who assisted in the management and conduct of these tests. The measurements reported for Tests 3 and 7 were funded by Dr. Larry Pater, Project Leader for Military Noise Management, ERDC-CERL.

Gary Leadore and Martha Turnbaugh of the U.S. Army Aberdeen Test Center are thanked for coordinating many of these tests. Steven Decato of ERDC-CRREL participated in all of these measurement efforts and was especially helpful in their successful completion.

The snow pistol shot data used to confirm the detailed model produced by the University of Hull was funded by the U.S. Army Corps of Engineers AT24 basic research program.

The authors thank the many colleagues from a number of agencies who assisted with the field tests. Demolitions and weapons experts included Jim Storey, U.S. Army Cold Regions Test Center, Fort Greely, AK, Robert A. Caudill, Frank Johnson, Chris Thomas, and Aubrey Edwards, Billy White, Aberdeen Test Center(ATC), and two Navy Seals. Others who assisted with arranging the tests included Danny Deal, Range Manager, ATC, Jeff Feldstein from the Naval Coastal Systems Station in Panama City, FL, Second Lieutenant Lisa Sherwood, and Range Officer Captain Guy Konietgko, Camp Ripley, Minnesota Army National Guard Center.

From ATC, Jessie Rommel, and Joe Ulrich assisted with photography. Steve Lay, George Trenkle, SGT Jim Wiseman, SGT William Kone, SPC Hamlin, Kevin Bannigan, Jason Eyler, and others at ATC assisted with the site preparation and in conducting the measurements. Jerry Daniels, Mark Lange, and Tom Ruffing provided surveying support.

Alan Cameron, Joe Donnelly, Joe Locy, and Karl Reiber and others on the Ft. Drum staff facilitated the tests at Ft. Drum. Dave Self, Jesse Stewart, and a number of other Lone Star Army Ammunition Plant personnel provided their assistance. The authors also received help from the staff at Camp Ripley, Minnesota Army National Guard Center, and from Naval Coastal Systems Station.

David Gonski and Chris Reiff of the Army Research Laboratory (ARL), Aldelphi, MD, assisted with some of the measurements.

The Netherlands Participants in one of the tests included Frank van den Berg, Jaap van't Hof, and Frits Van der Eerden, the Netherlands Organization for Applied Scientific Research (TNO), and Erik van Arkel, Netherlands Ministry of Defense (MOD-NL), via the Defense Coordinator for Spatial Planning and Environment (CROMD).

ERDC-CERL participants included Dr. Larry Pater, Dr. Michael J. White, Richard Racioppi, Jeff Mifflin, George Swenson, Brent Miller, Achal Modi, and Samantha Rawlings.

ERDC-CRREL participants in the measurements included Stephen N. Decato, David L. Carbee, Frank E. Perron, Jr., Dr. Joyce A. Nagle, and Dr. Donald G. Albert.

Dr. Robert H. Kennedy and Julian Richmond, U.S .Army European Research Office, were very helpful in arranging the financial transfer to support Dr. Keith Attenborough and Dr. Patrice Boulanger on this project.

Dr. Robert E. "Bert" Davis served as CRREL Military Programs Technical Director.

Alan Anderson is the Branch Chief, Ecological Processes Branch (CN-N) of the Installations Division (CN), and Dr. John Sandy is the Division Chief (CN). The Director of the Construction Engineering Research Laboratory is Dr. Ilker Adiguzel.

Professor Stephanie Haywood is the Head of the Department of Engineering, University of Hull, and Mr. Derek Willis is the Dean of the Faculty of Sciences.

This report was prepared under the general supervision of Janet Hardy, Chief, Geophysical Sciences Branch; Lance Hansen, Acting Deputy Director; and James Wuebben, Acting Director, CRREL. The Commander and Executive Director of the Engineer Research and Development Center is COL Richard B. Jenkins. The Director is Dr. James R. Houston.

Executive Summary

Increasingly, Army activities, including artillery or demolition training and demilitarization (detonating obsolete weapons), are subject to structural damage claims from civilian populations surrounding Army facilities. Currently, a simple procedure is used to assess damage claims that attribute ground motion to Army activities. In this procedure, empirical equations formulated by the Bureau of Land Management and the mining industry are used to estimate the peak level of ground vibration caused by the Army activity. A claim is viewed to have merit if the estimated ground particle velocity has a value of 1.0 in./s (25.4 mm/s) or larger based on these empirical equations. (Some mining regulations use a more stringent threshold value of 0.5 in./s or 12 mm/s). However, mining industry blasting significantly differs from Army activities, especially in the use of very large explosive charge sizes (typically thousands of pounds of TNT) spread over a relatively large area (to break the most rock). Thus, the empirical equations currently in use may not be accurate when applied to Army activities, which usually involve point sources much smaller in explosive size. In addition, many Army activities, including artillery training and demolitions work, use airborne explosives rather than the buried charges most often used in mining.

In this SERDP SEED project, a scientifically based empirical equation for predicting the maximum ground vibration induced by military activities is derived from existing field measurement data. Because of the project resource limitations, the research is limited to airborne detonations produced by explosive charges of C4 under a variety of environmental conditions.

The analysis of the experimental data shows that, although two separate seismic (ground vibrational) arrivals can be detected in all cases, the early seismic arrival from an underground path (Path B in Fig. 1) is always much smaller than the vibration induced by the air blast arrival (Path A in Fig. 1), so the early seismic arrival is neglected in the empirical equation.

A conservative empirical equation to predict ground vibration from explosions is given by eq 9 of the text. Equation 9 predicts that the vibrational damage criteria of 12 and 25 mm/s will be exceeded when the peak positive pressure exceeds 480 Pa (147.6 dB) or 1 kPa (154.0 dB), respectively. Either of these levels is much higher than the Army overpressure damage criterion of 159 Pa (138 dB). Thus, in

most situations, damage from blast overpressure will occur long before damaging levels of ground vibration are reached.

Detailed waveform modeling was also conducted to validate the simple model and to examine any frequency dependence in the process.

1 Objectives

This SERDP SEED research project directly addresses a portion of CPSON-04-03: *Characterization and Prediction of Potential Impact of Military Generated Noise on Structures*. The project addresses damage claims alleging that military activities cause substantial earth-borne vibration. The research provides a scientific analysis of this situation and develops a simple model based on existing data that can be used for assessing and predicting ground vibration levels.

The technical objective of this project was to produce a simple, accurate procedure for estimating the peak ground vibration produced by Army training and demilitarization activities. This procedure is based on the analysis of existing measurements of various Army activities and has a firm scientific foundation. To accomplish this goal, three following tasks were completed.

Task 1—Construct an accurate but simple model of induced ground motion from military activities

This was the main goal of this project: to develop a simple model, based on existing measurement data, to provide predictions of peak ground vibration from military noise sources for a variety of soil and ground conditions.

Task 2—Determine the acoustic-to-seismic coupling coefficients *C1* and *C2*

This task was a subtask of Task 1 above. These coefficients were needed in the empirical equation and were determined by analyzing a large database of explosion measurements conducted over different soil types and ground conditions.

Task 3—Computational modeling of acoustically induced ground motion

The simple model of blast sound interaction with the ground that was postulated above ignores any possible frequency dependence. To ensure that we fully understand the process of acoustically induced ground motion and its dependence on relevant factors, we also calculated the theoretically expected acoustic pressure and associated ground motion attributable to a point source in air using a frequency-domain program. This modeling provides additional scientific insight into the process of inducing ground motion from airborne explosive sources.

2 Background

DOD installations are increasingly dealing with complaints and structural damage claims allegedly caused by ground vibrations produced by military activities. Currently, a simple procedure is used to assess damage claims that attribute ground motion to Army activities (Wright 1994). In this procedure, empirical equations formulated by the mining industry are used to estimate the peak level of ground vibration caused by the Army activity. A claim is viewed to have merit if the estimated ground motion has a value of 1.0 in./s (25.4 mm/s) or larger based on these empirical equations. However, mining industry blasting significantly differs from Army activities, especially in the use of very large explosive charge sizes (typically thousands of pounds of TNT) spread over a relatively large area (to break the most rock). Thus, the empirical equations currently in use may not be accurate when applied to Army activities, which usually involve point sources much smaller in explosive size.

Wright (1994) presents the procedures currently used to evaluate civilian claims of damage from military activities at Army facilities. The procedures conservatively estimate the peak overpressure or peak ground motion (peak particle velocity, or PPV) and compare these predictions with peak level damage criteria. (By conservative, it is meant that the procedure favors the claimant.) If the criteria are met, the claim is then further evaluated to see if damage compensation is warranted. To predict ground motion, two equations are cited. Both of these equations are in the form

$$\dot{u}_{peak} = A_0 \left(R/W^{1/3} \right)^{-\alpha} \tag{1}$$

where

$\dot{u}_{peak}$ = peak particle velocity (m s^{-1} or inches s^{-1})
A_0 = Constant coefficient ($kg^{-1/3}$ m^1 or $lb^{-1/3}$ ft^1)
R = distance from explosion (m or ft)
$W^{1/3}$ = cube root of TNT equivalent explosive charge weight ($kg^{1/3}$ or $lb^{1/3}$)
α = an attenuation coefficient.

Wright cites Siskind et al. (1980) and Johnson et al. (1988) as sources for the values of the coefficients A_0 and α listed in columns 4 and 5 of Table 1 for surface

explosions and for buried explosions, respectively. For ground motion damage claims, Wright states that one of these two equations (columns 4 and 5 of Table 1) is used to estimate the peak ground particle velocity, and that the claim is rejected if the predicted peak motion is less than 1.0 in. s^{-1}. We note here an apparent typographical error in Wright (1994), as the surface explosion equation with coefficients in the first column does not predict reasonable values. (We were unable to find and correct this equation in the cited reference and could not contact Mr. Wright, who has apparently retired from the Army Research Laboratory.)

Table 1. Coefficients (in English units) for eq 1 used to estimate peak particle velocity.

	Dowding (1996), Fig. 4-4	Dowding (1996), eq 11-2	Surface explosions (Siskind 1980)	Buried explosions (Johnson 1988)
Equation number for this report:	2	3	—	
A_0	360	6.88	5.349×10^{15}	1.20×10^{3}
α	1.6	1.46	5.354	2.7
1 block C4 at 100 m (in./s):	0.045	0.0019	—	0.000 31
1 block C4 at 100 m (mm/s):	1.1	0.048		0.0079

More recently, Dowding (1996) presents additional relationships based on measured data from surface mining. The first relationship, appearing in Dowding's Figure 4-4, is reproduced from a study by Ambrayseys and Hendron (1968) and was developed from blasts ranging in size from 14 to 145,000 kg. The far field coefficients derived from these data are listed in the second column of Table 1 above. In addition, Dowding presents equations based on his own measurements of surface mining explosions. We have combined terms, dropped the dependence on soil or rock density, and reworked Dowding's equations into the same form as eq 1, and the resulting coefficients are listed in the third column of Table 1. The empirical equations of Dowding are

$$\dot{u}_{peak} = 360\left(R/W^{1/3}\right)^{-1.6} \tag{2}$$

$$\dot{u}_{peak} = 6.88\left(R/W^{1/3}\right)^{-1.46} \tag{3}$$

Note that predicted peak particle velocities will vary greatly depending on which equation is used. As an example, the predicted ground motion produced by the

detonation of one block (1.25 lb) of C4 a distance of 328 ft (100 m) was predicted using each of the equations and is shown in the last row of Table 1. The equation of Siskind et al. (1980) as quoted by Wright (1994) gave a value of 470 in./s, which is clearly erroneous and has been omitted from the table. The values predicted by the two surface blast equations (eq 2 and 3) given by Dowding vary by a factor of 20, and are less than our own measured value of about 0.077 in./s (2.0 mm/s) for typical soil conditions. Thus, the claim made by Wright (1994) that the current Army estimation procedure overpredicts the actual ground vibration might be erroneous.

The above equations and standards were adapted directly from the mining industry. While they can serve as a useful starting point, there are significant differences between mining and military activities. For example, in mining, explosive charge sizes are usually quite large in depth and area, as their purpose is to break as much rock as possible. Army sources (for example demilitarization [demolition of obsolete munitions] or artillery training) tend to be point sources, with much smaller physical dimensions and usually smaller charge size. In addition, the type of soil and geology, factors that might cause large variations in induced ground vibration, have not been specified or included in the mining relations. The purpose of this research project was to investigate these differences between mining and Army sources and to derive new, scientifically based equations (that include the variation in ground properties) to be used for predictions of the ground motion produced by military activities.

3 Materials and Methods

A number of acoustic and seismic signature measurements of explosions obtained under various environmental conditions were analyzed to determine the relationship between explosion parameters and the induced ground vibration. A simple model, based on existing measurement data, was developed to provide predictions of peak ground vibration from military noise sources for a variety of soil and ground conditions.

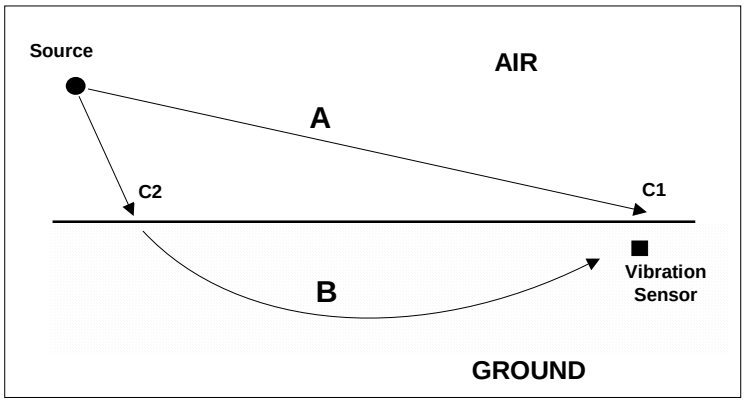

Figure 1. Ground vibration model. After source in the air or on the ground is detonated, waves will propagation to a vibration sensor following two paths: airborne (A) and predominantly subsurface (B). The ground vibration amplitude resulting from these two propagation paths is affected by the acoustic-to-seismic coupling coefficients *C1* and *C2*, respectively. The model is described by eq 4 in the text.

Figure 1 shows a sketch of the two propagation paths that may be important in this situation. Path A is a purely airborne path between source and ground, so that the coupling of airborne sound energy into the ground occurs near the reception point of interest. Path B in is a relatively short airborne path between source and ground and subsurface transmission thereafter. The ratio of incident sound pressure to acoustically induced particle motion can be described in terms of the acoustic-to-seismic coupling coefficients *C1* and *C2*, respectively. In most (but perhaps not all) cases, the airborne path induces the largest ground vibration, as it is least attenuated. If the airblast directly hits a structure, the dB Peak criterion already used is sufficient and was not further developed in this research. Instead, this project developed an estimate of the peak ground vibration caused by a source in the air for the two propagation paths, such as would affect a building foundation.

This model was developed using existing measured data. ANSI Standard S2.20 (1983) was used to predict the peak pressure from a given explosive charge size as a function of distance from the charge, *R*. This standard is initially used to predict the expected peak pressure at *R*, although it can be modified to account for different ground surface conditions. The peak ground vibration from this propagation path was determined using the coupling coefficient *C1*. Determining the values of *C1* for various soil and surface impedance conditions was a goal of this project.

The subsurface path (B in Fig. 1) can be predicted by multiplying the near-source peak pressure by a second coupling coefficient *C2* to determine the induced peak ground vibration near the source. This value was propagated to range *R* using a simple Rayleigh wave propagation model that includes seismic attenuation. Specifying the Rayleigh wave model, and determining appropriate values of *C2* for various ground and source conditions, was another goal of this project.

Summarizing this approach, we developed an equation of the form

$$\dot{u}_{peak} = C1\, P(R)\, e^{-\beta R} + C2\, P(R_0)\, G(R)\, e^{-\gamma R} \tag{4}$$

where

$\dot{u}_{peak}$ = peak particle velocity (m s^{-1})
R = distance from explosion (m)
β = pressure wave attenuation coefficient along the ground surface (m^{-1})
γ = Rayleigh wave attenuation coefficient (m^{-1})
$C1$ = far-field acoustic-to-seismic coupling coefficient (m s^{-1} Pa^{-1})
$C2$ = near-field acoustic-to-seismic coupling coefficient ($m^{1/2}$ s^{-1} Pa^{-1})
$P(R)$ = airblast pressure at distance *R*, from ANSI Standard (Pa)
$G(R)$ = geometrical spreading factor for induced seismic waves ($m^{-1/2}$).
R_0 = slant distance where maximum Rayleigh wave coupling occurs (m).

The first term in eq 4 represents the direct atmospheric wave from the charge to the ground measurement point, and the second an arrival that travels primarily through the ground as a Rayleigh wave. The direct wave decays with distance as approximately $R^{-1.1}$, the far-field attenuation of the ANSI standard pressure, plus

an additional attenuation caused by interaction of the airblast wave with the ground surface. The Rayleigh wave will decay geometrically by a factor $G(R)$, which reduces in the farfield to $R^{-1/2}$ dependence. The Rayleigh wave is also subject to a seismic material attenuation given by γ. Although the dependence with charge weight does not appear explicitly in eq 4, cube root scaling was still expected and is contained in the pressure terms P because of the ANSI Standard.

From the data analysis presented below, we found that the first term in eq 4 dominates the peak particle velocity response and the second term can be ignored. In these situations eq 5 is simplified by retaining only the first term

$$\dot{u}_{peak} = C1\, P(R)\, e^{-\beta R} \tag{5}$$

These coefficients have been determined by analyzing a large database of explosion measurements conducted over different soil types and ground conditions. Over the past few years, a few hundred digital waveform measurements of waves produced by detonations of various sized charges of C4 explosive have been recorded using collocated pressure sensors and geophones (ground vibration sensors) in a number of environments, including concrete, grass, snow, and thick tropical or forest vegetation. These measurements were used to:

1. Determine the coupling coefficients *C1* and *C2* in eq 4 for various soil and geological conditions.
2. Determine classifications of ground conditions where the path B is important and needs to be included in the response.
3. Test and evaluate the predictions of eq 1 and 4, the mining and Army predictive equations, vs. the measured ground vibration as a function of propagation range.

The simple model of blast sound interaction with the ground that is postulated above ignores any possible frequency dependence. To ensure that we fully understand the process of acoustically induced ground motion and its dependence on relevant factors, we also calculated acoustic pressure and associated ground motion from a point source in air using a frequency-domain program (Boulanger and Attenborough 2005a). This modeling provides additional scientific insight into the process of inducing ground motion from airborne explosive sources.

Overview of the measurements

The seven measurement data sets that will be analyzed in this report were conducted by ERDC-CRREL for other Army projects. Because the tests had differing

goals and because there were different restrictions on the test plans, depending on the Army range in which they were conducted, the parameters of the tests (including charge size, charge height, and propagation distance) vary from one test to another. Table 2 lists some of the parameters for these experimental measurements. (In fact, none of the original test goals required the measurement of ground vibration, but we were able to record some of this data without impacting the test schedules or costs, and thus the measurements became available for this study.)

For all of the measurements except one (Test 6), a Geometrics NZ digital seismograph was used to make the recordings, usually with a sampling rate of 5000 samples per second. For Test 6, a number of Summit two-channel distributed digitizers were used to record the signatures at a sampling rate of 8000 samples per second. Both recorders have 24 bit digitizers giving the measurements a very wide dynamic range. The recordings were started using either a signal from the blasting cap firing box or by using a break wire placed within the C4 charge itself.

Table 2. Test environments, charge sizes, and propagation distances.

Test #	Type	Location (State)	Charge heights (m)	Charge size range (blocks C4)	Charge size (kg)	Distance range (m)
1	Concrete	MD	1.5	1	0.57	8–91
2	Soil	MD	1.5	1–128	0.57, 5.7, 9.1, 18.2, 72.7	100–240
3	Soil and Gravel pile	MD	1.0, 1.5, 3.0	1	0.57	60–405
4	Tropical vegetation	FL	0.0, 1.5	0.5–8	0.28, 0.57, 2.3, 4.6	30–100
5	Low density snow cover	MN	0.0, 1.5	0.5–8	0.28, 0.57, 2.3, 4.6	30–100
6	Snow	NY	0.0, 1.5	0.5–8	0.28, 0.57, 2.3, 4.6	60, 150
7	Forest	TX	0.3, 1.2, 1.9, 3.0, 3.8	1–4	0.57, 2.3	30–565

At each measurement location, a solid state PCB pressure sensor or a Bruel and Kjaer ¼-in.-diameter microphone was used to record the air blast wave at the ground (or snow surface) level. The solid state sensors were capable of measuring higher pressure levels and so were usually used for propagation distances of 100 m and less, while the microphones were used at greater distances. Mark Products L-15 geophones with a resonant frequency of 4.5 Hz were used to record the ground vibrations. The geophones were oriented with one vertical component, and

either one (radial) or two (radial and transverse) horizontal components. These geophones produce a voltage output that is proportional to the ground particle velocity.

For most of the measurements, the sensors were located in a straight line at known distances away from a shot location. The main exception to this geometry was for Test 1, the measurements conducted on a concrete pad. In this case, two lines of sensors perpendicular to each other were installed and used to record the data, and the source location was also moved to different locations on the concrete pad. The number of fully instrumented sensor locations varied from one test to another.

C4 Charge heights and sizes

Because of site restrictions, only four of the tests allowed C4 charges to be placed at the ground surface (Tests 1, 4, 5, and 6, see Table 2). We found that the measured pressures and ground vibrations were similar to those for air shots in the same location, so we have combined all of the measurements in this analysis. The measurements would certainly have given different results if the explosive charges had been buried, but that situation is already covered by the measurements and standards from mining industry explosions. We also found little difference in the measurements done at various charge heights above the ground surface, so those measurements are also analyzed together for each location.

The tests also differed in the charge sizes that could be used. In two of the tests (Tests 1 and 3, see Table 2), only single blocks of C4 (1.25 lb or 0.57 kg) were used. The other tests all had at least two different charge sizes, and Test 2 had charge sizes up to 73 kg.

Charge scaling

Geometric and energy considerations predict that identical blast waves will be produced at identical *scaled distance*s for two different explosive charge sizes. The scaling is proportional to the cube root of the charge size, and the scaled distance is defined as

$$D = \frac{R}{W^{1/3}} \tag{5b}$$

where D is the scaled distance, R the actual distance, and W the charge weight.

For example, a single block of C4 produces a peak pressure of about 1 kPa at a distance of 100 m. To produce the same peak pressure when eight blocks are used, the measurement distance will need to be increased by a factor of $8^{1/3} = 2$, or at a distance of 200 m from the larger charge. To account for the different charge sizes used in the measurements, the propagation distances are scaled by the cube root of the charge size in the analysis below. These scaled distances are then given in units of m $kg^{-1/3}$. Once the data are scaled in this way, a regression (least squares) line can be derived, and that line can be used to predict the peak pressure as a function of distance for any charge size (see Fig. 2). This scaling is used in the analysis to account for charge size differences. Because the acoustic pressure and the ground vibration would scale in a similar manner, ratios of these two parameters do not need to be scaled.

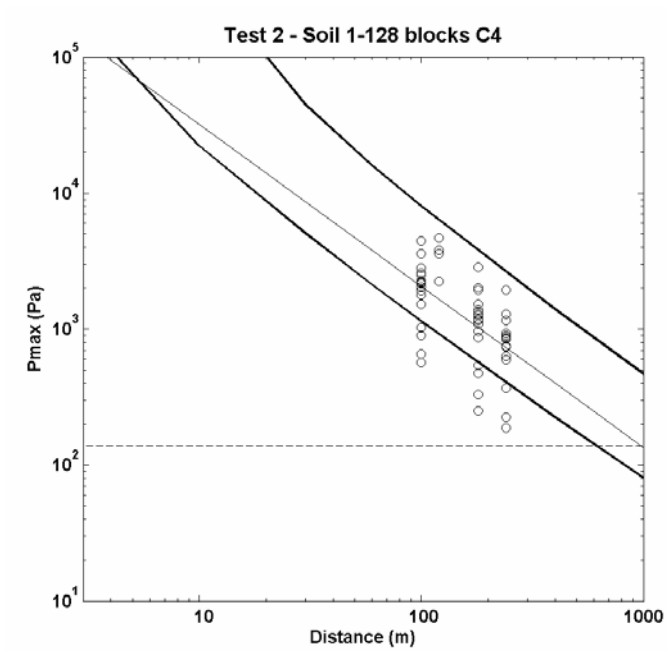

a. Measurements of peak pressure as a function of propagation distance from detonations of C4 explosive charges ranging in size from 1 to 128 blocks (0.57 to 72.7 kg). The vertical distribution of the measurements at each location is primarily from the difference in charge size.

Figure 2. Example of cube root scaling of the charge size.

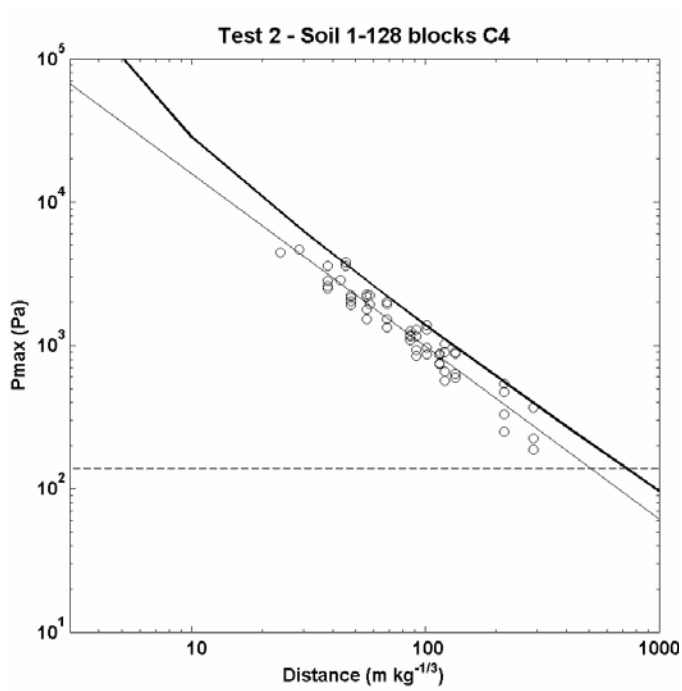

b. The same measurements plotted as a function of scaled distance. These measurements now fit a line reasonably well, and that line can be used to make predictions for any charge size or distance.

Figure 2 (cont'd). Example of cube root scaling of the charge size.

4 Results and Accomplishments

This section discusses the data analysis procedures and results, the development of a simple prediction model, and the detailed waveform modeling results.

Data Analysis of C4 airblast measurements

In this section several signature measurements using C4 explosions are analyzed. The C4 measurements analyzed here are similar to the impulsive sounds expected to be produced by artillery muzzle blasts. The goal of the analysis is to determine the validity of the equations presented in the previous section in describing the vibration produced by airborne explosive sources in a variety of environments and to determine the coefficients *C1* and *C2* for the propagation paths shown in Figure 1. The particular equation that is used will depend on whether Path A in Figure 1 is sufficient to give good predictions or whether both Paths A and B are needed.

Test 1—Propagation over concrete

Because concrete is a material that has a very high acoustic impedance, it also has a high reflection coefficient and for this reason the peak acoustic pressures for a given distance and explosive charge size are expected to be higher over concrete than for any other ground condition. But how the acoustic energy couples into this material is unknown.

Figure 3. Photo of some of the sensors used during Test 1, propagation measurements over concrete.

This experiment was conducted at the Aberdeen Test Center, Edgewood Area, in 2001 as part of the SYDET development project. The test was conducted over a 90- × 90-m flat concrete pad with a large concrete wall located at one edge of the pad (Fig. 3). The wall was 7 m tall, 14 m wide, and 2 m thick. Sensors (microphones and geophones) were arranged in lines parallel and perpendicular to the wall, and the geophones were drilled and cemented into place. Single blocks of C4 (1.25 lb or 0.57 kg) were detonated and the resulting signatures were measured using a digital seismograph. We were allowed to detonate a few charges at the base of the wall on the edge of the concrete pad, but all of the other detonations were at a height of 1.5 m to avoid damage to the concrete pad. The shots were fired at various locations around the concrete pad, giving propagation distances ranging from 10 to 93 m. The geometry of the measurements is shown in Figure 4, and additional details of the measurements are available in Carbee et al. (2001).

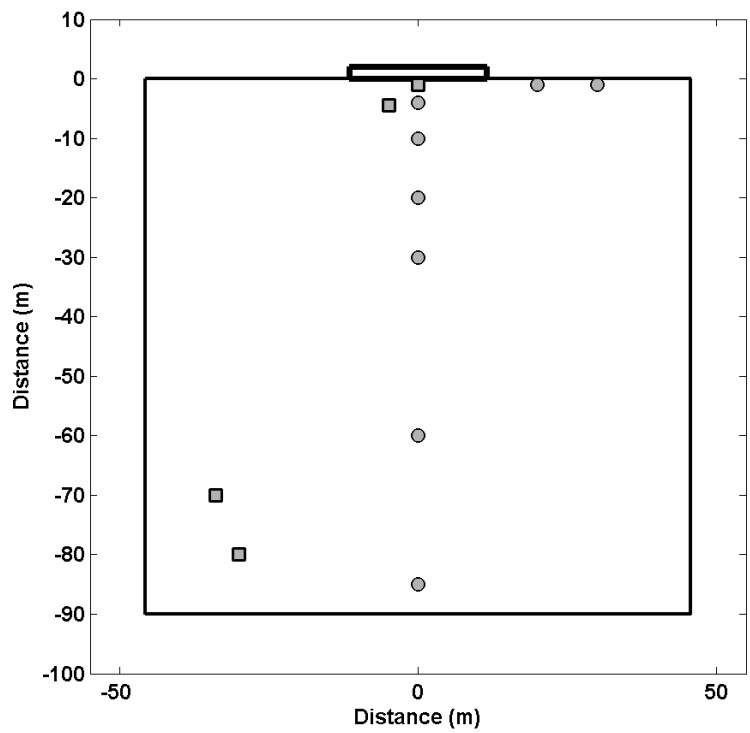

Figure 4. Geometry of the measurements over concrete. Single block (0.57 kg) charges of C4 were detonated at a height of 1.5 m above the surface at the four locations shown by the squares in the figure, and recorded by sensors at the locations shown by circles. At each sensor location, two pressure sensors were installed, one at the surface of the concrete and one at a height of 1.5 m. Two geophones were also installed at these locations, one sensitive to vertical motion, the other to horizontal motion. The horizontal component geophone was aligned to measure motion perpendicular to the wall, located at the top of this figure.

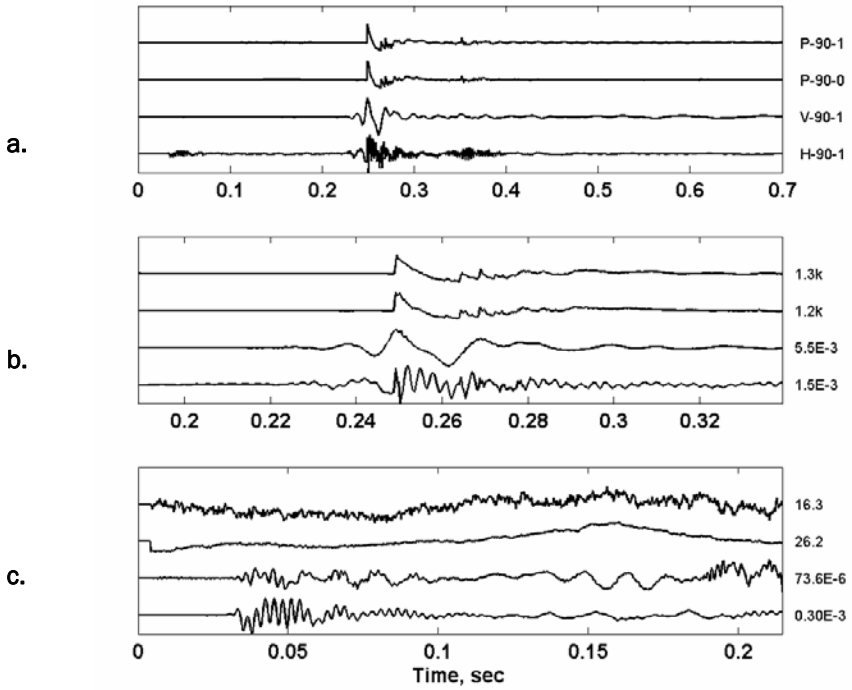

Figure 5. Waveforms measured during Test 1, for a single block of C4 (0.57 kg) detonated at a height of 1.5 m above a concrete pad. The sensors were located 90 m from the source. In 5a the main acoustic or blast wave arrives at about 0.25 seconds. 5b shows that the ground vibration starts about 0.03 s ahead of the acoustic arrival, but the maximum ground vibration is coincident with the acoustic arrival. In 5c no acoustic arrivals are present on the pressure sensors, but seismic waves are visible at about 0.035 s. These waves have much smaller amplitudes that the waves that arrive closer to the acoustic arrival time in 5b.*

Figure 5 shows examples of the time series or waveforms measured after a single block of C4 was detonated at a height of 1.5 m above the concrete pad. The sensors were located 90 m from the source. From Figure 5a, showing the full time series, the main acoustic or blast wave arrival can be seen at about 0.25 s, and a smaller seismic wave arrival is visible at an earlier time of about 0.035 s on the radial geophone. Figure 5b, giving more detail around the acoustic arrival time, shows that the ground vibration starts about 0.03 s ahead of the acoustic arrival, but the maximum ground vibration is coincident with the acoustic arrival. This wave corresponds to propagation path A in Figure 1. Figure 5c shows the early time part of the trace. Here, no acoustic arrivals are present on the pressure sen-

* This figure and similar figures for Tests 2–7 will all have the same format: For all three panels in the figure, the signal trace order from top to bottom the traces in each panel are 1) pressure sensor 1.5 m above the surface, 2) pressure sensor at the surface, 3) vertical component geophone (ground particle velocity), and 4) radial component geophone—a shows the full time series, b shows a close up time window near the acoustic arrival time, and c shows an early time window where seismic waves propagating at speeds higher than the atmospheric acoustic wave may appear. Numbers to the right of the traces in b and c indicate the maximum positive pressures in kPa for the pressure sensors, and maximum absolute ground particle velocities in m/s for the geophones for the time windows shown.

sors, but seismic waves are visible at about 0.035 seconds. These seismic waves correspond to propagation path B in Figure 1 and have much smaller amplitudes that the waves that arrive closer to the acoustic arrival time in Figure 5b.

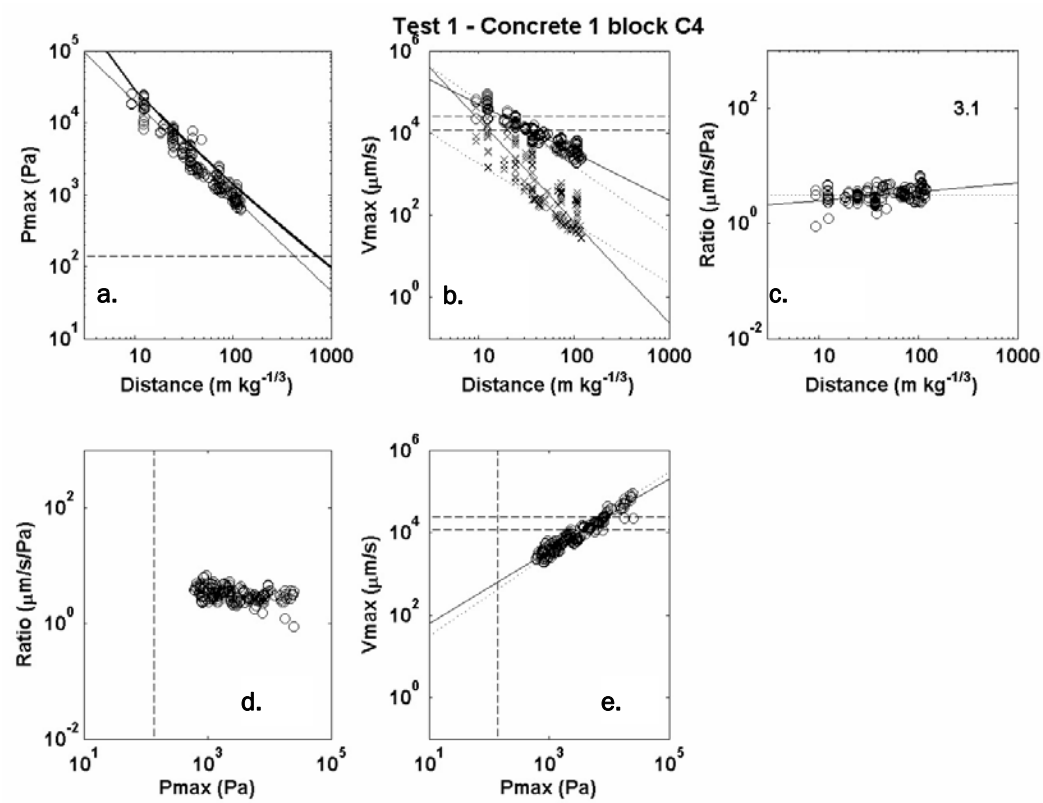

Figure 6. Measurement results for Test 1, propagation over concrete. Dashed lines in the Figure are acoustic or vibrational damage criteria of 159 Pa, 25 mm/s, or 12 mm/s. The slopes of the least squares line fits to the measured data in the panels appear in Table 3, and the pressure levels needed to exceed the vibration damage criteria are listed in Table 4. *

* The top row gives measured wave parameters as a function of scaled propagation distance and the bottom row plots parameters independent of the propagation distance. *a* is peak positive pressure vs. scaled distance. Circles are the measured peak pressures and the thin line is a least squares fit to the measured data. The thick line is the ANSI Standard S2.20 predicted line for a block of C4 and the dashed line is the Army airblast damage threshold of 138 dB (159 Pa). *b* is peak seismic amplitude vs. scaled propagation distance. Circles are seismic arrivals associated with the acoustic arrival and x's are the early seismic arrivals. These correspond to Path A and Path B in Figure 1. Solid lines are least squares fits to the measured data. Dashed lines are vibration damage criteria of 12 and 25 mm/s. The dotted lines are the empirical lines of eq 2 and 3. *c* is measured acoustic to seismic coupling ratio vs. scaled propagation distance. The solid line is the least squares line fit, the dotted line is the median value, which is also on the figure. *d* is peak positive pressure vs. acoustic-to-seismic coupling ratio. Circles are measured values, and the dashed line is the Army airblast damage criterion of 138 dB. *e* is peak positive pressure vs. maximum seismic amplitude. Vertical dashed line is the Army airblast damage criterion of 138 dB (159 Pa) while the horizontal dashed lines are the vibration damage criteria of 12 and 25 mm/s. The thicker line is a least squares fit to the data, and the dotted line is eq 8 in the form $V_{max} = P_{ANSI}$*(Median Ratio). Note that the measurements on the top row have been scaled to a charge size of 1 kg by dividing the distance by the cube root of the actual charge weight in kg.

These arrivals confirm the validity of the model proposed in Figure 1. As we will see in this and additional data sets, path A always produces a seismic arrival that is larger than path B. Because of these experimental observations, we will simplify the empirical prediction model eq 4 to include only path A as in eq 5.

The five plots in Figure 6 give the results of the data analysis for Test 1. In all of the plots and in the plots to follow for the other tests, the measured amplitudes for pressure and ground vibration have been scaled to a 1-kg charge size by dividing the measurement by the cube root of the actual charge weight. Vertical and horizontal dashed lines in the plots give the current threshold criteria for building cosmetic damage, either an airblast pressure value of 138 dB (159 Pa) or a vibration particle velocity value of 12 or 25 mm/s.

Figure 6a shows the peak positive pressure as a function of propagation distance. The thick line is the ANSI Standard S2.20 predicted line for a block of C4 and the thin line is a least squares fit to the measured data of the form

$$P(R) = P_0 R^{-\alpha} \tag{6}$$

with an attenuation rate α of –1.3 (Table 3). The peak pressure values lie very close to the ANSI Standard line.

Figure 6b shows the peak seismic amplitude as a function of propagation distance. The seismic amplitude V_{max} is the vector magnitude, calculated as

$$V_{max} = \left(\dot{u}_{max}^2 + \dot{v}_{max}^2\right)^{1/2} \tag{7}$$

where $\dot{u}_{max}^2$, etc., are the peak vertical, and radial particle velocities measured by the geophones during the appropriate time period.

Both the seismic arrivals associated with the acoustic arrival (circles) and the early seismic arrivals (x) are shown in Figure 6b. These correspond to Path A and Path B in Figure 1, and the graph shows that as the distance increases the early seismic arrival is two orders of magnitude or more below the amplitude of the acoustically-induced seismic vibration. (Close to the source, the arrivals are very close in time and the early arrival identification was somewhat arbitrary, so there is a lot of scatter in the amplitude of the early arrival for short propagation distances.) The solid lines are least squares lines fitted to the vibration measurements, and the line fitted to V_{max} gives an amplitude decay rate of -1.2 (listed in Table 3). The dotted lines are eq 2 and 3, the empirical mining equations of

Dowding (1996). For these measurements eq 2 is slightly lower than the measured peak vibration data and has a higher attenuation rate, and eq 3 is well below the measured data and is much closer to the early seismic arrival amplitudes. Equation 3 is clearly unsuitable for predicting the levels produced by this typical military case. Also, because the early seismic arrivals are so much smaller than the acoustic arrivals, they are omitted from Table 3 and from further consideration. These conclusions also apply to all of the other measurements as will be shown in the rest of this discussion. The plot also shows that the vibrational damage criteria of 12 and 25 mm/s are exceeded for scaled distances of 60 m $kg^{-1/3}$ and less.

Table 3. Attenuation rates and coupling ratios determined from the measured data.

Test #	Type	Charge size (kg)	Distance range (m)	*N*	P	V	Ratio	*S/A* ratio *C1* (median)	*P-V*
1	Concrete	0.57	8–91	166	–1.3	–1.2	0.15	3.1	0.88
2	Soil	0.57–72.7	100–240	54	–1.2	–1.6	–0.43	3.3	1.3
3	Soil and Gravel pile	0.57	60–405	292	–1.5	–1.1	0.36	5.7	0.76
4	Tropical vegetation	0.28–4.5	30–100	110	–1.3	–1.5	–0.18	13.2	1.1
5	Low density snow cover	0.28–4.5	30–100	143	–1.3	–1.1	0.22	1.0	0.87
6	Snow	0.28–4.5	60, 150	33	–1.5	–1.3	0.17	34.2	0.85
7	Forest	0.57–2.3	30–565	138	–1.3	–1.4	–0.12	5.2	1.1
1-5,7				**815**	**–1.40**	**–1.1**	**0.37**	**4.9**	**0.74**

N = number of data points; P = decay rate coefficient α for peak acoustic pressure; V = decay rate coefficient α for seismic amplitude, Ratio = slope of the *S/A* ratio vs. scaled distance plot, upper right panel in Figure 6, etc.; *S/A* Ratio = median value of seismic/acoustic amplitudes (μm/s)/Pa. This value corresponds to coefficient *C1* in eq 5 of the text; *P-V* = Slope of the *P-V* line in the lower center of Figure 6, etc.

Figure 6c shows the measured acoustic to seismic coupling ratio vs. propagation distance. The solid line is the least squares line fit (with a positive slope of 0.15), the dotted line is the median value (3.1), which is written on the figure and listed in Table 3. After examining all of the measured data, we determined that the median value is the best and most useful fit to the data. This value, 3.1 (μm/s)/Pa, is the estimate of the coefficient *C1* in eq 5.

For some Army range situations, the actual source and its distance from the measurement location may be unknown. Figures 6d and e may be useful in such situations. These panels show parameters that can be measured without knowing the source to sensor distance. Figure 6d shows the acoustic-to-seismic coupling ratio

as a function of peak positive pressure, and indicates that this value is nearly constant with respect to pressure. Figure 6e shows the peak seismic amplitude as a function of peak positive pressure. The thicker line is a least squares fit to the data with a slope of +0.88, and the dotted line is a variation of eq 5

$$\dot{u}_{peak} = C1 P_{ANSI}(R) \tag{8}$$

where P_{ANSI} is the peak pressure predicted by the ANSI Standard and the coefficient *C1* is given by the median of the acoustic-to-seismic coupling ratio (in µm/s/Pa) as determined by the data shown in the upper right panel of the Figure. Finally, the peak acoustic pressures corresponding to exceedance of the damage criteria of 12 and 25 mm/s are determined from the lines, and occur at 3.9 and 8.3 kPa, respectively (Table 4). The details of the measurements and all of the parameters determined from the data analysis are listed in Tables 3–4 for this test and the following tests.

Table 4. Peak acoustic pressure levels needed to exceed vibration damage criteria (peak pressure vs. peak ground vibration).

Test #	Type	Charge size (kg)	Distance range (m)	Pressure to exceed 12 mm/s ground velocity (kPa)	Pressure to exceed 12 mm/s ground velocity (dB)	Pressure to exceed 25 mm/s ground velocity (kPa)	Pressure to exceed 25 mm/s ground velocity (dB)
1	Concrete	0.57	8–91	3.9	165.8	8.3	172.4
2	Soil	0.57–72.7	100–240	2.3	161.2	3.7	165.3
3	Soil and Gravel pile	0.57	60–405	2.2	160.8	4.8	167.6
4	Tropical vegetation	0.28–4.5	30 – 100	1.0	154.0	1.6	158.1
5	Low density snow cover	0.28–4.5	30–100	12.3	175.8	25.6	182.1
6	Snow	0.28–4.5	60, 150	0.33	144.3	0.76	151.6
7	Forest	0.57–2.3	30–565	1.8	159.1	3.7	165.3
1–5,7				**2.0**	**160.0**	**3.5**	**164.9**

Test 2—Propagation over soil with light vegetation

This experiment was conducted at the Aberdeen Test Center, Edgewood Area, in 2004 as part of the SYDET (Sympathetic Detonator, an Army explosive detonator device) development project. The primary objective of the test was to determine the performance of the SYDET hardware for various charge sizes and distances

from the source. The test was conducted in a large field with sandy soil and vegetation consisting of grass, weeds, and a few scattered small trees. Figure 7 shows the sensor array and one of the sensor locations at the test site. For this test various charge sizes of C4, ranging from 1 to 128 blocks (0.57 to 73 kg), were detonated at 1.5 m above ground level and the resulting signatures were measured using a digital seismograph for propagation distances from 10 to 240 m. Geophones were installed at four locations, 100, 120, 180, and 240 m from the source location. Geophones were not installed at distances less than 100 m from the source as they would have been overdriven by the larger charge sizes at closer distances. Additional details of the measurements are presented in Perron et al. (in review, 2006b).

a. Blank pistol shot being fired at the C4 source location. Sensors in a linear array are spaced 10–240 m from the source point. The white sand bags were used to protect some of the sensor cables, as a maximum charge size of 73 kg might have damaged them. This photois intended to show the general ground and vegetative conditions during the tests. The sensors used in this report were 100 m or more from the source location, starting at about same distance away as the small tree visible to the left of the photograph.

Figure 7. Photo taken during Test 2 propagation over soil with grass/weed vegetative cover.

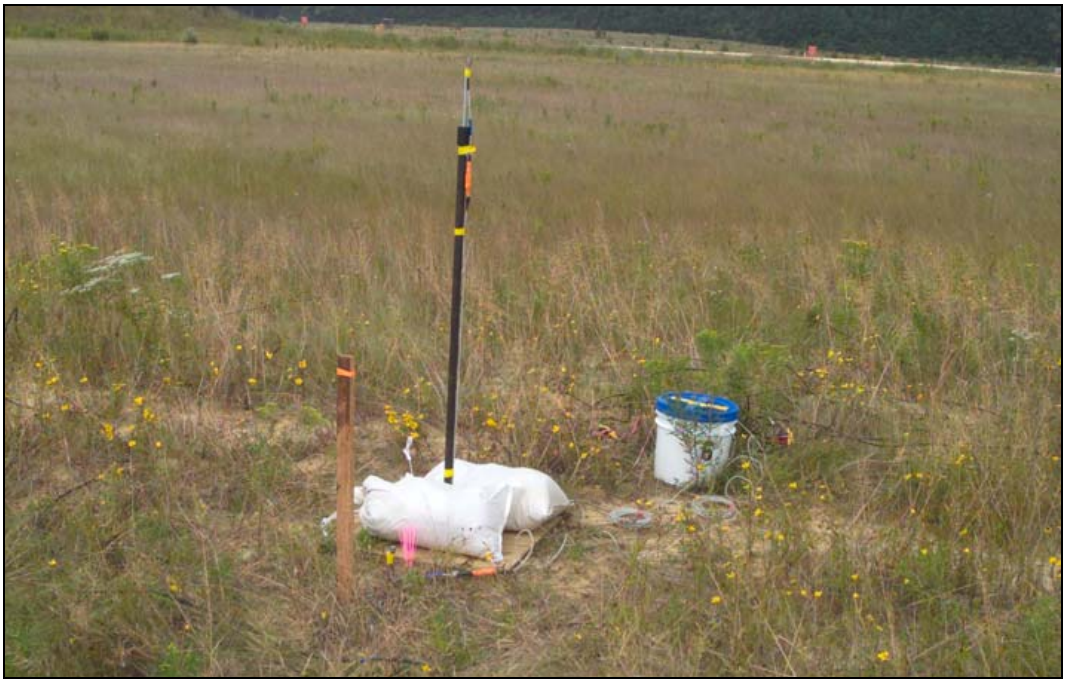

b. 100-m sensor location. Two blast pressure sensors are visible, one mounted on the pipe stand 1.5 m above the ground, and the other on a small metal rod near the ground surface. The white plastic bucket is used to protect the sensor power supplies. Note the tall grass.

c. Two orange geophones installed at the 100-m sensor location, one sensitive to vertical ground motion and the other sensitive to horizontal motion. These sensors are the same distance away from the source as the pressure sensors shown in 7b.

Figure 7 (cont'd). Photo taken during Test 2 propagation over soil with grass/weed vegetative cover.

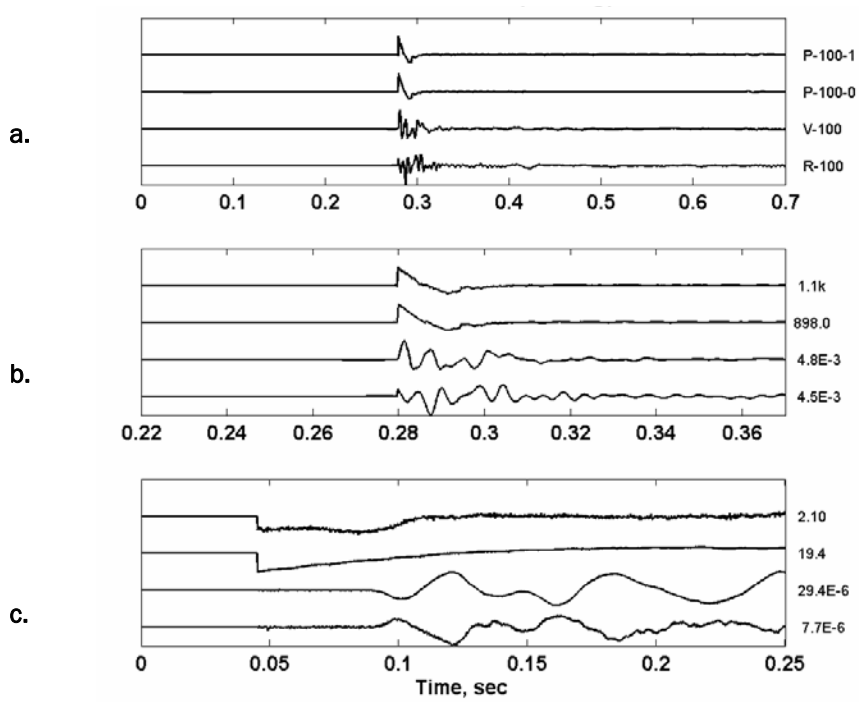

Figure 8. Waveforms measured during Test 2, for a single block (0.57 kg) of C4 detonated at 1.5 m above soil. The sensors were located 100 m from the source. In 8a, the main acoustic or blast wave arrives at about 0.28 s with a peak positive pressure of 900 Pa. 8b shows that the ground vibration starts coincident with the acoustic arrival. In 8c, low amplitude seismic waves are visible at about 0.09 s.

Figure 8 shows examples of the time series or waveforms measured after a single block of C4 was detonated at a height of 1.5 m, and Figure 9 shows the waveforms produced by a 32-block or 18.2-kg charge. In both figures, the sensors were located 100 m from the source. Both figures show that the primary acoustic and seismic arrivals are associated with the air wave, Path A in Figure 1. In this environment the seismic wave starts after the acoustic arrival, not before as in Test 1 for concrete. Smaller seismic arrivals corresponding to Path B as observed in both cases. Again, these arrivals confirm the validity of the model proposed in Figure 1 and the early seismic arrivals are small enough that eq 5 can be used instead of eq 4. Both charge sizes produced a shock waveform with a fast rise time and exponential decay. The slightly faster arrival time for the larger charge may be caused by nonlinear effects, as the propagation velocity will be proportional to the peak pressure (although changing atmospheric conditions can also be responsible for some of the time difference).

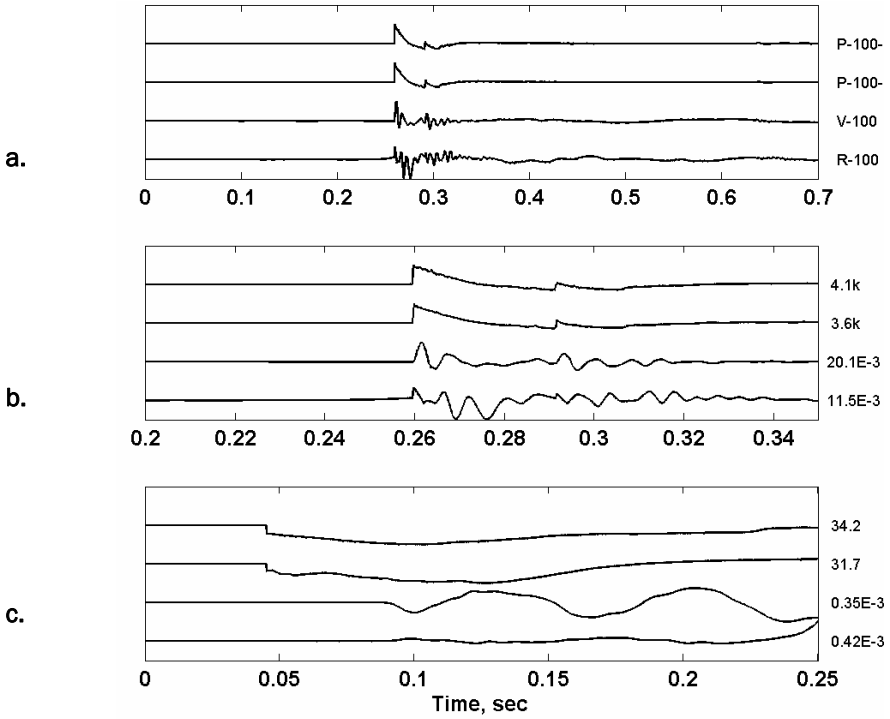

Figure 9. Waveforms measured during Test 2, for 32 blocks (18.2 kg) of C4 detonated at 1.5 m above soil. The sensors were located 100 m from the source. In 9a, the main acoustic or blast wave arrives at about 0.26 s with a peak positive pressure of 3.6 kPa. 9b shows that the ground vibration starts coincident with the acoustic arrival. In 9c, low amplitude seismic waves are visible at ~0.09 s.

Figure 10 shows the analysis results for this test, with numerical parameters listed in Tables 3–4. The scaled peak pressure measurements agree with and are slightly lower than the peak pressures predicted by the ANSI Standard, and the peak pressure attenuation rate vs. distance (–1.2) is similar to the attenuation rate measured for Test 1 over concrete. Maximum pressure values above the ANSI Standard occurred at all of the charge sizes, so it is probably caused by the relatively hard ground surface and not by a change in attenuation with charge size. The peak pressure may also have been enhanced for some of the measurements by wet ground from occasional rain showers and by atmospheric conditions related to a heavy, low altitude overcast that would tend to trap the acoustic energy near the ground surface.

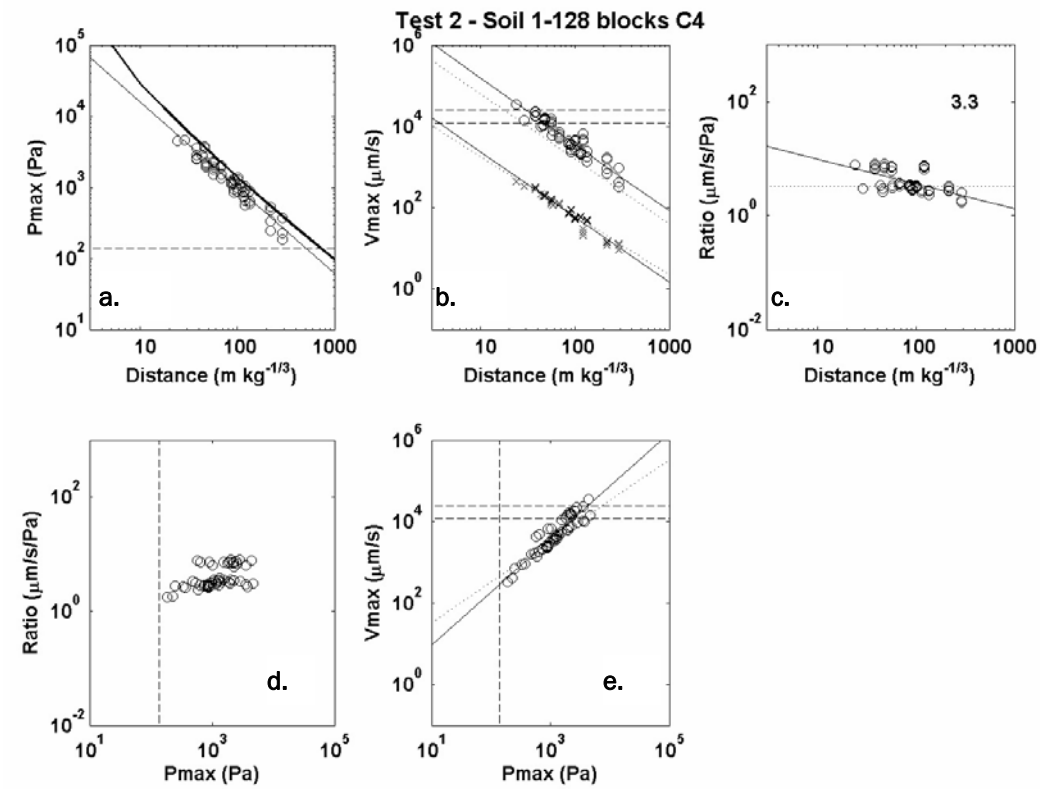

Figure 10. Measurement results for Test 2, propagation over soil. Dashed lines in the Figure are acoustic or vibrational damage criteria of 159 Pa, 25 mm/s, or 12 mm/s. The slopes of the least squares line fits to the measured data in the panels appear in Table 3, and the pressure levels needed to exceed the vibration damage criteria are listed in Table 4. See footnote to Figure 6 for more detailed information.

Figure 10a shows that the Path B seismic arrivals are two orders of magnitude lower in amplitude than those from Path A, and the measurements exceed the vibrational damage criteria at scaled distances less than approximately 70 m $kg^{-1/3}$. In this case the seismic attenuation rate of –1.6 is much higher than that measured for concrete. Line fits are used to predict peak pressure levels of 2.3 and 2.7 kPa (161.2 and 162.6 dB) that would be needed to induce vibrational damage levels of 12 and 25 mm/s.

Test 3—Propagation over soil with light vegetation, with a gravel pile

This experiment was conducted at the Aberdeen Test Center in 2004 as part of an Army Range Management project to determine whether a gravel pile could reduce the noise produced by artillery fire and ease civilian noise complaints. The test was conducted in a large field with light vegetation consisting of grass and weeds. A 15- × 15-m × 1.5-m tall coarse gravel pile was constructed in the field and used as part of these tests (see Fig. 11). All of the measurements were made using sin-

gle blocks of C4 as the source. For some of the measurements the explosives were detonated to the side of the gravel pile where all of the propagation occurred over undisturbed soil, while for other measurements the charge was detonated above or behind the gravel pile. The source height was varied from 1 to 3 m above the gravel or soil surface. Sensor locations from 60 to 405 m from the source are used in this analysis. Because there was very little difference in the measurement results from the various source locations for propagation distances of 100 m or greater, all of the measurements have been combined for this analysis. Full documentation of the measurements is presented in Perron et al. (in review, 2006a).

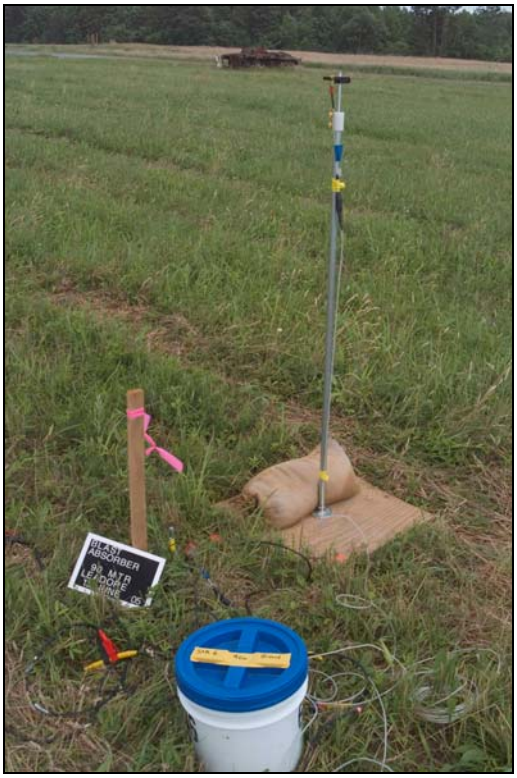

a. Sensors installed at 90 m. A solid state blast pressure sensor was installed on the pipe at 1.5 m above ground. Three ground level sensors were also used at this location but are partially obscured by the tall grass. A blast pressure sensor was installed on a small rod 10 cm above the ground (the rod has a piece of yellow tape on it, visible just above the message board), and the orange cases of two geophones are also visible nearby.

Figure 11. Photo from Test 3, soil and a gravel pile.

b. C4 charges detonated above or slightly behind the gravel pad, while others were detonated above normal ground away from the pile. The blast waves recorded by the sensors were similar in both cases so all of the source locations were combined for the analysis presented in this report.

c. Gravel pile constructed at the site, with a person standing on it for scale.

Figure 11 (cont'd). Test 3, soil and a gravel pile (Maryland, 2005).

Figure 12 shows a measurement made by sensors located 120 m from a detonation of a single block of C4 (0.57 kg) over bare ground. The figure shows that the

primary acoustic and seismic arrivals are associated with the air wave, Path A in Figure 1. In this environment the air-coupled seismic wave starts after the acoustic arrival, not before as in Test 1 for concrete (Fig. 5). Smaller seismic arrivals corresponding to Path B do occur in both cases. Again, these arrivals confirm the validity of the model proposed in Figure 1 and the early seismic arrivals are small enough that eq 5 can be used instead of eq 4. The seismic waves display relatively long duration oscillations occurring after the acoustic wave arrival, corresponding to air-coupled Rayleigh waves with a peak frequency of about 45 Hz. These properties are controlled by the shallow soil stratigraphy and seismic velocity structure.

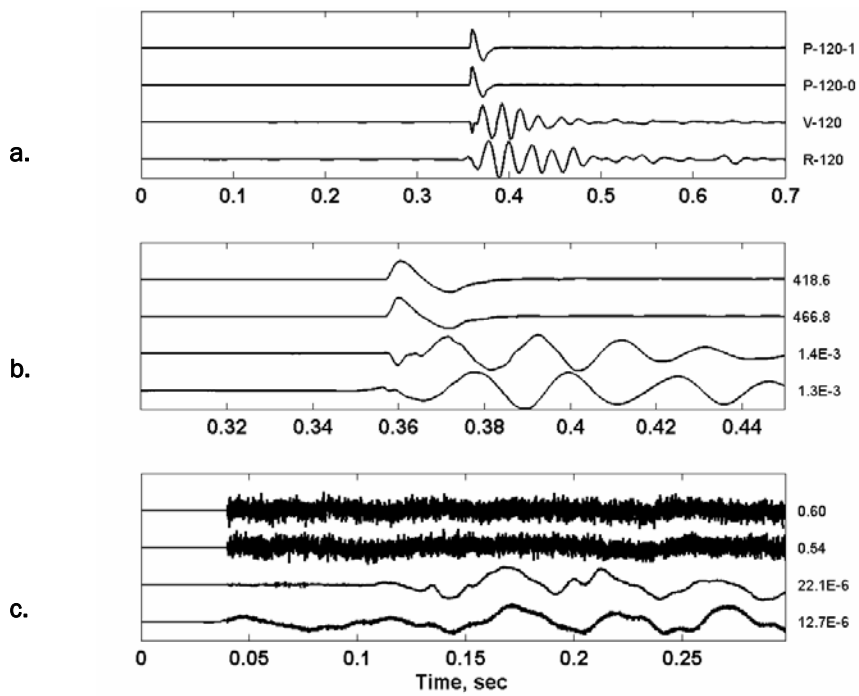

Figure 12. Waveforms measured during Test 3, for a single block of C4 (0.57 kg) detonated at 1.5 m above soil approximately 30 m to the side of a large gravel pile. The sensors were located 120 m from the source. The main acoustic or blast wave arrives at about 0.355 s with a peak positive pressure of 470 Pa. The ground vibration starts coincident with the acoustic arrival. In 12c, low amplitude seismic waves are visible at about 0.04 s, and additional waves arrive at 0.15 s, well before the acoustic arrival time.

Figure 13 shows the analysis results for this test, with numerical parameters listed in Tables 3–4. The scaled peak pressure measurements are all lower than the peak pressures predicted by the ANSI Standard, and the peak pressure attenuation rate vs. distance (–1.5) is higher than the attenuation rate measured for Test 1 over concrete. The Path B seismic arrivals are again two orders of magnitude lower in amplitude than those from Path A, and none of the measurements exceed the vibrational damage criteria. In this case the seismic attenuation rate of –1.1 is slightly less than that measured for concrete. Although concrete is theoretically

expected to have a lower attenuation rate than soil, the difference here is small, and might be caused by the different scaled distances where the measurements were made, with the concrete's measurements closer to the source than the soil's. Line fits are used to predict peak pressure levels of 2.2 and 4.8 kPa (160.8 and 167.6 dB) that would induce vibrational damage levels of 12 and 25 mm/s.

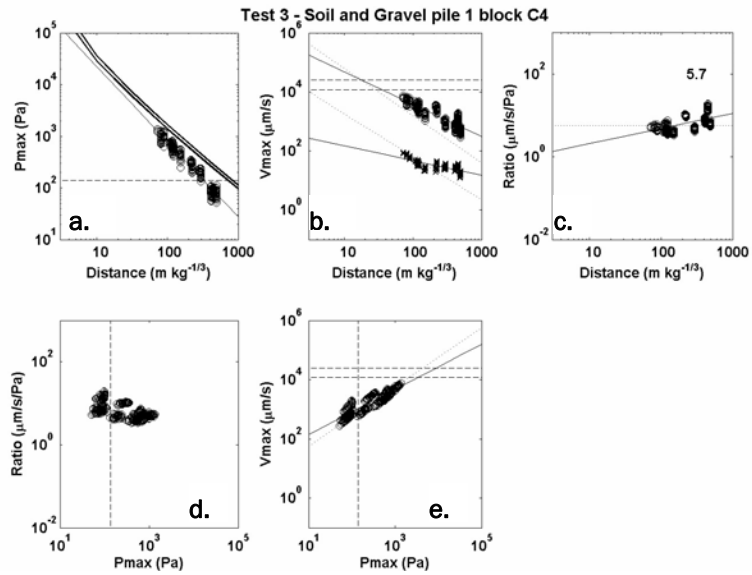

Figure 13. Measurement results for Test 1, propagation over concrete. Dashed lines in the Figure are acoustic or vibrational damage criteria of 159 Pa, 25 mm/s, or 12 mm/s. The slopes of the least squares line fits to the measured data in the panels appear in Table 3, and the pressure levels needed to exceed the vibration damage criteria are listed in Table 4. See footnote to Figure 6 for more detailed information.

Test 4—Propagation through heavy tropical vegetation

This experiment was conducted at the Eglin Air Force Base, Florida, in 2001 as part of the SYDET development project. The primary objective of the test was to determine the performance of the SYDET hardware in this environment. The test was conducted in an area of very thick vegetation that limited the visibility to less than 30 m in most locations. There was an extensive amount of vegetative debris on the ground. Figure 14 shows the test site. For this test various charge sizes of C4, ranging from 0.5 to 8 blocks (0.28 to 4.5 kg) were detonated on the ground and also at 1.5 m above ground level, and the resulting signatures were measured using a digital seismograph for propagation distances of 30 to 100 m. Additional details of the measurements are presented in Decato et al. (in review, 2006).

a. Looking down a path cut through the thick vegetation to access the sensor locations. The acoustic propagation path was through uncut vegetation similar to that shown in the photograph, and consisted of very dense, small diameter woody trunks.

b. Typical sensor location. Two high pressure microphones are covered with waterproof bags to protect them from rainfall. With the bags left open at the bottom there is no effect on the low frequency pressure wave recordings. Two orange geophones were also installed at this location and are visible in the leafy ground cover. This porous ground surface is similar to a snow cover in its absorptive properties.

Figure 14. Photos of Test 4, tropical vegetation (Eglin AFB, Florida, 2002).

Figure 15 shows a measurement made by sensors located 100 m from a detonation of a single block of C4 (0.57 kg). The figure shows that the primary acoustic

and seismic arrivals are associated with the air wave, Path A in Figure 1, and that the main seismic wave starts after the acoustic arrival. Smaller seismic arrivals corresponding to Path B were also detected. Again, the early seismic arrivals are small enough that eq 5 can be used instead of eq 4. The seismic waves display relatively long duration oscillations at a frequency of about 55 Hz, occurring after the acoustic wave arrival.

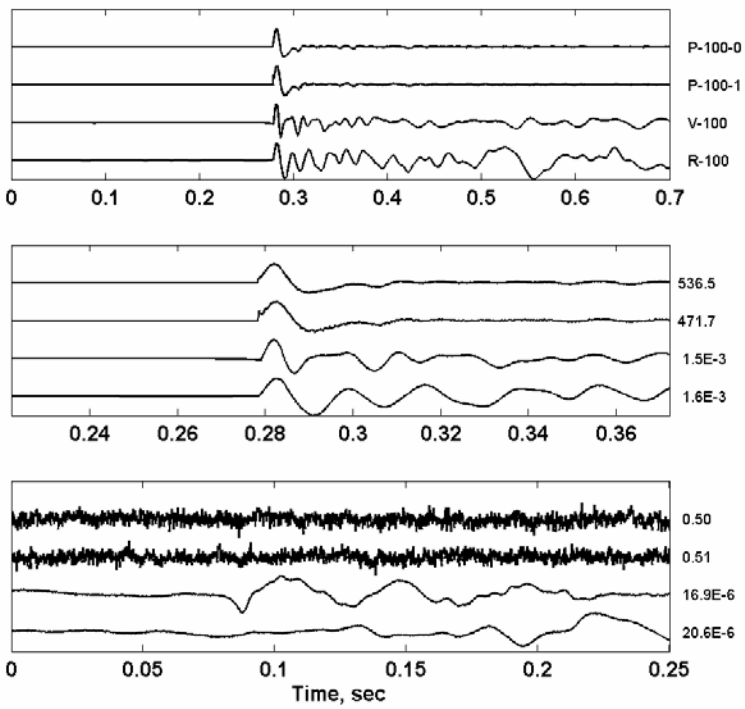

Figure 15. Waveforms measured during Test 4, for a single block of C4 (0.57 kg) detonated at a height of 1.5 m through tropical vegetation. The sensors were located 100 m from the source. The main acoustic wave arrives at about 0.28 s with a peak positive pressure of 470 Pa. The ground vibration starts coincident with the acoustic arrival, and low amplitude seismic waves are visible at about 0.09 s.

Figure 16 shows the analysis results for this test, with numerical parameters listed in Tables 3–4. The scaled peak pressure measurements are all lower than the peak pressures predicted by the ANSI Standard, and the peak pressure attenuation rate vs. distance was determined to be –1.3, similar to the attenuation rate measured for Test 1 over concrete. The Path B seismic arrivals are again two orders of magnitude lower in amplitude than those from Path A. Although the seismic attenuation rate of –1.5 is a relatively high value that would tend to predict low ground vibration levels, the ratio of induced seismic vibration to incident acoustic pressure is 13.2, the second highest value measured for any of these C4 tests. Because of this high ratio, some of the ground vibration levels exceed the vibrational damage levels of 12 and 25 mm/s at distances as much as 100 m $kg^{-1/3}$ from the

source. Line fits to the measurements predict that relatively low peak pressure levels of 1.0 and 1.6 kPa (154.0 and 158.1 dB) would be capable of inducing vibrational damage levels of 12 and 25 mm/s. The vegetative ground cover is apparently a good material for coupling acoustic energy into the ground. This behavior can be explained by the lower acoustic and vibrational impedance of this porous material compared to other materials like concrete.

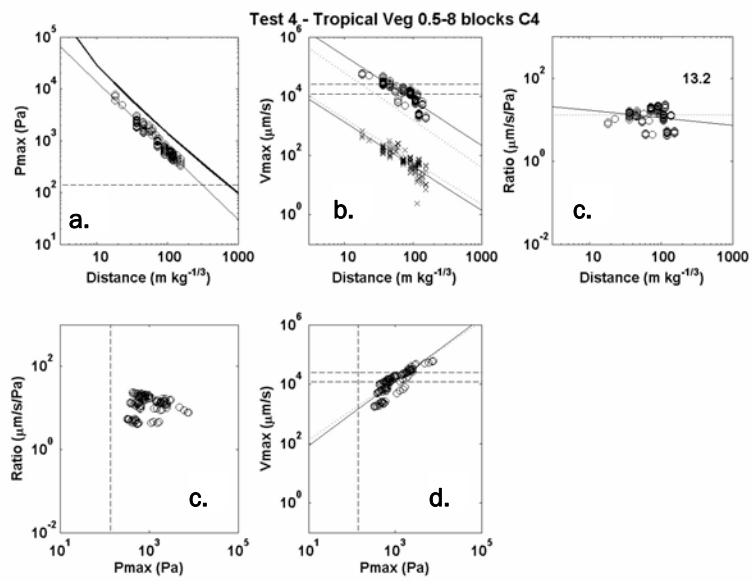

Figure 16. Measurement results for Test 4, propagation through tropical vegetation. Dashed lines in the Figure are acoustic or vibrational damage criteria of 159 Pa, 25 mm/s, or 12 mm/s. The slopes of the least squares line fits to the measured data in the panels appear in Table 3, and the pressure levels needed to exceed the vibration damage criteria are listed in Table 4. See footnote to Figure 6 for more detailed information.

Test 5—Propagation at a site with a low density snow cover over frozen ground

This experiment was conducted at the Camp Ripley, Minnesota, in 2002 as part of the SYDET development project. The primary objective of the test was to determine the performance of the SYDET hardware in this winter environment. A very low density and low strength snow cover was present at the site during the tests, and the geophones were drilled into the frozen soil because the snow cover was not strong enough to support them. Figure 17 shows the test site. The snow cover ranged from 10 to 15 cm in thickness and had an extremely low density of 60–90 kg m^{-3} (compared to a density of 1000 kg m^{-3} for water). For this test various charge sizes of C4, ranging from 0.5 to 8 blocks (0.28 to 4.5 kg) were detonated on the surface and at 1.5 m above ground level and the resulting signatures were measured using a digital seismograph for propagation distances of 30 to 100 m. Additional details of the measurements are presented in Decato et al. (2003).

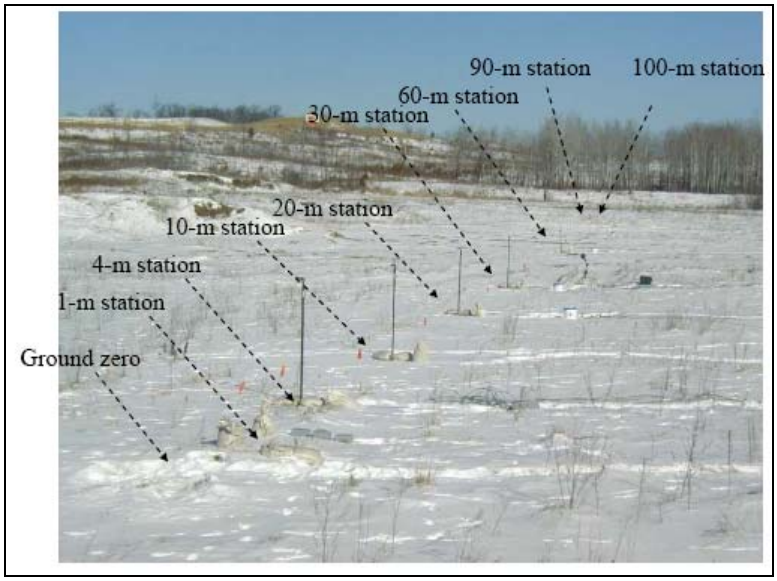

a. Sensor array before any C4 charges were detonated. Pressure sensors were mounted at the snow surface level and at 1.5 m height on the pipe stands.

b. Test 5 experiment after some shots were detonated. The large dark patch with a person standing within is the location where the C4 charges were detonated. The sensor array extends in a straight line away from the camera, starting near that point. The ground was very rough in this location, and the snow cover was not continuous or uniform.

Figure 17. Photographs of Test 5 experiment, with a low density snow cover (10–15 cm) over frozen ground present (Camp Ripley, MN, 2002).

Figure 18 shows a measurement made by sensors located 100 m from a detonation of a single block of C4 (0.57 kg). The figure shows that the primary acoustic

and seismic arrivals are associated with the air wave, Path A in Figure 1 and the main seismic wave starts after the acoustic arrival. The pressure waves are longer in duration than those measured in the other tests (approximately 30 ms compared to 20 ms or less). The vertical seismic arrival closely follows the acoustic waveform, with a longer following wavetrain, while the radial seismic signal has a constant higher frequency imposed on the lower frequency acoustic waveform. Smaller seismic arrivals corresponding to Path B were also detected. Again, the early seismic arrivals are small enough that eq 5 can be used instead of eq 4.

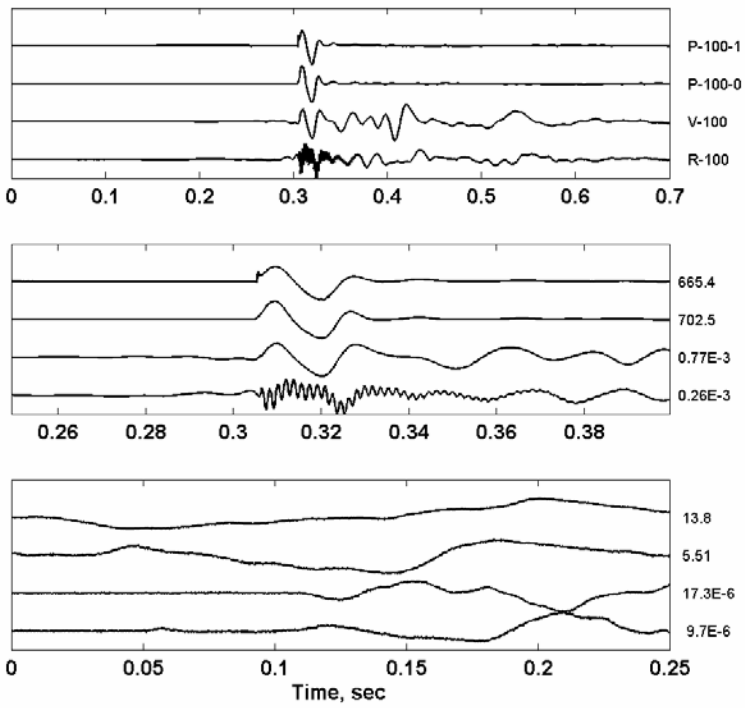

Figure 18. Waveforms measured during Test 5, for a single block of C4 (0.57 kg) detonated at 1.5 m above a low density snow cover over frozen ground. The sensors were located 100 m from the source. The main acoustic wave arrives at about 0.305 s with a peak positive pressure of 700 Pa. The ground vibration starts coincident with the acoustic arrival, and low amplitude seismic waves are visible at about 0.110 s. The radial geophone signal is a high frequency resonance modulated by a low frequency wave similar to the vertical component geophone.

Figure 19 shows the analysis results for this test, with numerical parameters listed in Tables 3–4. A few of the scaled peak pressure measurements exceed the peak pressures predicted by the ANSI Standard, and the peak pressure attenuation rate vs. distance was determined to be –1.3, the same as the attenuation rate measured for Test 1 over concrete. The acoustically induced seismic arrivals are all well below the damage criteria even at 30 m $kg^{-1/3}$ distance, although they have a relatively low attenuation coefficient of –1.1. The Path B seismic arrivals are again two orders of magnitude lower in amplitude than those from Path A. The ratio of

induced seismic vibration to incident acoustic pressure is 1.0, the lowest value measured for any of these C4 tests. Line fits to the measurements predict that very high peak pressure levels of 12.3 and 25.6 kPa (175.8 and 182.1 dB), respectively, would be needed to induce vibrational damage levels of 12 and 25 mm/s. This behavior is probably the result of the very hard frozen ground present at this site. (The geophones were measuring the frozen ground motion, not the snow cover motion.)

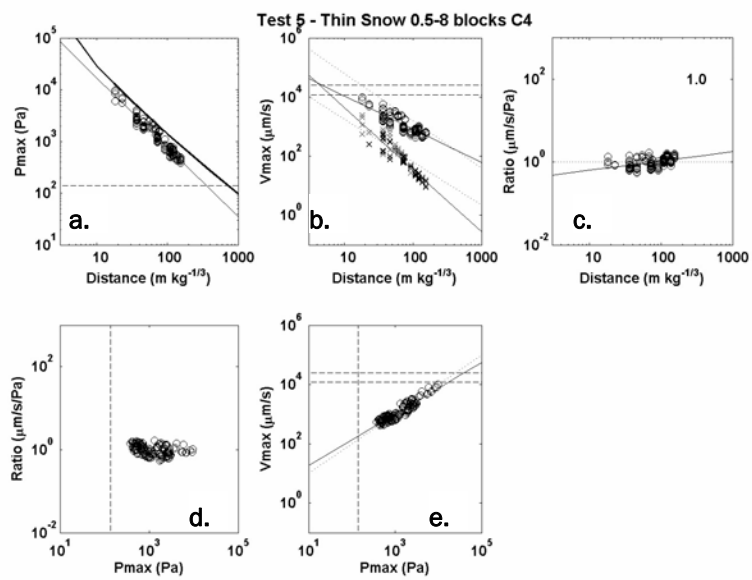

Figure 19. Measurement results from Test 5, propagation over a low density snow cover 10 to 15 cm thick over frozen ground. Dashed lines in the Figure are acoustic or vibrational damage criteria of 159 Pa, 25 mm/s, or 12 mm/s. The slopes of the least squares line fits to the measured data in the panels appear in Table 3, and the pressure levels needed to exceed the vibration damage criteria are listed in Table 4. See footnote to Figure 6 for more detailed information.

Test 6—Propagation over a high density snow cover

This experiment was conducted at Ft. Drum, New York, in 2004 as part of the SYDET development project. The primary objective of the test was to determine the performance of the SYDET hardware in this winter environment. A snow cover with an average density of 110 kg m^{-3} and depth ranging from 8 to 25 cm was present at the site (Fig. 20). There was a thick wind crust with a density of 225 kg m^{-3} present throughout the site, and this sintered, high-strength snow layer allowed the geophones to be installed at the snow surface, not at the ground surface as for the previous test. For this test various charge sizes of C4, ranging from 0.5 to 8 blocks (0.28 to 4.5 kg) were detonated on the surface and at 1.5 m above ground level, and the resulting signatures were measured using a digital seismograph for propagation distances of 60 and 150 m only. At these locations the snow

depth was 9 and 16 cm, respectively. A report documenting these measurements in more detail is in preparation.

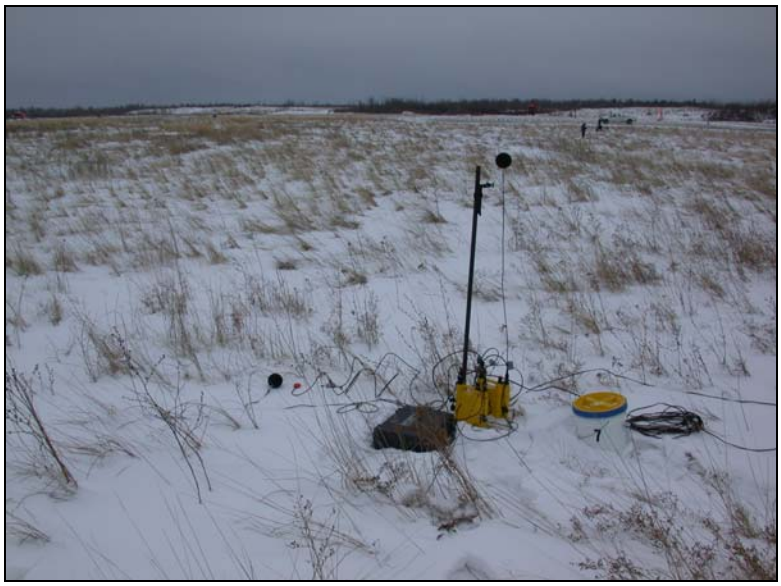

Figure 20. Photo of Test 6 experiment, measurements for propagation with a sintered snow cover present (Fort Drum, NY, 2004). Two high pressure microphones are visible with their black round foam wind screens. Two orange geophones were also installed at this location at the surface of the snow cover itself. The yellow boxes are waterproof digitizers, and the black case and white bucket are used to protect the power supplies from the weather. Although there are many bushes poking through the snow, the snow cover at this site was continuous and relatively deep (ranging from 8 to 25 cm) compared to the Test 5.

Figure 21a shows a measurement made by sensors located 60 m from a detonation of a single block of C4 (0.57 kg), while Figure 21b shows the same shot measured 150 m from the source. Again, the primary acoustic and seismic arrivals are associated with the air wave, Path A in Figure 1, and the main seismic wave starts after the acoustic arrival. Smaller seismic arrivals corresponding to Path B were also detected in both cases but the early seismic arrivals are small enough that eq 5 can be used instead of eq 4. The seismic waves are display relatively long duration oscillations occurring after the acoustic wave arrival and the acoustic arrivals have a long duration of 30 ms at 60 m, 40 ms at 150 m. In this case the peak vibrational levels (of the snow cover) are much higher than the levels measured for any of the previous tests.

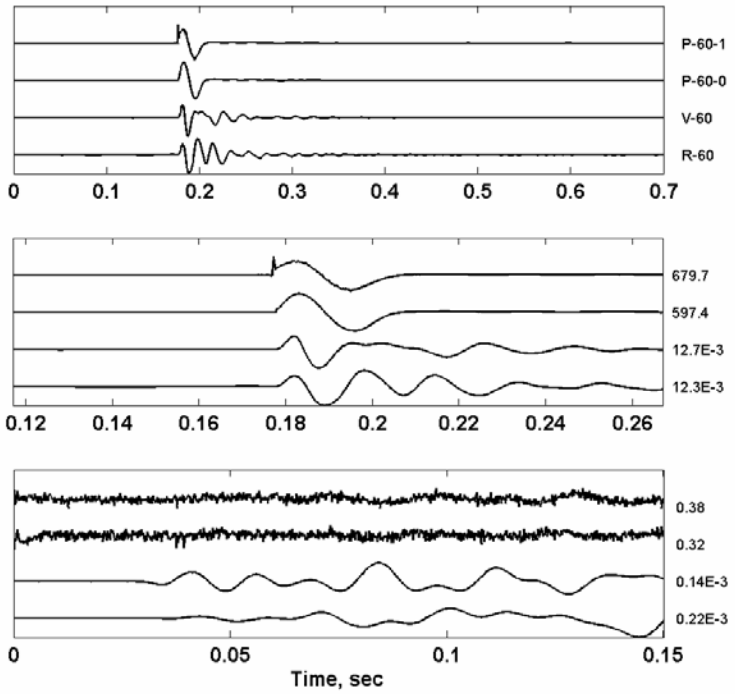

a. Sensors located 60 m from the source. The main acoustic wave arrives at about 0.18 s with a peak positive pressure of 600 Pa. The ground vibration starts coincident with the acoustic arrival, and low amplitude seismic waves are visible at about 0.04 s.

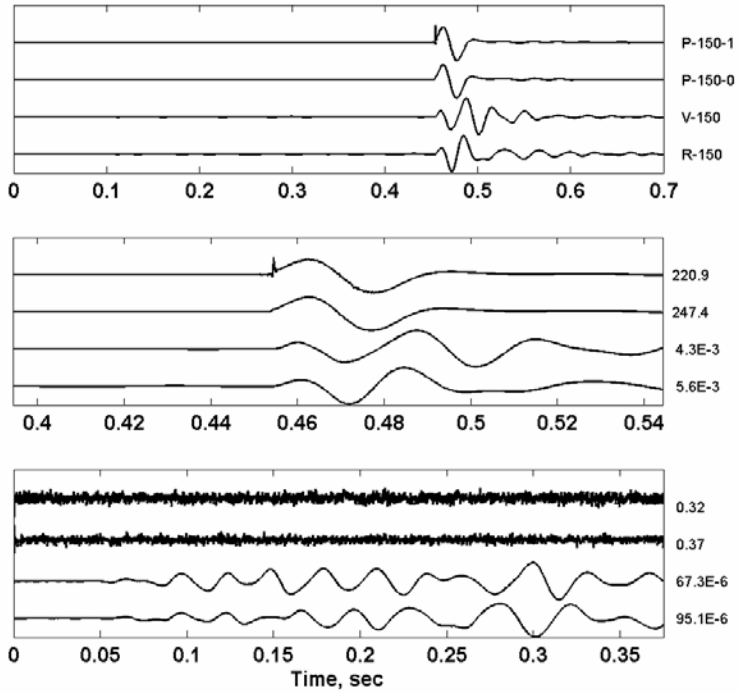

b. Sensors located 150 m from the source. The main acoustic wave arrives at about 0.455 s with a peak positive pressure of 250 Pa. The ground vibration starts coincident with the acoustic arrival, and low amplitude seismic waves are visible at about 0.05 s.

Figure 21. Waveforms measured during Test 6, for a single block of C4 (0.57 kg) detonated at a height of 1.5 m over a snow cover.

Figure 22 shows the analysis results for this test, with numerical parameters listed in Tables 3–4. The scaled peak pressure measurements are all lower than the peak pressures predicted by the ANSI Standard, and the peak pressure attenuation rate vs. distance was determined to be –1.5, a relatively high attenuation rate compared to the other tests.

The Path A seismic arrivals are very high compared to the other tests and indicate that the damage levels are exceeded for scaled distances less than 110 m $kg^{-1/3}$. The Path B seismic arrivals are again two orders of magnitude lower in amplitude than those from Path A.

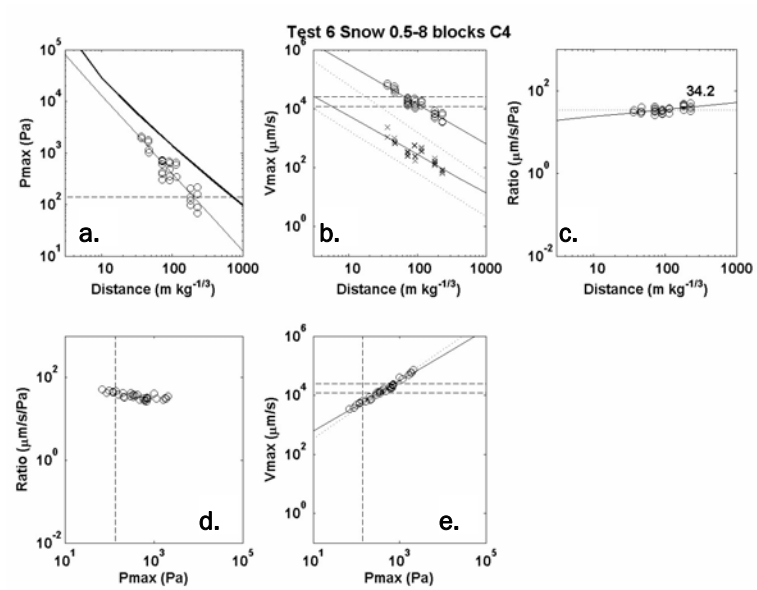

Figure 22. Measurement results from Test 6, a sintered snow cover 8 to 25 cm deep. Dashed lines in the Figure are acoustic or vibrational damage criteria of 159 Pa, 25 mm/s, or 12 mm/s. The slopes of the least squares line fits to the measured data in the panels appear in Table 3, and the pressure levels needed to exceed the vibration damage criteria are listed in Table 4. See footnote to Figure 6 for more detailed information.

The seismic attenuation rate is measured at a value of –1.3. The ratio of induced seismic vibration to incident acoustic pressure is 34, the highest value measured for any of these C4 tests. Line fits to the measurements predict that low peak pressure levels of 330 and 760 Pa (144.3 and 151.6 dB) would be needed to induce vibrational damage levels of 12 and 25 mm/s. In this case the relatively low strength of the snow cover compared to most soils has a significant effect and greatly increases the induced ground motion. However, the vibration experienced by a building is not expected to reach these high levels, because the foundation would rest on more competent soil rather than on the snow cover. For this reason,

the results of this experiment will not be included when the damage criteria are derived below.

It should be emphasized that the different results for the snow cover situations in Tests 5 and 6 are primarily attributable to differences in the way the vibration measurements were conducted. Because the snow cover could not support the geophones for Test 5, they were installed in the frozen soil with properties similar to concrete. For Test 6, however, the geophones were installed at the snow surface, so in this test much larger induced vibrations were recorded.

Test 7—Propagation through a conifer forest

This experiment was conducted at the Lone Star Army Ammunition Plant, Texas, in 2002 as part of an Army land management project to determine the effect of a forest on acoustic pulse propagation. Five sensor stations were installed in the forest starting 30 m from the forest edge and spaced 30 m apart. There was a thick layer of pine needles on the ground at the sensor locations. Figure 23 shows the conditions at the test site. Two charge sizes of C4, one and four blocks (0.57 and 2.3 kg), were detonated at various heights ranging from 0.3 to 3.8 m above ground level and the resulting signatures were measured using a digital seismograph for propagation distances of 30 to 565 m. Four different source locations were used. For two of the source locations, the propagation path was entirely in the forest (with propagation distances of 30–281 m), while for the other two source locations, some of the path was outside of the forest. In the latter case, the propagation distance over open ground was either 61 or 415 m, depending on the source location, followed by 30–150 m of propagation through the forest to reach the various sensor locations. For the analysis presented here all, of the source locations and source heights have been combined. Additional details of the measurements are presented in Decato et al. (2005).

Figure 24 shows a measurement made by sensors located 505 m from a detonation of a four blocks of C4 (2.3 kg) 1.9 m above the ground level. The primary acoustic and seismic arrivals are associated with the air wave, Path A in Figure 1, and the main seismic wave starts after the acoustic arrival. There are some very small seismic waves arriving just before the acoustic wave, and even smaller seismic arrivals corresponding to Path B were also detected. The early seismic arrivals are small enough that eq 5 can be used instead of eq 4.

a. Sensor locations giving a general view of the tree and vegetation density within the forest.

b. Close view of typical ground conditions within the forest, showing a horizontal and a vertical component geophone installed in the ground. The tick marks on the scale are in cm, the large divisions and numbers indicate 10-cm intervals.

Figure 23. Photo of Test 7 experiment, propagation through a conifer forest (Lone Star Army Ammunition Plant, Texas, 2002).

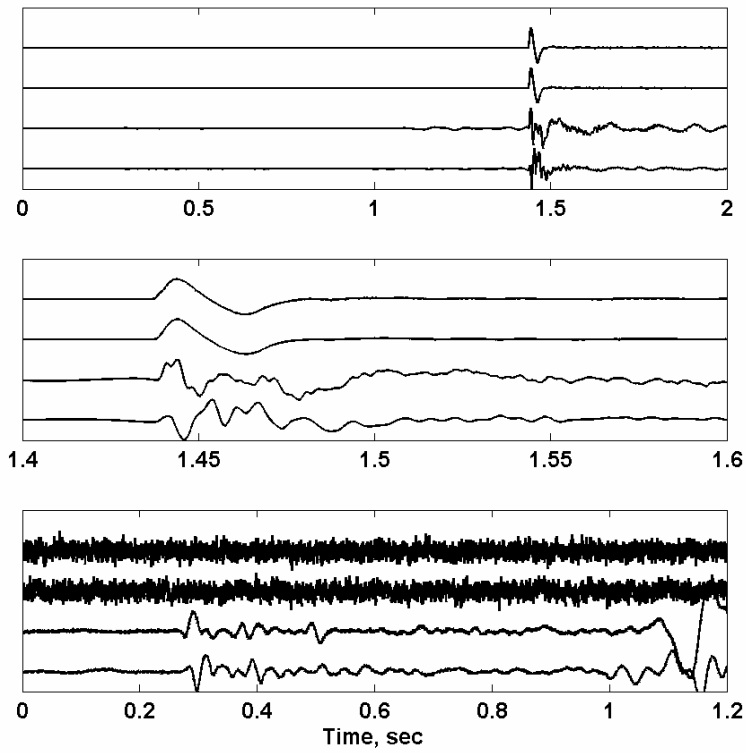

Figure 24. Waveforms measured during Test 7, produced by a 2.3-kg charge of C4 detonated 1.9 m above the ground level, after propagation through a conifer forest. The sensors were located 505 m from the source. The main acoustic wave arrives at about 1.44 s with a peak positive pressure of 148 Pa. The ground vibration starts coincident with the acoustic arrival, and low amplitude seismic waves are visible at about 0.28 s.

Figure 25 shows the analysis results for this test, with numerical parameters listed in Tables 3–4. The scaled peak pressure measurements are all lower than the peak pressures predicted by the ANSI Standard, and the peak pressure attenuation rate vs. distance was determined to be –1.3. The Path B seismic arrivals are again two orders of magnitude lower in amplitude than those from Path A. The seismic attenuation rate is measured at a value of –1.4 and the ratio of induced seismic vibration to incident acoustic pressure is 5.2, both "typical" values compared to the other measurements. Except for a single measurement at 30 m $kg^{-1/3}$, the other measurements at 90 m $kg^{-1/3}$ and greater propagation distance are all well below the damage criteria for vibration. Line fits to the measurements predict that peak pressure levels of 1.8 and 3.7 kPa (159.1 and 165.3 dB) would be needed to induce vibrational damage levels of 12 and 25 mm/s.

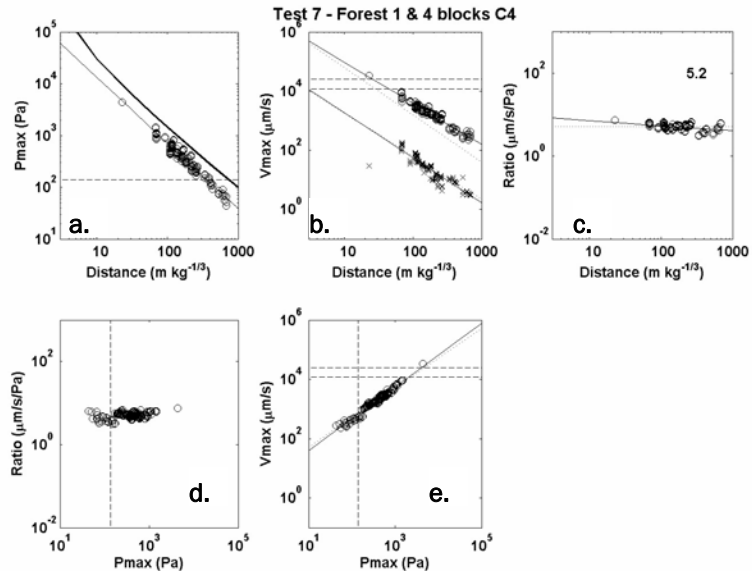

Figure 25. Measurement results for Test 7, propagation through a conifer forest. Dashed lines in the Figure are acoustic or vibrational damage criteria of 159 Pa, 25 mm/s, or 12 mm/s. The slopes of the least squares line fits to the measured data in the panels appear in Table 3, and the pressure levels needed to exceed the vibration damage criteria are listed in Table 4. See footnote to Figure 6 for more detailed information.

Combination of Tests 1–5 and 7—Propagation in various environments

Figure 26 shows the analysis results for all of the measurements, except for Test 6, the test over a relatively thick sintered snow cover that had very high vibrational levels. The snow test was excluded because building foundations do not rest on a snow cover. The figure shows that most of the 815 data points in the measurement set have peak pressure levels above the Army airblast criterion of 138 dB for cosmetic damage, and that the ANSI standard prediction of peak pressure is equaled or exceeded by a small percentage of the measurements. These measurements are from Tests 1, 5, and 2, which were conducted over very hard ground surfaces (concrete and frozen ground) or over a hard soil (with a loose gravel pad). The acoustic peak pressure for all of the measurements has an attenuation coefficient of –1.40, and the seismic of about –1.1. The vibrational damage criteria are exceeded only for propagation distances of 100 m $kg^{-1/3}$ or less. The overall average ratio of induced seismic vibration to incident acoustic pressure is found to be 4.9. Line fits to the measurements predict that peak pressure levels of 2.0 and 3.5 kPa (159.1 and 164.9 dB), well above the acoustic airblast damage criterion of 138 dB, would be needed to induce vibrational damage levels of 12 and 25 mm/s. These results agree with those of Sabatier and Respet (1988). In all cases the seismic path (Path B in Figure 1) had substantially lower vibration levels, and can be ignored in damage predictions. The highest levels for

this early seismic arrival were for Test 1, the measurement over concrete, and these levels are from a wave that arrives just before the acoustic arrival.

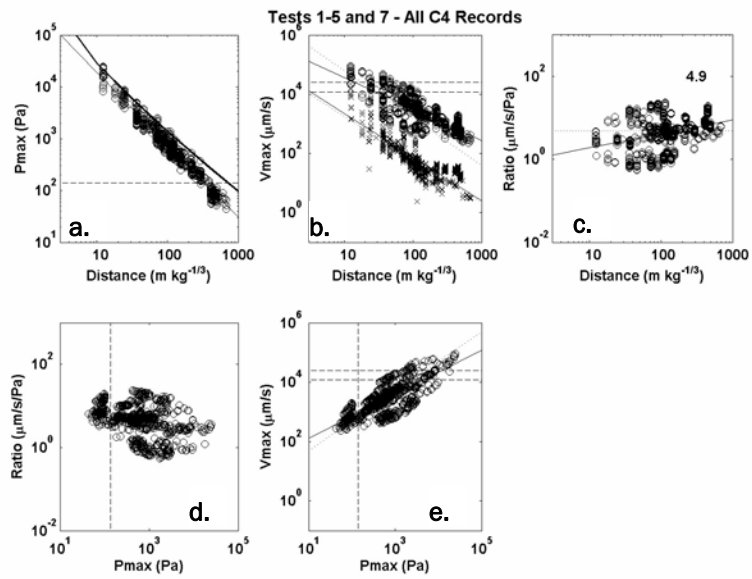

Figure 26. Combined measurement results from Tests 1–5 and Test 7, propagation in a variety of environments, including concrete, frozen and unfrozen soil, forest, and tropical vegetation. Dashed lines in the Figure are acoustic or vibrational damage criteria of 159 Pa, 25 mm/s, or 12 mm/s. The slopes of the least squares line fits to the measured data in the panels appear in Table 3, and the pressure levels needed to exceed the vibration damage criteria are listed in Table 4. See footnote to Figure 6 for more detailed information.

Prediction method

A conservative method to predict when ground vibration from military explosions in the air or on the ground might cause cosmetic building damage can be derived from the measurement data presented above. The data have shown that vibration levels from Path B in Figure 1 are always much smaller that those associated with the arrival of the air wave (Path A), so these Path B waves are neglected in the prediction method. Data analysis also showed that the median value of the acoustic-to-seismic coupling coefficient *C1* in eq 8 was 4.9 (μm/s)/Pa. Excluding the snow cover test (Test 6), the highest measured value was 23.6 (μm/s)/Pa for a "springy" sensor location in tropical vegetation. In other locations the highest measured value was 19.7 (μm/s)/Pa. To be conservative and over-predict the possible ground vibration, a coupling coefficient $C_{\max}$ is specified as 25 (μm/s)/Pa, higher than any value measured in any ground experiment, and eq 8 is modified to read

$$\dot{u}_{\text{peak}} = C_{\max} P(R) \tag{9}$$

This equation can be applied in two different ways. If an acoustic measurement of some military activity at the desired distance has been made or is available from past measurements, the peak positive pressure can be used as $P(R)$ in eq 9. Or, if a standard demolition event is planned (detonation of a known type and size explosive charge a known distance away), the ANSI Standard can be used to determine $P(R)$. In either case, eq 9 states that simply by multiplying the peak pressure (in kPa) by 25 determines the predicted peak particle velocity in mm/s. If the value is less than the damage criterion of 12 or 25 mm/s, the activity should not cause any vibrational cosmetic damage.

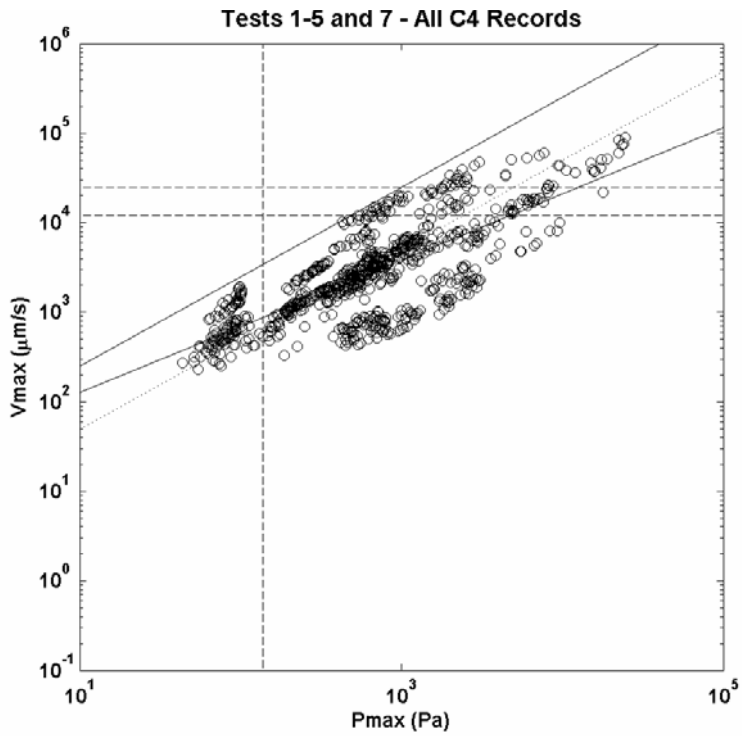

Figure 27. P_{max} vs. V_{max} for Tests 1–5 and Test 7, propagation in a variety of environments. The dashed vertical and horizontal lines are the damage criteria of 138 dB, 12 mm/s, and 25 mm/s. The solid line running through the data is a least squares fit to the measured data. The lightest dotted line through the data is a prediction given by eq 8 using the median coupling ratio of 4.9 (μm/s)/Pa, and the solid line above the data points parallel to this line is the prediction given by eq 9.

Figure 27 shows this equation plotted vs. the measured data from all of the tests. The figure shows that the equation over-predicts the measured ground vibration as desired. Equation 9 predicts that the vibrational damage criteria of 12 and 25 mm/s will be exceeded when the peak positive pressure exceeds 480 Pa (147.6 dB) or 1 kPa (154.0 dB), respectively. Either of these levels is much higher than the Army overpressure damage criterion of 159 Pa (138 dB). Thus, in most situa-

tions, damage from blast overpressure will occur long before damaging levels of ground vibration are reached.

Detailed modeling of ground vibrations produced by explosions

This task was accomplished by P. Boulanger and K. Attenborough of the University of Hull, United Kingdom, and is fully documented in their final reports (Boulanger and Attenborough 2005a, b). An existing frequency domain computer program (Tooms et al. 1993) was modified and extended to incorporate predictions of impulsive sound sources above porous and elastic grounds. These modifications were tested on measured acoustic and seismic spectra and waveforms for short (60 m) and long (3 km) ranges and found to agree tolerably well.

Two examples of the modeling work for a blank pistol shot source are included here to illustrate these results. Figures 28 and 29 show the measured acoustic and seismic waveforms and spectra for one particular snow cover (experiment no. 8 of Albert 2001), and Figures 30 and 31 show the results for a second snow cover with different parameters (experiment no. 4 of Albert 2001). Both modeling examples show relatively good agreement with the measured acoustic pulses and very good agreement with the seismic waveforms. The seismic results are especially noteworthy as they explain a phenomenon frequently seen for shallow snow covers: a high frequency ground vibration modulated by a lower frequency (Fig. 31). See Figure 18 for an example of this type of response for a low density snow cover in the blast wave measurements. The interpretation of this result is that it is caused by resonances within the thin snow cover, visible as the relatively high level between 200 and 500 Hz in Figure 32a compared to the lower level in that bandwidth for Figure 29a. These effects had not been satisfactorily modeled prior to this work.

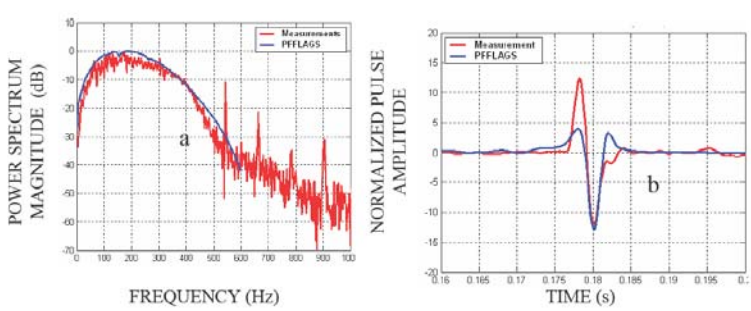

Figure 28. Acoustical power spectral magnitude (a) and (b) pulse shapes predicted and measured in experiment 8 of Albert (2001). (Reproduced from Figure 4 from Boulanger and Attenborough 2005b, with permission.)

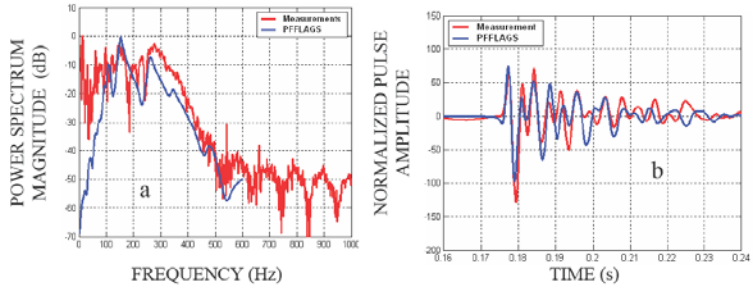

Figure 29. Seismic power spectral magnitude (a) and (b) pulse shapes predicted and measured in experiment 8 of Albert (2001). (Reproduced from Figure 5 from Boulanger and Attenborough 2005b, with permission).

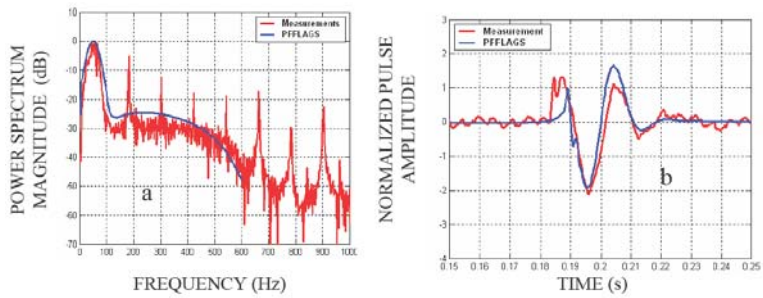

Figure 30. Acoustical power spectral magnitude (a) and pulse (b) shapes predicted and measured in experiment 4 of Albert (2001). (Reproduced from Figure 6 from Boulanger and Attenborough 2005b, with permission.)

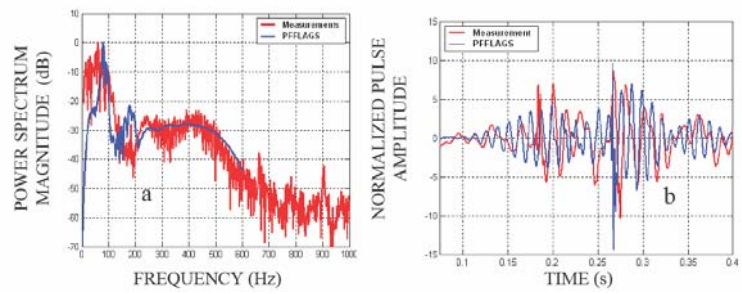

Figure 31. Seismic power spectral magnitude (a) and (b) pulse shapes predicted and measured in experiment 4 of Albert (2001). (Reproduced from Figure 7 from Boulanger and Attenborough 2005b, with permission.)

Comparisons with various measurements (Boulanger and Attenborough 2005a, b) show that the computational model seems to capture the physics of the induced ground motion correctly. The main problem in applying this model generally is that many ground parameters are needed as input to the model, and some are not easily measured. Further work on the sensitivity of the model to the ground parameters would be useful.

5 Conclusions

DOD installations are increasingly dealing with complaints and damage claims alleging that military activities are producing bothersome ground vibrations. While some civilian regulations exist addressing ground vibration, DOD has not formally adopted any methods to regulate vibration or assess these complaints. In this report, existing measurement data were analyzed to determine the noise and vibration produced by explosive detonations. The objective of this analysis was to produce a simple, accurate procedure for estimating the peak ground vibration produced by Army training and demilitarization activities.

Analysis of the measured data showed that cube-root charge weight scaling is appropriate for predicting peak positive acoustic amplitudes, and the ANSI Standard S2.20 (1983) provides good predictions of peak pressures for small C4 explosions in different terrains. Measured acoustic pressure decay rates range from $r^{-1.2}$ to $r^{-1.5}$, compared to the ANSI Standard prediction of $r^{-1.2}$. The measured peak positive airblast pressures may exceed ANSI Standard prediction if the ground is very hard, or under highly favorable atmospheric conditions.

Two mechanisms and propagation paths for ground vibration were detected in all experiments as postulated. The seismic wave always arrived first, followed by the atmospheric coupled wave. However, the ground vibration induced by the arrival of the atmospheric wave is always greater than vibration from seismic waves induced near the explosion source. The acoustic-to-seismic coupling ratio *C1* for the atmospheric wave is a constant with respect to distance and peak pressure at a given location, but varies from site to site. For airborne explosions the value is usually between 1 and 13 (μm/s)/Pa (see Table 3).

A conservative empirical equation to predict ground vibration from explosions is given by eq 9. Equation 9 predicts that the vibrational damage criteria of 12 and 25 mm/s will be exceeded when the peak positive pressure exceeds 480 Pa (147.6 dB) or 1 kPa (154.0 dB), respectively. Either of these levels is much higher than the Army overpressure damage criterion of 159 Pa (138 dB). Thus, in most situations damage from blast overpressure will occur long before damaging levels of ground vibration are reached.

The following paragraphs provide an explanation of how the project goals were met by documenting the progress and accomplishments in relation to specific tasks and milestones.

Task 1—Construct an accurate but simple model of induced ground motion from military activities

This objective has been met. A simple model, based on existing measurement data, was developed to predict peak ground vibration from military noise sources for a variety of soil and ground conditions. Analysis of the measured data showed that only the air-coupled vibration (Path A in Fig. 1) is significant, so eq 9 is a sufficiently accurate model to use for Army predictions and evaluations. By using a very conservative value of 25 (μm/s)/Pa for the coupling coefficient C_{max} in the equation, an overestimate of the ground vibration for all of the environments was obtained as shown in Figure 27. The predicted peak ground motion can be determined either from an ANSI Standard prediction of peak pressure (if charge type, size, and distance are known) or from a measurement or other estimate of the expected peak pressure. The equation predicts that the vibrational damage criteria of 12 and 25 mm/s will be exceeded when the peak positive pressure exceeds 480 Pa (147.6 dB) or 1 kPa (154.0 dB), respectively. Either of these levels is much higher than the Army overpressure damage criterion of 159 Pa (138 dB). Thus, in most situations, damage from blast overpressure will occur long before damaging levels of ground vibration are reached.

Task 2—Determine the acoustic-to-seismic coupling coefficients *C1* and *C2*

This objective has been met. Analysis of the measured data showed that the coefficient *C2* was typically more than two orders of magnitude less than the coefficient *C1*, so it was dropped from the predictive equation. The experimentally determined values of *C1* for various ground conditions are summarized in Table 4. For all of the experimental measurements combined, a value of 4.9 (μm/s)/Pa was determined. A maximum single measurement value of 23.6 was obtained for a location in a tropically vegetated area. Values for a sintered snow cover were found to be high, indicating that induced motion of the snow will be higher than for other ground types. However, building foundations always rest upon competent soils, so this case is not a realistic one to use for building damage predictions.

Task 3—Computational modeling of acoustically induced ground motion

This objective has been met. An existing propagation model (Tooms et al. 1993) was successfully modified to include acoustic pulse sources and validated by comparison with measured waveforms under a wide range of conditions. The model also successfully predicted observations of high frequency modulation that sometimes arise when a snow cover is present.

References

Albert, D. G. 2002. Observations of acoustic to seismic coupling under winter conditions, *J. Acoust. Soc. Amer*. **111**.

Albert, D. G. 2001. Acoustic waveform inversion with application to seasonal snow covers *J. Acoust. Soc. Am.* **22**: 539–546.

Ambrayseys, N. R., and A. J. Hendron. 1968. Dynamic behavior of rock masses. In *Rock Mechanics and Engineering Practice* (K.G. Stagg and O.C. Zienkiewicz, eds.). London: John Wiley & Sons, Inc., pp. 203–227.

American National Standard Institute. 1983. *Estimating airblast characteristics for single point explosions in air, with a guide to evaluating atmospheric and propagation effects*. ANSI Standard S2.20.

Baker, W. E. 1973. *Explosions in air*. Austin: University of Texas Press.

Boulanger, P., and K. Attenborough., 2005a. *Prediction of ground vibration from explosions*. Final Report for Contract Number N62588-05-P-0247. Hull, UK: University of Hull.

Boulanger, P., and K. Attenborough. 2005b. *Supplement to final report: Prediction of ground vibration from explosions*. Hull, UK: University of Hull.

Carbee, D. L., D. G. Albert, S. N. Decato, and J. A. Nagle. 2001. *Barrier wall signal data II, SYDET Wall Experiment II*. U.S. Army Engineer Research and Development Center, Cold Regions Research and Engineering Laboratory, CRREL Contract Report.

Decato, S. N., D. L. Carbee , D. G. Albert, and J. A. Nagle. 2003. *XM153 Sympathetic Detonator (SYDET) acoustic signature measurements winter engineering test*. U.S. Army Engineer Research and Development Center, Cold Regions Research and Engineering Laboratory, CRREL Contract Report.

Decato, S. N., D. G. Albert, F. E. Perron, Jr., and D. L. Carbee. 2005. *Short-range seismic and acoustic signature measurements through forest*. U.S. Army Engineer Research and Development Center, Cold Regions Research and Engineering Laboratory, ERDC/CRREL TR-05-10.

Decato, S. N., D. G. Albert, F. E. Perron, Jr., and D. L. Carbee. In review. *Acoustic signature measurements from the XM153 Sympathetic Detonator (SYDET) tropical engineering test*. U.S. Army Engineer Research and Development Center, Cold Regions Research and Engineering Laboratory, ERDC/CRREL TR-06-xx.

Dowding, C. H. 1996. *Construction vibrations*. Upper Saddle River, NJ: Prentice-Hall.

Johnson et al. 1988. Underground storage in unlined rock tunnels: Rock mechanics considerations in estimating damage levels. *DOD Explosives Safety Board, Minutes of the Twenty-Third Explosives Safety Seminar*, vol. 2, pp. 1815.

Kinney, G. F., and K. J. Graham. 1985. *Explosive shocks in air*. New York: Springer-Verlag..

Perron, F. E., Jr., S. N. Decato, D. G. Albert, and D. L. Carbee. In review, 2006a. *Blast absorber feasibility test—short range measurements*. U.S. Army Engineer Research and Development Center, Cold Regions Research and Engineering Laboratory, ERDC/CRREL TR-06-xx.

Perron, F. E., Jr., S. N. Decato, D. G. Albert, and D. L. Carbee. In review, 2006b. Seismic and acoustic signature measurements from the XM153 Sympathetic Detonator (SYDET) large explosive charge engineering test. U.S. Army Engineer Research and Development Center, Cold Regions Research and Engineering Laboratory, ERDC/CRREL TR-06-xx.

Reed, J. 1977. *Atmospheric attenuation of explosive waves*, J. *Acoust. Soc. Am*. **61**: 39–47.

Sabatier, J. M., and R. Raspet. 1988. Investigation of possibility of damage from acoustically coupled seismic waveform from blast and artillery. *J. Acoust. Soc. Amer*., 84: 1478–1482.

Siskind, D. E., M. S. Stagg, J. W. Kopp, and C. H. Dowding. 1980. *Structure response and damage produced by ground vibration from surface blasting*. Bureau of Mines Report of Investigation RI-8507.

Tooms, S., S. Taherzadeh, and K. Attenborough. 1993. Sound propagation in a refracting fluid above a layered porous and elastic medium. *J. Acoust. Soc. Amer.,* 93: 173–181.

Wright, W. P. 1994. *Army blast claims evaluation procedures*. Army Research Laboratory Report ARL-MR-131, AD-A277-909.

Umnova, O., K.. Attenborough, and A. Cummings. 2001. Nonlinear behavior of poroelastic absorbing materials. *J. Acoust. Soc. Am*., **109** (5): Abstract 4pAA6.

Appendix A: Supporting Data

```
%Pressures in Pa, Seis units micro-m/s, Ratios micro-m/s / Pa
% C:\DDrive\FY05Coupling\PlotCoupling02\AllAcousticToSeismicResults.m
% Lists the data used for all experiments
%Pressures in Pa, Seis units micro-m/s, Ratios micro-m/s / Pa

% MD 2002 Wall 2 over concrete Acoustic-to-seismic measurements
% MD01brk1A = source on wall, all horizontal geos are radial
% MD01brk1B = source off wall, horizontal geos have various orientations

%Test 1 - Concrete -----------------------------------------
% Rec Chan rx sz size   Dist  Vratio  Hratio  Pmax   Vmax   Hmax   Vratio  Hratio  Pmax   Vmax   Hmax
MD01brk1A = [...
  10  27   0 1.5 0.57     20.2   2.22e+0  1.31e+0  7.02e+3  1.56e+4  9.19e+3   2.21e+0  1.00e+0  7.02e+3  1.56e+4  7.05e+3
  10  31   0 1.5 0.57     30.2   2.57e+0  1.11e+0  4.91e+3  1.26e+4  5.46e+3   5.55e-1  4.21e-1  4.91e+3  2.73e+3  2.07e+3
  10  35   0 1.5 0.57     60.2   3.26e+0  1.07e+0  2.14e+3  6.98e+3  2.30e+3   1.00e-1  1.41e-1  2.14e+3  2.15e+2  3.03e+2
  10  39   0 1.5 0.57     90.2   4.66e+0  1.35e+0  1.18e+3  5.52e+3  1.59e+3   4.39e-2  2.96e-1  1.18e+3  5.20e+1  3.50e+2
  10  11 -20 1.5 0.57     20.1   2.05e+0  9.22e-1  7.59e+3  1.56e+4  6.99e+3   2.10e-1  2.14e-1  7.59e+3  1.59e+3  1.62e+3
  10   7 -30 1.5 0.57     30.2   2.44e+0  1.32e+0  2.96e+3  7.24e+3  3.90e+3   1.72e-2  1.57e-1  2.96e+3  5.11e+1  4.64e+2
  11  24   0 1.5 0.57     10.2   3.11e+0  1.89e+0  2.46e+4  7.66e+4  4.66e+4   3.11e+0  1.27e+0  2.46e+4  7.66e+4  3.12e+4
  11  27   0 1.5 0.57     20.2   3.05e+0  1.09e+0  8.13e+3  2.48e+4  8.87e+3   2.10e+0  1.09e+0  8.13e+3  1.70e+4  8.87e+3
  11  31   0 1.5 0.57     30.2   2.57e+0  9.45e-1  4.92e+3  1.27e+4  4.65e+3   6.70e-1  4.00e-1  4.92e+3  3.30e+3  1.97e+3
  11  35   0 1.5 0.57     60.2   3.47e+0  1.02e+0  2.21e+3  7.70e+3  2.26e+3   1.69e-1  2.09e-1  2.21e+3  3.74e+2  4.63e+2
  11  39   0 1.5 0.57     90.2   4.45e+0  1.24e+0  1.25e+3  5.55e+3  1.54e+3   3.45e-2  2.38e-1  1.25e+3  4.30e+1  2.96e+2
  11  15 -10 1.5 0.57     10.2   2.50e+0  1.01e+0  2.23e+4  5.59e+4  2.25e+4   6.40e-1  2.11e-1  2.23e+4  1.43e+4  4.72e+3
  11  11 -20 1.5 0.57     20.1   2.81e+0  8.77e-1  8.02e+3  2.25e+4  7.04e+3   2.02e-1  2.38e-1  8.02e+3  1.62e+3  1.91e+3
  11   7 -30 1.5 0.57     30.2   2.10e+0  9.05e-1  3.22e+3  6.76e+3  2.91e+3   1.77e-2  1.42e-1  3.22e+3  5.70e+1  4.58e+2
  12  24   0 1.5 0.57     10.2   2.68e+0  1.65e+0  2.34e+4  6.27e+4  3.87e+4   2.68e+0  1.12e+0  2.34e+4  6.27e+4  2.62e+4
  12  27   0 1.5 0.57     20.2   2.72e+0  1.07e+0  8.76e+3  2.38e+4  9.41e+3   1.43e+0  1.06e+0  8.76e+3  1.25e+4  9.27e+3
  12  31   0 1.5 0.57     30.2   2.40e+0  1.02e+0  4.97e+3  1.19e+4  5.09e+3   5.87e-1  3.04e-1  4.97e+3  2.92e+3  1.51e+3
  12  35   0 1.5 0.57     60.2   2.79e+0  1.07e+0  2.50e+3  6.98e+3  2.67e+3   8.17e-2  1.09e-1  2.50e+3  2.04e+2  2.72e+2
  12  39   0 1.5 0.57     90.2   5.03e+0  1.40e+0  1.25e+3  6.27e+3  1.74e+3   3.31e-2  1.95e-1  1.25e+3  4.13e+1  2.43e+2
  12  15 -10 1.5 0.57     10.2   2.53e+0  1.02e+0  1.89e+4  4.79e+4  1.93e+4   4.54e-1  1.94e-1  1.89e+4  8.60e+3  3.66e+3
  12  11 -20 1.5 0.57     20.1   2.41e+0  9.48e-1  7.27e+3  1.76e+4  6.89e+3   1.63e-1  1.82e-1  7.27e+3  1.19e+3  1.32e+3
  12   7 -30 1.5 0.57     30.2   1.80e+0  9.21e-1  2.98e+3  5.35e+3  2.74e+3   1.99e-2  1.30e-1  2.98e+3  5.94e+1  3.88e+2
  13  24   0 1.5 0.57     10.2   2.70e+0  1.58e+0  2.41e+4  6.51e+4  3.79e+4   2.69e+0  7.44e-1  2.41e+4  6.47e+4  1.79e+4
  13  27   0 1.5 0.57     20.2   2.79e+0  1.14e+0  8.11e+3  2.26e+4  9.26e+3   1.70e+0  8.70e-1  8.11e+3  1.38e+4  7.06e+3
  13  31   0 1.5 0.57     30.2   2.50e+0  1.00e+0  4.83e+3  1.21e+4  4.85e+3   5.16e-1  3.04e-1  4.83e+3  2.49e+3  1.47e+3
  13  35   0 1.5 0.57     60.2   3.25e+0  1.09e+0  2.35e+3  7.66e+3  2.57e+3   7.79e-2  1.47e-1  2.35e+3  1.83e+2  3.46e+2
  13  39   0 1.5 0.57     90.2   4.38e+0  1.48e+0  1.38e+3  6.02e+3  2.04e+3   3.26e-2  1.71e-1  1.38e+3  4.48e+1  2.35e+2
  13  15 -10 1.5 0.57     10.2   2.69e+0  1.03e+0  1.76e+4  4.74e+4  1.81e+4   3.95e-1  2.50e-1  1.76e+4  6.96e+3  4.40e+3
  13  11 -20 1.5 0.57     20.1   2.50e+0  1.01e+0  6.80e+3  1.70e+4  6.84e+3   1.42e-1  2.13e-1  6.80e+3  9.63e+2  1.45e+3
  13   7 -30 1.5 0.57     30.2   1.90e+0  9.85e-1  2.95e+3  5.61e+3  2.91e+3   1.93e-2  1.37e-1  2.95e+3  5.70e+1  4.06e+2
  14  24   0 1.5 0.57     10.2   3.18e+0  2.01e+0  2.23e+4  7.10e+4  4.47e+4   3.18e+0  1.31e+0  2.23e+4  7.10e+4  2.92e+4
  14  27   0 1.5 0.57     20.2   2.87e+0  1.14e+0  8.29e+3  2.38e+4  9.42e+3   1.94e+0  1.13e+0  8.29e+3  1.61e+4  9.35e+3
  14  31   0 1.5 0.57     30.2   2.44e+0  9.83e-1  4.79e+3  1.17e+4  4.71e+3   5.56e-1  3.37e-1  4.79e+3  2.67e+3  1.62e+3
  14  35   0 1.5 0.57     60.2   3.64e+0  1.08e+0  1.80e+3  6.56e+3  1.94e+3   1.18e-1  2.36e-1  1.80e+3  2.13e+2  4.25e+2
  14  39   0 1.5 0.57     90.2   4.82e+0  1.29e+0  1.01e+3  4.88e+3  1.31e+3   4.65e-2  2.32e-1  1.01e+3  4.72e+1  2.35e+2
  14  15 -10 1.5 0.57     10.2   2.98e+0  8.78e-1  1.51e+4  4.50e+4  1.32e+4   6.74e-1  2.78e-1  1.51e+4  1.02e+4  4.20e+3
  14  11 -20 1.5 0.57     20.1   2.35e+0  9.53e-1  6.11e+3  1.44e+4  5.82e+3   2.57e-1  2.59e-1  6.11e+3  1.57e+3  1.58e+3
  14   7 -30 1.5 0.57     30.2   1.77e+0  1.10e+0  2.59e+3  4.60e+3  2.84e+3   2.59e-2  1.53e-1  2.59e+3  6.71e+1  3.97e+2
  15  24   0 0.0 0.57     10.2   2.09e+0  1.07e+0  1.57e+4  3.27e+4  1.67e+4   9.45e-1  4.43e-1  1.57e+4  1.48e+4  6.94e+3
  15  27   0 0.0 0.57     20.2   2.73e+0  1.17e+0  6.05e+3  1.65e+4  7.08e+3   8.54e-1  4.49e-1  6.05e+3  5.17e+3  2.72e+3
  15  31   0 0.0 0.57     30.2   2.08e+0  9.89e-1  3.97e+3  8.24e+3  3.92e+3   1.63e-1  2.15e-1  3.97e+3  6.46e+2  8.51e+2
  15  35   0 0.0 0.57     60.2   3.02e+0  9.54e-1  1.69e+3  5.10e+3  1.61e+3   5.33e-2  1.31e-1  1.69e+3  9.00e+1  2.21e+2
  15  39   0 0.0 0.57     90.2   4.76e+0  1.57e+0  1.10e+3  5.25e+3  1.73e+3   3.66e-2  1.90e-1  1.10e+3  4.04e+1  2.09e+2
  15  15 -10 0.0 0.57     10.3   2.81e+0  1.10e+0  1.20e+4  3.38e+4  1.33e+4   6.08e-1  2.21e-1  1.20e+4  7.32e+3  2.66e+3
  15  11 -20 0.0 0.57     20.1   2.73e+0  1.24e+0  5.38e+3  1.47e+4  6.66e+3   1.05e-1  2.05e-1  5.38e+3  5.67e+2  1.10e+3
  15   7 -30 0.0 0.57     30.2   1.90e+0  1.12e+0  2.51e+3  4.76e+3  2.81e+3   2.88e-2  1.70e-1  2.51e+3  7.21e+1  4.28e+2
  16  24   0 0.0 0.57     10.2   1.90e+0  1.90e+0  8.20e+3  1.56e+4  1.56e+4   1.90e+0  1.90e+0  8.20e+3  1.56e+4  1.56e+4
  16  27   0 0.0 0.57     20.2   2.71e+0  1.16e+0  4.60e+3  1.25e+4  5.32e+3   8.59e-1  1.16e+0  4.60e+3  3.95e+3  5.32e+3
  16  31   0 0.0 0.57     30.2   2.32e+0  6.92e-1  2.94e+3  6.83e+3  2.03e+3   3.24e-1  4.84e-1  2.94e+3  9.52e+2  1.42e+3
  16  35   0 0.0 0.57     60.2   3.62e+0  6.32e-1  1.48e+3  5.35e+3  9.34e+2   5.77e-2  1.26e-1  1.48e+3  8.53e+1  1.87e+2
  16  39   0 0.0 0.57     90.2   4.80e+0  1.31e+0  8.48e+2  4.07e+3  1.11e+3   3.23e-2  1.27e-1  8.48e+2  2.74e+1  1.07e+2
  16  15 -10 0.0 0.57     10.3   8.65e-1  8.65e-1  1.80e+4  1.56e+4  1.56e+4   6.77e-2  4.24e-2  1.80e+4  1.22e+3  7.63e+2
  16  11 -20 0.0 0.57     20.1   2.34e+0  1.00e+0  6.64e+3  1.56e+4  6.66e+3   6.38e-2  6.86e-2  6.64e+3  4.24e+2  4.56e+2
  16   7 -30 0.0 0.57     30.2   2.17e+0  1.17e+0  2.84e+3  6.18e+3  3.32e+3   8.24e-3  8.32e-2  2.84e+3  2.34e+1  2.37e+2
  17  24   0 0.0 0.57     10.2   2.63e+0  2.56e+0  1.06e+4  2.79e+4  2.72e+4   2.63e+0  2.56e+0  1.06e+4  2.79e+4  2.72e+4
  17  27   0 0.0 0.57     20.2   3.07e+0  1.22e+0  4.84e+3  1.49e+4  5.91e+3   8.94e-1  1.22e+0  4.84e+3  4.32e+3  5.91e+3
  17  31   0 0.0 0.57     30.2   2.31e+0  8.00e-1  3.01e+3  6.95e+3  2.41e+3   4.13e-1  6.75e-1  3.01e+3  1.24e+3  2.03e+3
  17  35   0 0.0 0.57     60.2   3.24e+0  7.42e-1  1.47e+3  4.77e+3  1.09e+3   8.90e-2  2.03e-1  1.47e+3  1.31e+2  2.99e+2
  17  39   0 0.0 0.57     90.2   4.18e+0  1.12e+0  8.11e+2  3.39e+3  9.08e+2   4.28e-2  2.28e-1  8.11e+2  3.47e+1  1.85e+2
  17  15 -10 0.0 0.57     10.3   2.07e+0  1.12e+0  1.73e+4  3.59e+4  1.94e+4   2.07e-1  5.13e-2  1.73e+4  3.58e+3  8.89e+2
  17  11 -20 0.0 0.57     20.1   2.60e+0  1.04e+0  6.63e+3  1.72e+4  6.91e+3   7.08e-2  9.64e-2  6.63e+3  4.70e+2  6.40e+2
  17   7 -30 0.0 0.57     30.2   2.00e+0  1.18e+0  3.01e+3  6.01e+3  3.53e+3   1.08e-2  1.05e-1  3.01e+3  3.24e+1  3.15e+2
  18  24   0 0.0 0.57     10.2   4.04e+0  2.11e+0  9.59e+3  3.88e+4  2.02e+4   4.04e+0  2.11e+0  9.59e+3  3.88e+4  2.02e+4
  18  27   0 0.0 0.57     20.2   3.40e+0  1.45e+0  3.86e+3  1.31e+4  5.61e+3   1.46e+0  1.45e+0  3.86e+3  5.64e+3  5.61e+3
  18  31   0 0.0 0.57     30.2   2.72e+0  1.07e+0  2.26e+3  6.16e+3  2.43e+3   5.91e-1  7.35e-1  2.26e+3  1.34e+3  1.66e+3
  18  35   0 0.0 0.57     60.2   4.16e+0  8.09e-1  1.13e+3  4.69e+3  9.12e+2   1.28e-1  2.94e-1  1.13e+3  1.44e+2  3.32e+2
  18  39   0 0.0 0.57     90.2   4.94e+0  9.59e-1  6.77e+2  3.35e+3  6.50e+2   5.13e-2  2.81e-1  6.77e+2  3.47e+1  1.90e+2
  18  15 -10 0.0 0.57     10.3   2.12e+0  1.05e+0  1.60e+4  3.39e+4  1.68e+4   6.62e-2  6.29e-2  1.60e+4  1.06e+3  1.01e+3
  18  11 -20 0.0 0.57     20.1   2.56e+0  1.04e+0  6.14e+3  1.57e+4  6.40e+3   8.57e-2  1.13e-1  6.14e+3  5.26e+2  6.93e+2
  18   7 -30 0.0 0.57     30.2   2.04e+0  1.03e+0  2.74e+3  5.61e+3  2.84e+3   1.22e-2  1.16e-1  2.74e+3  3.35e+1  3.17e+2
  19  24   0 0.0 0.57     10.2   4.21e+0  2.00e+0  9.44e+3  3.97e+4  1.89e+4   4.21e+0  2.00e+0  9.44e+3  3.97e+4  1.89e+4
  19  27   0 0.0 0.57     20.2   2.97e+0  1.09e+0  5.67e+3  1.68e+4  6.15e+3   6.54e-1  5.88e-1  5.67e+3  3.71e+3  3.33e+3
  19  31   0 0.0 0.57     30.2   2.27e+0  8.93e-1  3.31e+3  7.54e+3  2.96e+3   2.89e-1  3.99e-1  3.31e+3  9.57e+2  1.32e+3
  19  35   0 0.0 0.57     60.2   3.13e+0  8.34e-1  1.60e+3  5.01e+3  1.34e+3   7.90e-2  1.50e-1  1.60e+3  1.26e+2  2.41e+2
  19  39   0 0.0 0.57     90.2   4.76e+0  1.24e+0  7.76e+2  3.70e+3  9.64e+2   3.21e-2  1.77e-1  7.76e+2  2.49e+1  1.38e+2
```

```
  19  15 -10 0.0 0.57     10.3   2.27e+0  1.20e+0  1.54e+4  3.50e+4  1.85e+4   2.12e-1  6.54e-2  1.54e+4  3.26e+3  1.01e+3
  19  11 -20 0.0 0.57     20.1   2.62e+0  1.06e+0  6.24e+3  1.63e+4  6.64e+3   8.61e-2  9.71e-2  6.24e+3  5.37e+2  6.06e+2
  19   7 -30 0.0 0.57     30.2   1.95e+0  1.24e+0  2.75e+3  5.37e+3  3.40e+3   1.02e-2  1.18e-1  2.75e+3  2.79e+1  3.23e+2
];
%Test 1 - Concrete -------------------------------------------
% Rec Chan rx sz size     Dist   Vratio   Hratio   Pmax     Vmax     Hmax      Vratio   Hratio   Pmax     Vmax     Hmax
MD01brk1B = [...
  20  24   0 1.5 0.57      7.7   6.18e-1  6.18e-1  2.52e+4  1.56e+4  1.56e+4   2.31e-1  8.56e-2  2.52e+4  5.81e+3  2.15e+3
  20  27   0 1.5 0.57     16.4   1.92e+0  1.16e+0  8.11e+3  1.56e+4  9.38e+3   1.48e+0  3.72e-1  8.11e+3  1.20e+4  3.02e+3
  20  31   0 1.5 0.57     26.1   2.29e+0  9.10e-1  4.73e+3  1.08e+4  4.30e+3   4.72e-1  3.01e-1  4.73e+3  2.23e+3  1.42e+3
  20  35   0 1.5 0.57     55.9   3.30e+0  1.03e+0  1.84e+3  6.08e+3  1.89e+3   6.01e-2  1.97e-1  1.84e+3  1.11e+2  3.63e+2
  20  39   0 1.5 0.57     85.8   6.03e+0  1.33e+0  8.48e+2  5.12e+3  1.13e+3   5.58e-2  2.04e-1  8.48e+2  4.74e+1  1.73e+2
  20  15 -10 1.5 0.57     15.2   2.04e+0  1.37e+0  7.62e+3  1.56e+4  1.04e+4   1.42e-1  9.20e-2  7.62e+3  1.08e+3  7.01e+2
  20  11 -20 1.5 0.57     25.1   3.31e+0  1.41e+0  3.93e+3  1.30e+4  5.52e+3   4.78e-2  8.82e-2  3.93e+3  1.88e+2  3.47e+2
  20   7 -30 1.5 0.57     35.3   2.49e+0  1.31e+0  2.43e+3  6.06e+3  3.18e+3   1.63e-2  7.33e-2  2.43e+3  3.97e+1  1.78e+2
  21  24   0 1.5 0.57      7.7   3.60e+0  1.06e+0  1.79e+4  6.43e+4  1.90e+4   4.10e-1  2.06e-1  1.79e+4  7.31e+3  3.67e+3
  21  27   0 1.5 0.57     16.4   3.42e+0  9.58e-1  9.62e+3  3.29e+4  9.22e+3   7.90e-1  3.64e-1  9.62e+3  7.60e+3  3.51e+3
  21  31   0 1.5 0.57     26.1   2.62e+0  1.01e+0  4.55e+3  1.19e+4  4.62e+3   3.94e-1  3.10e-1  4.55e+3  1.79e+3  1.41e+3
  21  35   0 1.5 0.57     55.9   3.39e+0  9.13e-1  1.88e+3  6.38e+3  1.72e+3   7.21e-2  2.04e-1  1.88e+3  1.36e+2  3.84e+2
  21  39   0 1.5 0.57     85.8   6.35e+0  1.41e+0  8.76e+2  5.57e+3  1.24e+3   6.17e-2  2.50e-1  8.76e+2  5.40e+1  2.19e+2
  21  15 -10 1.5 0.57     15.2   2.56e+0  1.21e+0  7.53e+3  1.92e+4  9.13e+3   1.67e-1  1.34e-1  7.53e+3  1.26e+3  1.01e+3
  21  11 -20 1.5 0.57     25.1   3.13e+0  1.36e+0  3.76e+3  1.18e+4  5.13e+3   6.36e-2  1.15e-1  3.76e+3  2.39e+2  4.34e+2
  21   7 -30 1.5 0.57     35.3   2.30e+0  9.54e-1  2.42e+3  5.57e+3  2.31e+3   2.68e-2  7.32e-2  2.42e+3  6.47e+1  1.77e+2
  22  24   0 1.5 0.57      7.7   3.00e+0  8.98e-1  1.86e+4  5.57e+4  1.67e+4   2.20e+0  5.92e-1  1.86e+4  4.10e+4  1.10e+4
  22  27   0 1.5 0.57     16.4   3.15e+0  1.14e+0  9.20e+3  2.90e+4  1.04e+4   1.26e+0  3.59e-1  9.20e+3  1.16e+4  3.30e+3
  22  31   0 1.5 0.57     26.1   2.68e+0  8.97e-1  4.43e+3  1.19e+4  3.97e+3   5.83e-1  4.08e-1  4.43e+3  2.58e+3  1.81e+3
  22  35   0 1.5 0.57     55.9   3.48e+0  9.33e-1  1.96e+3  6.81e+3  1.83e+3   7.75e-2  2.36e-1  1.96e+3  1.52e+2  4.62e+2
  22  39   0 1.5 0.57     85.8   6.62e+0  1.51e+0  9.47e+2  6.27e+3  1.43e+3   6.33e-2  2.52e-1  9.47e+2  6.00e+1  2.39e+2
  22  15 -10 1.5 0.57     15.2   2.70e+0  1.13e+0  7.08e+3  1.91e+4  8.04e+3   2.47e-1  2.09e-1  7.08e+3  1.75e+3  1.48e+3
  22  11 -20 1.5 0.57     25.1   3.54e+0  1.36e+0  3.69e+3  1.31e+4  5.00e+3   1.26e-1  1.24e-1  3.69e+3  4.65e+2  4.57e+2
  22   7 -30 1.5 0.57     35.3   2.26e+0  9.81e-1  2.38e+3  5.37e+3  2.33e+3   3.91e-2  9.01e-2  2.38e+3  9.29e+1  2.14e+2
  23  24   0 1.5 0.57     76.4   2.45e+0  9.55e-1  1.40e+3  3.44e+3  1.34e+3   1.46e-2  2.73e-2  1.40e+3  2.05e+1  3.82e+1
  23  27   0 1.5 0.57     67.3   2.68e+0  7.02e-1  1.25e+3  3.34e+3  8.76e+2   2.12e-2  4.56e-2  1.25e+3  2.65e+1  5.69e+1
  23  31   0 1.5 0.57     58.6   2.98e+0  8.19e-1  1.18e+3  3.52e+3  9.66e+2   2.86e-2  5.26e-2  1.18e+3  3.37e+1  6.21e+1
  23  35   0 1.5 0.57     36.4   4.57e+0  3.71e-1  1.94e+3  8.88e+3  7.22e+2   7.80e-2  8.79e-2  1.94e+3  1.52e+2  1.71e+2
  23  39   0 1.5 0.57     31.8   1.96e+0  3.84e-1  6.10e+3  1.20e+4  2.34e+3   1.81e-2  3.38e-2  6.10e+3  1.11e+2  2.06e+2
  23  15 -10 1.5 0.57     87.9   2.30e+0  4.08e-1  8.28e+2  1.90e+3  3.38e+2   2.67e-2  4.36e-2  8.28e+2  2.21e+1  3.61e+1
  23  11 -20 1.5 0.57     92.8   3.56e+0  6.16e-1  7.49e+2  2.67e+3  4.61e+2   3.65e-2  4.55e-2  7.49e+2  2.74e+1  3.41e+1
  23   7 -30 1.5 0.57     99.0   3.72e+0  3.85e-1  6.20e+2  2.30e+3  2.39e+2   3.31e-2  2.76e-2  6.20e+2  2.05e+1  1.71e+1
  24  24   0 1.5 0.57     76.4   2.27e+0  6.76e-1  1.42e+3  3.21e+3  9.56e+2   1.59e-2  2.64e-2  1.42e+3  2.26e+1  3.73e+1
  24  27   0 1.5 0.57     67.3   2.62e+0  7.70e-1  1.19e+3  3.12e+3  9.16e+2   2.12e-2  4.71e-2  1.19e+3  2.52e+1  5.60e+1
  24  31   0 1.5 0.57     58.6   2.91e+0  8.62e-1  1.21e+3  3.52e+3  1.04e+3   3.09e-2  4.98e-2  1.21e+3  3.74e+1  6.04e+1
  24  35   0 1.5 0.57     36.4   4.34e+0  4.17e-1  2.02e+3  8.78e+3  8.44e+2   7.97e-2  9.90e-2  2.02e+3  1.61e+2  2.00e+2
  24  39   0 1.5 0.57     31.8   1.46e+0  3.04e-1  7.82e+3  1.14e+4  2.38e+3   1.45e-2  2.78e-2  7.82e+3  1.14e+2  2.17e+2
  24  15 -10 1.5 0.57     87.9   2.27e+0  3.92e-1  8.15e+2  1.85e+3  3.19e+2   2.94e-2  4.11e-2  8.15e+2  2.40e+1  3.35e+1
  24  11 -20 1.5 0.57     92.8   4.33e+0  6.91e-1  6.47e+2  2.80e+3  4.47e+2   4.54e-2  5.16e-2  6.47e+2  2.94e+1  3.34e+1
  24   7 -30 1.5 0.57     99.0   3.85e+0  5.00e-1  6.16e+2  2.37e+3  3.08e+2   3.76e-2  2.70e-2  6.16e+2  2.32e+1  1.66e+1
  25  24   0 1.5 0.57     76.4   2.23e+0  7.54e-1  1.49e+3  3.33e+3  1.13e+3   1.75e-2  2.57e-2  1.49e+3  2.61e+1  3.83e+1
  25  27   0 1.5 0.57     67.3   2.52e+0  7.06e-1  1.25e+3  3.16e+3  8.85e+2   2.32e-2  4.65e-2  1.25e+3  2.91e+1  5.82e+1
  25  31   0 1.5 0.57     58.6   3.01e+0  6.92e-1  1.20e+3  3.63e+3  8.34e+2   3.35e-2  5.19e-2  1.20e+3  4.04e+1  6.25e+1
  25  35   0 1.5 0.57     36.4   4.37e+0  3.69e-1  2.15e+3  9.40e+3  7.94e+2   7.81e-2  9.88e-2  2.15e+3  1.68e+2  2.13e+2
  25  39   0 1.5 0.57     31.8   5.17e+0  1.09e+0  2.27e+3  1.17e+4  2.48e+3   5.29e-2  9.97e-2  2.27e+3  1.20e+2  2.26e+2
  25  15 -10 1.5 0.57     87.9   2.41e+0  4.25e-1  8.11e+2  1.96e+3  3.45e+2   2.93e-2  4.19e-2  8.11e+2  2.38e+1  3.40e+1
  25  11 -20 1.5 0.57     92.8   4.15e+0  4.79e-1  7.47e+2  3.10e+3  3.58e+2   3.82e-2  4.72e-2  7.47e+2  2.85e+1  3.53e+1
  25   7 -30 1.5 0.57     99.0   4.01e+0  4.52e-1  6.52e+2  2.61e+3  2.94e+2   3.64e-2  2.51e-2  6.52e+2  2.38e+1  1.64e+1
  26  24   0 1.5 0.57     64.5   3.88e+0  7.39e-1  1.31e+3  5.06e+3  9.64e+2   3.32e-2  7.40e-2  1.31e+3  4.33e+1  9.66e+1
  26  27   0 1.5 0.57     55.3   2.84e+0  6.91e-1  1.51e+3  4.28e+3  1.04e+3   3.12e-2  5.97e-2  1.51e+3  4.71e+1  9.00e+1
  26  31   0 1.5 0.57     46.5   3.30e+0  1.11e+0  1.73e+3  5.70e+3  1.91e+3   3.66e-2  8.02e-2  1.73e+3  6.31e+1  1.38e+2
  26  35   0 1.5 0.57     25.9   4.14e+0  2.17e-1  3.28e+3  1.36e+4  7.11e+2   1.28e-1  7.41e-2  3.28e+3  4.21e+2  2.43e+2
  26  39   0 1.5 0.57     31.3   4.22e+0  1.09e+0  3.50e+3  1.48e+4  3.82e+3   1.58e-1  1.17e-1  3.50e+3  5.52e+2  4.09e+2
  26  15 -10 1.5 0.57     75.8   2.58e+0  3.94e-1  9.89e+2  2.55e+3  3.89e+2   3.03e-2  4.69e-2  9.89e+2  3.00e+1  4.64e+1
  26  11 -20 1.5 0.57     80.8   4.10e+0  6.43e-1  1.03e+3  4.24e+3  6.65e+2   3.94e-2  5.18e-2  1.03e+3  4.07e+1  5.35e+1
  26   7 -30 1.5 0.57     87.0   4.55e+0  5.07e-1  7.69e+2  3.50e+3  3.90e+2   3.09e-2  4.15e-2  7.69e+2  2.38e+1  3.19e+1
  27  24   0 1.5 0.57     69.0   4.00e+0  9.30e-1  1.24e+3  4.96e+3  1.15e+3   3.38e-2  3.38e-2  1.24e+3  4.19e+1  4.20e+1
  27  27   0 1.5 0.57     60.5   2.89e+0  6.03e-1  1.28e+3  3.70e+3  7.73e+2   2.20e-2  4.19e-2  1.28e+3  2.82e+1  5.37e+1
  27  31   0 1.5 0.57     52.6   3.30e+0  7.06e-1  1.37e+3  4.51e+3  9.66e+2   3.37e-2  6.79e-2  1.37e+3  4.60e+1  9.28e+1
  27  35   0 1.5 0.57     35.7   3.74e+0  1.36e-1  2.33e+3  8.74e+3  3.18e+2   4.73e-2  6.39e-2  2.33e+3  1.10e+2  1.49e+2
  27  39   0 1.5 0.57     39.7   4.60e+0  9.47e-1  2.25e+3  1.04e+4  2.13e+3   3.01e-2  9.18e-2  2.25e+3  6.77e+1  2.06e+2
  27  15 -10 1.5 0.57     81.0   2.31e+0  5.33e-1  1.06e+3  2.44e+3  5.63e+2   2.31e-2  3.44e-2  1.06e+3  2.43e+1  3.63e+1
  27  11 -20 1.5 0.57     86.8   4.00e+0  7.51e-1  8.40e+2  3.36e+3  6.31e+2   3.53e-2  5.87e-2  8.40e+2  2.97e+1  4.93e+1
  27   7 -30 1.5 0.57     93.8   2.91e+0  6.46e-1  8.68e+2  2.53e+3  5.61e+2   2.33e-2  3.68e-2  8.68e+2  2.02e+1  3.19e+1
  28  24   0 1.5 0.57     69.0   3.97e+0  9.18e-1  1.24e+3  4.92e+3  1.14e+3   3.35e-2  3.27e-2  1.24e+3  4.16e+1  4.05e+1
  28  27   0 1.5 0.57     60.5   3.02e+0  6.91e-1  1.24e+3  3.75e+3  8.59e+2   2.39e-2  4.90e-2  1.24e+3  2.97e+1  6.10e+1
  28  31   0 1.5 0.57     52.6   3.44e+0  6.81e-1  1.33e+3  4.58e+3  9.08e+2   3.41e-2  5.56e-2  1.33e+3  4.54e+1  7.41e+1
  28  35   0 1.5 0.57     35.7   4.16e+0  1.72e-1  2.24e+3  9.32e+3  3.85e+2   5.04e-2  5.34e-2  2.24e+3  1.13e+2  1.20e+2
  28  39   0 1.5 0.57     39.7   1.75e+0  3.83e-1  5.82e+3  1.02e+4  2.23e+3   1.09e-2  3.49e-2  5.82e+3  6.32e+1  2.03e+2
  28  15 -10 1.5 0.57     81.0   2.61e+0  6.23e-1  9.28e+2  2.43e+3  5.78e+2   3.23e-2  4.13e-2  9.28e+2  3.00e+1  3.83e+1
  28  11 -20 1.5 0.57     86.8   4.50e+0  9.45e-1  7.72e+2  3.48e+3  7.30e+2   3.92e-2  5.63e-2  7.72e+2  3.03e+1  4.35e+1
  28   7 -30 1.5 0.57     93.8   3.07e+0  5.02e-1  8.35e+2  2.56e+3  4.19e+2   2.38e-2  3.54e-2  8.35e+2  1.99e+1  2.95e+1
  29  24   0 1.5 0.57     70.9   3.97e+0  5.97e-1  1.04e+3  4.12e+3  6.20e+2   2.46e-2  3.41e-2  1.04e+3  2.55e+1  3.54e+1
  29  27   0 1.5 0.57     62.6   2.90e+0  6.07e-1  1.08e+3  3.12e+3  6.54e+2   2.34e-2  4.66e-2  1.08e+3  2.52e+1  5.02e+1
  29  31   0 1.5 0.57     54.8   3.06e+0  4.17e-1  1.21e+3  3.71e+3  5.06e+2   3.50e-2  6.29e-2  1.21e+3  4.25e+1  7.64e+1
  29  35   0 1.5 0.57     38.3   3.27e+0  1.66e-1  2.34e+3  7.64e+3  3.88e+2   3.28e-2  5.90e-2  2.34e+3  7.66e+1  1.38e+2
  29  39   0 1.5 0.57     41.5   4.66e+0  1.10e+0  1.77e+3  8.26e+3  1.95e+3   3.72e-2  1.27e-1  1.77e+3  6.59e+1  2.26e+2
  29  15 -10 1.5 0.57     83.0   2.80e+0  6.51e-1  7.95e+2  2.22e+3  5.17e+2   4.07e-2  6.86e-2  7.95e+2  3.24e+1  5.45e+1
  29  11 -20 1.5 0.57     89.0   3.99e+0  7.35e-1  7.53e+2  3.01e+3  5.53e+2   5.40e-2  7.09e-2  7.53e+2  4.07e+1  5.34e+1
  29   7 -30 1.5 0.57     96.0   3.15e+0  8.55e-1  7.31e+2  2.30e+3  6.25e+2   3.54e-2  4.32e-2  7.31e+2  2.58e+1  3.15e+1
  30  24   0 1.5 0.57     71.6   3.52e+0  6.70e-1  1.27e+3  4.47e+3  8.50e+2   2.04e-2  4.84e-2  1.27e+3  2.58e+1  6.14e+1
  30  27   0 1.5 0.57     63.4   2.83e+0  6.27e-1  1.22e+3  3.45e+3  7.65e+2   3.07e-2  7.42e-2  1.22e+3  3.74e+1  9.05e+1
  30  31   0 1.5 0.57     55.9   3.21e+0  6.55e-1  1.26e+3  4.04e+3  8.24e+2   3.58e-2  1.39e-1  1.26e+3  4.51e+1  1.75e+2
  30  35   0 1.5 0.57     40.1   4.06e+0  2.19e-1  2.05e+3  8.33e+3  4.48e+2   5.24e-2  1.09e-1  2.05e+3  1.07e+2  2.23e+2
  30  39   0 1.5 0.57     43.5   4.78e+0  1.08e+0  1.91e+3  9.13e+3  2.05e+3   4.40e-2  2.00e-1  1.91e+3  8.40e+1  3.82e+2
  30  15 -10 1.5 0.57     83.8   2.42e+0  5.39e-1  9.13e+2  2.21e+3  4.92e+2   2.57e-2  6.79e-2  9.13e+2  2.35e+1  6.20e+1
  30  11 -20 1.5 0.57     90.0   3.79e+0  9.21e-1  8.12e+2  3.08e+3  7.48e+2   3.66e-2  1.10e-1  8.12e+2  2.97e+1  8.91e+1
  30   7 -30 1.5 0.57     97.1   2.78e+0  6.98e-1  8.21e+2  2.28e+3  5.74e+2   3.07e-2  6.00e-2  8.21e+2  2.52e+1  4.93e+1
```

```
];
%Test 2 - Soil ---------------------------------------------
% Rec Chan rx  sz size     Dist   Vratio   Hratio   Pmax     Vmax     Hmax      Vratio   Hratio   Pmax     Vmax     Hmax
MD04brk1 = [...
  76   9 100 1.5 0.57    100.0   5.32e+0  5.03e+0  6.56e+2  3.49e+3  3.30e+3   3.06e-2  7.35e-3  6.56e+2  2.01e+1  4.83e+0
  76  20 180 1.5 0.57    180.0   1.59e+0  2.19e+0  3.31e+2  5.26e+2  7.25e+2   3.18e-2  1.89e-2  3.31e+2  1.05e+1  6.27e+0
  76  16 240 1.5 0.57    240.0   1.18e+0  1.42e+0  2.25e+2  2.66e+2  3.20e+2   3.27e-2  2.48e-2  2.25e+2  7.38e+0  5.59e+0
  77   9 100 1.5 0.57    100.0   5.52e+0  5.37e+0  5.67e+2  3.13e+3  3.04e+3   4.21e-2  1.08e-2  5.67e+2  2.39e+1  6.11e+0
  77  20 180 1.5 0.57    180.0   1.63e+0  2.26e+0  2.49e+2  4.07e+2  5.64e+2   4.60e-2  3.09e-2  2.49e+2  1.15e+1  7.69e+0
  77  16 240 1.5 0.57    240.0   1.09e+0  1.38e+0  1.87e+2  2.04e+2  2.57e+2   4.75e-2  5.41e-2  1.87e+2  8.88e+0  1.01e+1
  88   9 100 1.5 0.57    100.0   4.76e+0  4.40e+0  1.03e+3  4.92e+3  4.55e+3   2.80e-2  6.26e-3  1.03e+3  2.90e+1  6.47e+0
  88  20 180 1.5 0.57    180.0   2.39e+0  2.05e+0  5.39e+2  1.29e+3  1.10e+3   2.21e-2  1.42e-2  5.39e+2  1.19e+1  7.63e+0
  88  16 240 1.5 0.57    240.0   2.03e+0  1.59e+0  3.68e+2  7.47e+2  5.86e+2   2.79e-2  1.84e-2  3.68e+2  1.03e+1  6.76e+0
  89   9 100 1.5 0.57    100.0   5.33e+0  4.97e+0  8.98e+2  4.79e+3  4.47e+3   3.27e-2  8.57e-3  8.98e+2  2.94e+1  7.70e+0
  89  20 180 1.5 0.57    180.0   2.46e+0  2.26e+0  4.75e+2  1.17e+3  1.07e+3   2.56e-2  1.62e-2  4.75e+2  1.21e+1  7.69e+0
];
MD04brk10 = [...
  78   9 100 1.5 5.68    100.0   5.59e+0  4.69e+0  1.53e+3  8.55e+3  7.18e+3   7.94e-2  1.87e-2  1.53e+3  1.22e+2  2.86e+1
  78  20 180 1.5 5.68    180.0   1.80e+0  2.48e+0  8.69e+2  1.56e+3  2.15e+3   4.86e-2  3.18e-2  8.69e+2  4.22e+1  2.76e+1
  78  16 240 1.5 5.68    240.0   1.31e+0  1.94e+0  5.93e+2  7.74e+2  1.15e+3   6.14e-2  5.89e-2  5.93e+2  3.64e+1  3.49e+1
  79   9 100 1.5 5.68    100.0   5.74e+0  4.16e+0  1.78e+3  1.02e+4  7.41e+3   7.56e-2  1.71e-2  1.78e+3  1.34e+2  3.05e+1
  79  20 180 1.5 5.68    180.0   1.88e+0  2.58e+0  9.66e+2  1.82e+3  2.49e+3   4.84e-2  2.84e-2  9.66e+2  4.68e+1  2.75e+1
  79  16 240 1.5 5.68    240.0   2.06e+0  1.94e+0  6.36e+2  1.31e+3  1.24e+3   6.22e-2  4.18e-2  6.36e+2  3.96e+1  2.66e+1
  90   9 100 1.5 5.68    100.0   5.06e+0  3.40e+0  2.28e+3  1.15e+4  7.74e+3   6.59e-2  1.65e-2  2.28e+3  1.50e+2  3.75e+1
  90  20 180 1.5 5.68    180.0   2.52e+0  2.38e+0  1.29e+3  3.25e+3  3.07e+3   3.78e-2  2.03e-2  1.29e+3  4.87e+1  2.62e+1
  90  16 240 1.5 5.68    240.0   2.26e+0  1.53e+0  8.81e+2  1.99e+3  1.35e+3   4.52e-2  2.61e-2  8.81e+2  3.98e+1  2.29e+1
  91   9 100 1.5 5.68    100.0   6.05e+0  3.98e+0  2.18e+3  1.32e+4  8.67e+3   7.39e-2  1.87e-2  2.18e+3  1.61e+2  4.07e+1
  91  20 180 1.5 5.68    180.0   2.53e+0  2.13e+0  1.39e+3  3.52e+3  2.97e+3   3.67e-2  2.09e-2  1.39e+3  5.11e+1  2.91e+1
  91  16 240 1.5 5.68    240.0   2.32e+0  1.57e+0  8.92e+2  2.07e+3  1.40e+3   4.53e-2  3.03e-2  8.92e+2  4.05e+1  2.71e+1
];
MD04brk16 = [...
  80   9 100 1.5 9.09    100.0   6.16e+0  4.09e+0  1.92e+3  1.18e+4  7.86e+3   9.51e-2  2.57e-2  1.92e+3  1.83e+2  4.93e+1
  80  20 180 1.5 9.09    180.0   2.01e+0  2.42e+0  1.18e+3  2.37e+3  2.85e+3   5.11e-2  3.20e-2  1.18e+3  6.02e+1  3.77e+1
  80  16 240 1.5 9.09    240.0   1.92e+0  1.73e+0  8.72e+2  1.68e+3  1.51e+3   5.75e-2  4.06e-2  8.72e+2  5.02e+1  3.54e+1
  81   9 100 1.5 9.09    100.0   5.84e+0  3.81e+0  2.16e+3  1.26e+4  8.24e+3   8.30e-2  2.30e-2  2.16e+3  1.79e+2  4.97e+1
  81  20 180 1.5 9.09    180.0   2.20e+0  2.49e+0  1.16e+3  2.56e+3  2.89e+3   5.16e-2  3.02e-2  1.16e+3  5.99e+1  3.51e+1
  81  16 240 1.5 9.09    240.0   2.15e+0  1.89e+0  7.45e+2  1.60e+3  1.41e+3   6.43e-2  4.40e-2  7.45e+2  4.79e+1  3.28e+1
  92   9 100 1.5 9.09    100.0   5.87e+0  3.79e+0  2.25e+3  1.32e+4  8.53e+3   8.69e-2  1.91e-2  2.25e+3  1.96e+2  4.31e+1
  92  20 180 1.5 9.09    180.0   2.42e+0  2.64e+0  1.09e+3  2.64e+3  2.88e+3   5.96e-2  3.79e-2  1.09e+3  6.49e+1  4.13e+1
  92  16 240 1.5 9.09    240.0   2.31e+0  1.60e+0  7.40e+2  1.71e+3  1.18e+3   6.73e-2  4.24e-2  7.40e+2  4.98e+1  3.14e+1
  93   9 100 1.5 9.09    100.0   6.83e+0  4.33e+0  2.04e+3  1.39e+4  8.84e+3   9.88e-2  2.14e-2  2.04e+3  2.02e+2  4.37e+1
  93  20 180 1.5 9.09    180.0   2.47e+0  2.41e+0  1.25e+3  3.08e+3  3.01e+3   4.89e-2  3.10e-2  1.25e+3  6.10e+1  3.87e+1
  93  16 240 1.5 9.09    240.0   2.41e+0  1.53e+0  8.50e+2  2.05e+3  1.30e+3   5.84e-2  3.56e-2  8.50e+2  4.96e+1  3.03e+1
  93  24 120 1.5 9.09    120.0   2.25e+0  2.64e+0  2.25e+3  5.04e+3  5.93e+3   4.75e-2  1.99e-2  2.25e+3  1.07e+2  4.46e+1
];
MD04brk32 = [...
  83   9 100 1.5 18.18    100.0   5.81e+0  3.68e+0  2.59e+3  1.51e+4  9.54e+3   1.21e-1  2.80e-2  2.59e+3  3.15e+2  7.27e+1
  83  20 180 1.5 18.18    180.0   2.12e+0  3.18e+0  1.33e+3  2.81e+3  4.22e+3   8.12e-2  4.37e-2  1.33e+3  1.08e+2  5.80e+1
  83  16 240 1.5 18.18    240.0   2.02e+0  1.93e+0  8.49e+2  1.72e+3  1.64e+3   8.68e-2  6.39e-2  8.49e+2  7.37e+1  5.42e+1
  86   9 100 1.5 18.18    100.0   6.38e+0  4.03e+0  2.50e+3  1.59e+4  1.01e+4   1.20e-1  2.74e-2  2.50e+3  3.00e+2  6.86e+1
  86  20 180 1.5 18.18    180.0   2.39e+0  2.76e+0  1.53e+3  3.65e+3  4.21e+3   6.86e-2  3.65e-2  1.53e+3  1.05e+2  5.57e+1
  86  16 240 1.5 18.18    240.0   2.26e+0  1.76e+0  9.27e+2  2.10e+3  1.63e+3   8.03e-2  6.07e-2  9.27e+2  7.44e+1  5.63e+1
  95   9 100 1.5 18.18    100.0   5.65e+0  3.22e+0  3.57e+3  2.01e+4  1.15e+4   7.50e-2  2.02e-2  3.57e+3  2.68e+2  7.21e+1
  95  20 180 1.5 18.18    180.0   2.48e+0  2.14e+0  1.93e+3  4.78e+3  4.12e+3   5.73e-2  3.43e-2  1.93e+3  1.11e+2  6.62e+1
  95  16 240 1.5 18.18    240.0   2.55e+0  1.54e+0  1.16e+3  2.96e+3  1.78e+3   6.51e-2  4.61e-2  1.16e+3  7.55e+1  5.34e+1
  95  24 120 1.5 18.18    120.0   2.07e+0  1.70e+0  3.80e+3  7.87e+3  6.45e+3   5.14e-2  1.45e-2  3.80e+3  1.95e+2  5.49e+1
  96   9 100 1.5 18.18    100.0   6.87e+0  4.33e+0  2.80e+3  1.92e+4  1.21e+4   9.96e-2  2.49e-2  2.80e+3  2.79e+2  6.98e+1
  96  20 180 1.5 18.18    180.0   2.60e+0  2.51e+0  2.02e+3  5.26e+3  5.08e+3   5.69e-2  3.12e-2  2.02e+3  1.15e+2  6.31e+1
  96  16 240 1.5 18.18    240.0   2.46e+0  1.54e+0  1.28e+3  3.14e+3  1.97e+3   5.71e-2  3.78e-2  1.28e+3  7.29e+1  4.84e+1
  96  24 120 1.5 18.18    120.0   2.13e+0  2.09e+0  3.57e+3  7.60e+3  7.46e+3   5.08e-2  1.55e-2  3.57e+3  1.81e+2  5.54e+1
];
MD04brk128 = [...
  98   9 100 1.5 72.73    100.0   6.73e+0  4.07e+0  4.45e+3  2.99e+4  1.81e+4   9.26e-2  3.37e-2  4.45e+3  4.12e+2  1.50e+2
  98  20 180 1.5 72.73    180.0   2.48e+0  2.35e+0  2.85e+3  7.07e+3  6.71e+3   6.69e-2  3.29e-2  2.85e+3  1.91e+2  9.39e+1
  98  16 240 1.5 72.73    240.0   2.61e+0  1.63e+0  1.95e+3  5.09e+3  3.18e+3   6.76e-2  3.52e-2  1.95e+3  1.32e+2  6.88e+1
  98  24 120 1.5 72.73    120.0   2.25e+0  2.07e+0  4.66e+3  1.05e+4  9.64e+3   6.65e-2  3.01e-2  4.66e+3  3.10e+2  1.40e+2
];

%Test 3 - Soil and Gravel Pile ----------------------------
% Rec Chan rx  sz size     Dist   Vratio   Hratio   Pmax     Vmax     Hmax      Vratio   Hratio   Pmax     Vmax     Hmax
MD05Bare05 = [...
  37   8  62 3.0 0.57     73.4   2.98e+0  4.43e+0  9.07e+2  2.70e+3  4.01e+3   4.91e-2  4.29e-2  9.07e+2  4.45e+1  3.89e+1
  37   3  92 3.0 0.57    101.5   3.20e+0  4.99e+0  5.51e+2  1.76e+3  2.75e+3   4.62e-2  2.83e-2  5.51e+2  2.55e+1  1.56e+1
  37  16  92 3.0 0.57     97.0   3.34e+0  2.86e+0  6.02e+2  2.01e+3  1.72e+3   2.52e-2  5.51e-2  6.02e+2  1.51e+1  3.32e+1
  37  36 120 3.0 0.57    125.9   3.02e+0  2.72e+0  4.41e+2  1.33e+3  1.20e+3   5.21e-2  2.09e-2  4.41e+2  2.30e+1  9.25e+0
  37  32 180 3.0 0.57    185.6   7.56e+0  6.92e+0  2.55e+2  1.93e+3  1.76e+3   1.22e-1  5.37e-2  2.55e+2  3.11e+1  1.37e+1
  37  28 240 3.0 0.57    245.5   2.64e+0  4.93e+0  1.60e+2  4.21e+2  7.87e+2   1.26e-1  7.94e-2  1.60e+2  2.01e+1  1.27e+1
  37  48 340 3.0 0.57    345.3   4.09e+0  7.18e+0  7.07e+1  2.89e+2  5.08e+2   2.50e-1  1.41e-1  7.07e+1  1.77e+1  9.99e+0
  37  44 370 3.0 0.57    375.3   3.65e+0  1.41e+1  8.12e+1  2.97e+2  1.15e+3   2.60e-1  2.19e-1  8.12e+1  2.11e+1  1.78e+1
  37  40 400 3.0 0.57    405.3   3.38e+0  6.29e+0  6.74e+1  2.27e+2  4.24e+2   2.71e-1  8.41e-2  6.74e+1  1.83e+1  5.66e+0
  43   8  62 3.0 0.57     73.4   3.30e+0  4.36e+0  1.16e+3  3.81e+3  5.04e+3   3.72e-2  2.61e-2  1.16e+3  4.30e+1  3.02e+1
  43   3  92 3.0 0.57    101.5   2.84e+0  5.34e+0  6.37e+2  1.81e+3  3.40e+3   4.04e-2  3.31e-2  6.37e+2  2.57e+1  2.11e+1
  43  16  92 3.0 0.57     97.0   3.03e+0  2.58e+0  6.73e+2  2.04e+3  1.73e+3   2.79e-2  4.84e-2  6.73e+2  1.88e+1  3.26e+1
  43  32 180 3.0 0.57    185.6   7.78e+0  7.00e+0  2.51e+2  1.95e+3  1.76e+3   1.42e-1  5.54e-2  2.51e+2  3.56e+1  1.39e+1
  43  28 240 3.0 0.57    245.5   2.44e+0  4.84e+0  1.89e+2  4.62e+2  9.17e+2   1.05e-1  6.91e-2  1.89e+2  2.00e+1  1.31e+1
  43  48 340 3.0 0.57    345.3   4.56e+0  7.47e+0  9.04e+1  4.12e+2  6.75e+2   2.10e-1  1.22e-1  9.04e+1  1.90e+1  1.10e+1
  43  44 370 3.0 0.57    375.3   3.79e+0  1.55e+1  1.00e+2  3.81e+2  1.55e+3   2.23e-1  2.19e-1  1.00e+2  2.23e+1  2.20e+1
  43  40 400 3.0 0.57    405.3   3.61e+0  5.70e+0  9.34e+1  3.37e+2  5.32e+2   1.96e-1  7.01e-2  9.34e+1  1.83e+1  6.55e+0
  45   8  62 3.0 0.57     73.4   3.18e+0  4.24e+0  1.20e+3  3.83e+3  5.10e+3   3.57e-2  2.42e-2  1.20e+3  4.29e+1  2.91e+1
  45   3  92 3.0 0.57    101.5   2.84e+0  5.14e+0  6.99e+2  1.98e+3  3.59e+3   3.66e-2  2.63e-2  6.99e+2  2.56e+1  1.84e+1
  45  16  92 3.0 0.57     97.0   2.82e+0  2.59e+0  7.51e+2  2.12e+3  1.94e+3   1.91e-2  4.26e-2  7.51e+2  1.43e+1  3.20e+1
  45  32 180 3.0 0.57    185.6   7.99e+0  6.23e+0  3.17e+2  2.53e+3  1.98e+3   9.74e-2  4.15e-2  3.17e+2  3.09e+1  1.32e+1
  45  28 240 3.0 0.57    245.5   2.46e+0  4.40e+0  1.92e+2  4.72e+2  8.42e+2   1.06e-1  6.45e-2  1.92e+2  2.03e+1  1.24e+1
  45  48 340 3.0 0.57    345.3   4.14e+0  6.82e+0  6.80e+1  2.81e+2  4.64e+2   2.60e-1  1.62e-1  6.80e+1  1.76e+1  1.10e+1
  45  44 370 3.0 0.57    375.3   3.52e+0  1.36e+1  7.39e+1  2.60e+2  1.01e+3   3.07e-1  2.39e-1  7.39e+1  2.27e+1  1.77e+1
```

```
  45  40 400 3.0 0.57    405.3   3.28e+0  5.57e+0  6.25e+1  2.05e+2  3.48e+2   2.70e-1  9.88e-2  6.25e+1  1.69e+1  6.17e+0
  % Rec Chan rx  sz size     Dist   Vratio   Hratio   Pmax     Vmax     Hmax      Vratio   Hratio   Pmax     Vmax     Hmax
  81   8  62 3.0 0.57     73.4   2.87e+0  4.14e+0  1.02e+3  2.94e+3  4.23e+3   5.03e-2  3.12e-2  1.02e+3  5.14e+1  3.19e+1
  81   3  92 3.0 0.57    101.5   2.85e+0  6.09e+0  6.18e+2  1.76e+3  3.76e+3   4.21e-2  3.13e-2  6.18e+2  2.60e+1  1.93e+1
  81  16  92 3.0 0.57     97.0   3.50e+0  3.07e+0  6.34e+2  2.22e+3  1.94e+3   2.32e-2  5.37e-2  6.34e+2  1.47e+1  3.41e+1
  81  36 120 3.0 0.57    125.9   2.86e+0  2.36e+0  4.94e+2  1.41e+3  1.16e+3   3.61e-2  2.11e-2  4.94e+2  1.78e+1  1.04e+1
  81  32 180 3.0 0.57    185.6   8.00e+0  6.66e+0  2.80e+2  2.24e+3  1.87e+3   1.16e-1  4.75e-2  2.80e+2  3.26e+1  1.33e+1
  81  28 240 3.0 0.57    245.5   2.43e+0  4.68e+0  1.95e+2  4.73e+2  9.11e+2   1.08e-1  6.22e-2  1.95e+2  2.11e+1  1.21e+1
  81  48 340 3.0 0.57    345.3   4.14e+0  6.92e+0  9.38e+1  3.89e+2  6.49e+2   2.18e-1  1.37e-1  9.38e+1  2.04e+1  1.28e+1
  81  44 370 3.0 0.57    375.3   3.84e+0  1.48e+1  9.99e+1  3.84e+2  1.48e+3   2.50e-1  1.96e-1  9.99e+1  2.50e+1  1.96e+1
  81  40 400 3.0 0.57    405.3   3.39e+0  5.40e+0  8.96e+1  3.04e+2  4.84e+2   2.10e-1  5.94e-2  8.96e+1  1.88e+1  5.32e+0
  83   8  62 3.0 0.57     73.4   3.10e+0  4.06e+0  1.26e+3  3.90e+3  5.12e+3   3.62e-2  2.32e-2  1.26e+3  4.56e+1  2.92e+1
  83   3  92 3.0 0.57    101.5   2.81e+0  5.48e+0  6.82e+2  1.91e+3  3.74e+3   3.90e-2  2.69e-2  6.82e+2  2.66e+1  1.84e+1
  83  20  62 3.0 0.57     67.0   2.10e+0  5.78e+0  9.87e+2  2.07e+3  5.70e+3   5.01e-2  3.65e-2  9.87e+2  4.95e+1  3.60e+1
  83  16  92 3.0 0.57     97.0   3.49e+0  2.75e+0  5.63e+2  1.96e+3  1.54e+3   2.65e-2  6.03e-2  5.63e+2  1.49e+1  3.39e+1
  83  36 120 3.0 0.57    125.9   3.24e+0  2.61e+0  4.09e+2  1.33e+3  1.07e+3   4.63e-2  1.77e-2  4.09e+2  1.90e+1  7.23e+0
  83  32 180 3.0 0.57    185.6   7.24e+0  6.32e+0  2.59e+2  1.87e+3  1.63e+3   1.28e-1  5.10e-2  2.59e+2  3.30e+1  1.32e+1
  83  28 240 3.0 0.57    245.5   2.18e+0  4.24e+0  1.79e+2  3.91e+2  7.61e+2   1.18e-1  5.80e-2  1.79e+2  2.12e+1  1.04e+1
  83  48 340 3.0 0.57    345.3   3.96e+0  6.37e+0  7.76e+1  3.07e+2  4.94e+2   2.47e-1  1.54e-1  7.76e+1  1.91e+1  1.20e+1
  83  44 370 3.0 0.57    375.3   3.58e+0  1.24e+1  8.90e+1  3.19e+2  1.10e+3   2.75e-1  2.64e-1  8.90e+1  2.45e+1  2.35e+1
  83  40 400 3.0 0.57    405.3   3.19e+0  5.11e+0  7.70e+1  2.46e+2  3.93e+2   2.46e-1  7.84e-2  7.70e+1  1.90e+1  6.04e+0
  85   8  62 3.0 0.57     73.4   3.11e+0  4.06e+0  1.00e+3  3.12e+3  4.06e+3   4.87e-2  2.77e-2  1.00e+3  4.88e+1  2.78e+1
  85   3  92 3.0 0.57    101.5   3.21e+0  4.84e+0  5.80e+2  1.86e+3  2.81e+3   4.72e-2  3.55e-2  5.80e+2  2.74e+1  2.06e+1
  85  20  62 3.0 0.57     67.0   2.00e+0  4.44e+0  1.29e+3  2.58e+3  5.73e+3   3.94e-2  2.73e-2  1.29e+3  5.08e+1  3.53e+1
  85  16  92 3.0 0.57     97.0   2.86e+0  2.46e+0  7.36e+2  2.10e+3  1.81e+3   2.02e-2  5.00e-2  7.36e+2  1.48e+1  3.68e+1
  85  36 120 3.0 0.57    125.9   3.22e+0  2.63e+0  4.60e+2  1.48e+3  1.21e+3   4.03e-2  2.26e-2  4.60e+2  1.86e+1  1.04e+1
  85  32 180 3.0 0.57    185.6   7.54e+0  6.39e+0  3.01e+2  2.27e+3  1.93e+3   1.14e-1  4.88e-2  3.01e+2  3.45e+1  1.47e+1
  85  28 240 3.0 0.57    245.5   2.22e+0  4.14e+0  1.98e+2  4.40e+2  8.20e+2   1.11e-1  6.93e-2  1.98e+2  2.19e+1  1.37e+1
  85  48 340 3.0 0.57    345.3   4.12e+0  6.50e+0  8.26e+1  3.41e+2  5.37e+2   2.47e-1  1.44e-1  8.26e+1  2.04e+1  1.19e+1
  85  44 370 3.0 0.57    375.3   3.60e+0  1.30e+1  9.27e+1  3.34e+2  1.20e+3   2.75e-1  2.27e-1  9.27e+1  2.55e+1  2.10e+1
  85  40 400 3.0 0.57    405.3   3.39e+0  5.22e+0  7.90e+1  2.68e+2  4.12e+2   2.39e-1  8.66e-2  7.90e+1  1.89e+1  6.84e+0
  69   8  62 1.0 0.57     73.4   2.90e+0  4.28e+0  9.23e+2  2.68e+3  3.95e+3   5.90e-2  3.71e-2  9.23e+2  5.45e+1  3.42e+1
  69   3  92 1.0 0.57    101.5   3.19e+0  5.23e+0  5.87e+2  1.87e+3  3.07e+3   5.11e-2  3.32e-2  5.87e+2  3.00e+1  1.95e+1
  69  16  92 1.0 0.57     97.0   3.16e+0  2.42e+0  6.59e+2  2.08e+3  1.59e+3   2.64e-2  6.36e-2  6.59e+2  1.74e+1  4.19e+1
  69  36 120 1.0 0.57    125.9   3.08e+0  2.63e+0  4.38e+2  1.35e+3  1.15e+3   4.97e-2  2.47e-2  4.38e+2  2.18e+1  1.08e+1
  69  32 180 1.0 0.57    185.6   7.88e+0  6.89e+0  2.77e+2  2.18e+3  1.91e+3   1.39e-1  5.71e-2  2.77e+2  3.85e+1  1.58e+1
  69  28 240 1.0 0.57    245.5   2.26e+0  4.52e+0  1.98e+2  4.47e+2  8.95e+2   1.24e-1  6.38e-2  1.98e+2  2.45e+1  1.26e+1
  69  48 340 1.0 0.57    345.3   4.16e+0  7.33e+0  9.22e+1  3.84e+2  6.76e+2   2.22e-1  1.34e-1  9.22e+1  2.05e+1  1.23e+1
  69  44 370 1.0 0.57    375.3   4.47e+0  1.52e+1  9.86e+1  4.40e+2  1.49e+3   2.71e-1  1.99e-1  9.86e+1  2.67e+1  1.96e+1
  69  40 400 1.0 0.57    405.3   3.32e+0  5.58e+0  9.30e+1  3.09e+2  5.19e+2   2.05e-1  6.21e-2  9.30e+1  1.91e+1  5.77e+0
  71   8  62 1.0 0.57     73.4   2.93e+0  4.35e+0  1.04e+3  3.03e+3  4.51e+3   5.42e-2  3.28e-2  1.04e+3  5.61e+1  3.40e+1
  71   3  92 1.0 0.57    101.5   2.97e+0  5.34e+0  6.86e+2  2.04e+3  3.66e+3   4.80e-2  3.08e-2  6.86e+2  3.29e+1  2.11e+1
  71  16  92 1.0 0.57     97.0   3.29e+0  2.68e+0  7.68e+2  2.53e+3  2.06e+3   2.31e-2  5.76e-2  7.68e+2  1.77e+1  4.42e+1
  71  36 120 1.0 0.57    125.9   2.87e+0  2.58e+0  5.47e+2  1.57e+3  1.41e+3   4.36e-2  1.68e-2  5.47e+2  2.38e+1  9.19e+0
  71  32 180 1.0 0.57    185.6   7.89e+0  6.66e+0  3.33e+2  2.63e+3  2.22e+3   1.23e-1  4.78e-2  3.33e+2  4.08e+1  1.59e+1
  71  28 240 1.0 0.57    245.5   2.49e+0  4.56e+0  2.33e+2  5.81e+2  1.06e+3   1.16e-1  6.43e-2  2.33e+2  2.72e+1  1.50e+1
  71  48 340 1.0 0.57    345.3   3.99e+0  6.91e+0  1.12e+2  4.48e+2  7.77e+2   2.00e-1  1.22e-1  1.12e+2  2.24e+1  1.37e+1
  71  44 370 1.0 0.57    375.3   5.00e+0  1.91e+1  9.92e+1  4.96e+2  1.89e+3   2.87e-1  2.31e-1  9.92e+1  2.85e+1  2.29e+1
  71  40 400 1.0 0.57    405.3   3.36e+0  5.24e+0  1.13e+2  3.79e+2  5.91e+2   1.70e-1  5.55e-2  1.13e+2  1.92e+1  6.26e+0
  73   8  62 1.5 0.57     73.4   2.93e+0  4.19e+0  9.95e+2  2.92e+3  4.17e+3   5.63e-2  3.56e-2  9.95e+2  5.60e+1  3.54e+1
  73   3  92 1.5 0.57    101.5   3.29e+0  5.95e+0  6.83e+2  2.25e+3  4.06e+3   4.83e-2  2.58e-2  6.83e+2  3.30e+1  1.77e+1
  73  16  92 1.5 0.57     97.0   3.23e+0  2.75e+0  8.23e+2  2.65e+3  2.26e+3   2.19e-2  5.40e-2  8.23e+2  1.80e+1  4.45e+1
  73  36 120 1.5 0.57    125.9   2.88e+0  2.74e+0  5.54e+2  1.59e+3  1.52e+3   4.13e-2  1.63e-2  5.54e+2  2.28e+1  9.01e+0
  73  32 180 1.5 0.57    185.6   8.13e+0  6.98e+0  3.33e+2  2.71e+3  2.33e+3   1.19e-1  4.94e-2  3.33e+2  3.98e+1  1.65e+1
  73  28 240 1.5 0.57    245.5   2.54e+0  4.73e+0  2.40e+2  6.12e+2  1.14e+3   1.14e-1  6.16e-2  2.40e+2  2.74e+1  1.48e+1
  73  48 340 1.5 0.57    345.3   4.45e+0  7.32e+0  1.06e+2  4.70e+2  7.73e+2   2.29e-1  1.48e-1  1.06e+2  2.42e+1  1.57e+1
  73  44 370 1.5 0.57    375.3   4.83e+0  1.88e+1  9.78e+1  4.72e+2  1.84e+3   3.09e-1  2.38e-1  9.78e+1  3.02e+1  2.32e+1
  73  40 400 1.5 0.57    405.3   3.57e+0  5.85e+0  1.01e+2  3.62e+2  5.93e+2   1.94e-1  7.06e-2  1.01e+2  1.97e+1  7.16e+0
  87   8  62 1.0 0.57     73.4   3.04e+0  3.99e+0  1.03e+3  3.15e+3  4.12e+3   5.70e-2  3.33e-2  1.03e+3  5.89e+1  3.44e+1
  87   3  92 1.0 0.57    101.5   3.51e+0  6.73e+0  6.42e+2  2.26e+3  4.33e+3   5.35e-2  3.97e-2  6.42e+2  3.44e+1  2.55e+1
  87  20  62 1.0 0.57     67.0   2.32e+0  5.09e+0  1.25e+3  2.91e+3  6.38e+3   5.42e-2  2.74e-2  1.25e+3  6.79e+1  3.43e+1
  87  16  92 1.0 0.57     97.0   3.62e+0  3.00e+0  6.42e+2  2.33e+3  1.93e+3   2.44e-2  7.39e-2  6.42e+2  1.56e+1  4.74e+1
  87  36 120 1.0 0.57    125.9   3.30e+0  3.02e+0  4.73e+2  1.56e+3  1.43e+3   5.20e-2  2.18e-2  4.73e+2  2.46e+1  1.03e+1
  87  32 180 1.0 0.57    185.6   8.00e+0  6.94e+0  3.03e+2  2.43e+3  2.11e+3   1.40e-1  5.13e-2  3.03e+2  4.24e+1  1.56e+1
  87  28 240 1.0 0.57    245.5   2.58e+0  4.67e+0  2.11e+2  5.44e+2  9.84e+2   1.44e-1  6.56e-2  2.11e+2  3.03e+1  1.38e+1
  87  48 340 1.0 0.57    345.3   4.33e+0  7.00e+0  9.19e+1  3.98e+2  6.44e+2   2.57e-1  1.54e-1  9.19e+1  2.36e+1  1.41e+1
  87  44 370 1.0 0.57    375.3   4.38e+0  1.57e+1  9.37e+1  4.10e+2  1.47e+3   3.28e-1  2.50e-1  9.37e+1  3.08e+1  2.34e+1
  87  40 400 1.0 0.57    405.3   3.41e+0  5.38e+0  8.81e+1  3.00e+2  4.74e+2   2.21e-1  7.82e-2  8.81e+1  1.95e+1  6.89e+0
  89   8  62 1.0 0.57     73.4   3.04e+0  4.20e+0  9.29e+2  2.82e+3  3.90e+3   6.63e-2  3.91e-2  9.29e+2  6.16e+1  3.63e+1
  89   3  92 1.0 0.57    101.5   2.99e+0  5.63e+0  6.03e+2  1.80e+3  3.39e+3   5.76e-2  4.06e-2  6.03e+2  3.47e+1  2.45e+1
  89  20  62 1.0 0.57     67.0   2.13e+0  4.78e+0  1.13e+3  2.42e+3  5.41e+3   5.99e-2  2.96e-2  1.13e+3  6.78e+1  3.35e+1
  89  16  92 1.0 0.57     97.0   3.64e+0  2.89e+0  5.77e+2  2.10e+3  1.67e+3   3.17e-2  8.25e-2  5.77e+2  1.83e+1  4.77e+1
  89  32 180 1.0 0.57    185.6   7.55e+0  6.47e+0  2.64e+2  2.00e+3  1.71e+3   1.63e-1  6.56e-2  2.64e+2  4.31e+1  1.73e+1
  89  28 240 1.0 0.57    245.5   2.59e+0  4.82e+0  1.73e+2  4.50e+2  8.35e+2   1.69e-1  8.81e-2  1.73e+2  2.93e+1  1.53e+1
  89  48 340 1.0 0.57    345.3   4.52e+0  8.12e+0  6.89e+1  3.11e+2  5.59e+2   3.75e-1  2.31e-1  6.89e+1  2.58e+1  1.59e+1
  89  44 370 1.0 0.57    375.3   4.47e+0  1.57e+1  7.79e+1  3.48e+2  1.22e+3   4.04e-1  2.96e-1  7.79e+1  3.14e+1  2.31e+1
  89  40 400 1.0 0.57    405.3   3.95e+0  6.96e+0  6.55e+1  2.59e+2  4.56e+2   3.21e-1  1.10e-1  6.55e+1  2.10e+1  7.20e+0
  91   8  62 1.0 0.57     73.4   3.00e+0  4.07e+0  9.28e+2  2.78e+3  3.78e+3   6.66e-2  3.82e-2  9.28e+2  6.18e+1  3.54e+1
  91   3  92 1.0 0.57    101.5   3.23e+0  5.87e+0  6.13e+2  1.98e+3  3.60e+3   5.89e-2  3.92e-2  6.13e+2  3.61e+1  2.40e+1
  91  20  62 1.0 0.57     67.0   2.39e+0  5.20e+0  1.12e+3  2.67e+3  5.81e+3   6.23e-2  3.16e-2  1.12e+3  6.95e+1  3.52e+1
  91  16  92 1.0 0.57     97.0   3.70e+0  3.02e+0  6.25e+2  2.31e+3  1.89e+3   2.85e-2  7.74e-2  6.25e+2  1.78e+1  4.84e+1
  91  36 120 1.0 0.57    125.9   3.51e+0  3.07e+0  4.12e+2  1.45e+3  1.27e+3   6.27e-2  2.87e-2  4.12e+2  2.58e+1  1.18e+1
  91  32 180 1.0 0.57    185.6   7.64e+0  6.75e+0  2.78e+2  2.12e+3  1.88e+3   1.59e-1  5.69e-2  2.78e+2  4.43e+1  1.58e+1
  91  28 240 1.0 0.57    245.5   2.32e+0  4.36e+0  2.07e+2  4.80e+2  9.01e+2   1.48e-1  7.33e-2  2.07e+2  3.07e+1  1.52e+1
  91  48 340 1.0 0.57    345.3   4.28e+0  7.06e+0  8.21e+1  3.51e+2  5.80e+2   2.96e-1  1.89e-1  8.21e+1  2.43e+1  1.55e+1
  91  44 370 1.0 0.57    375.3   3.67e+0  1.38e+1  9.31e+1  3.42e+2  1.28e+3   3.28e-1  2.57e-1  9.31e+1  3.05e+1  2.39e+1
  91  40 400 1.0 0.57    405.3   3.33e+0  5.38e+0  8.12e+1  2.71e+2  4.37e+2   2.50e-1  7.86e-2  8.12e+1  2.03e+1  6.38e+0
];

% Rec Chan rx  sz size     Dist   Vratio   Hratio   Pmax     Vmax     Hmax      Vratio   Hratio   Pmax     Vmax     Hmax
MD05Bare02 = [...
  38   8  62 1.5 0.57     67.1   3.00e+0  4.10e+0  1.16e+3  3.47e+3  4.75e+3   5.22e-2  3.00e-2  1.16e+3  6.05e+1  3.48e+1
  38   3  92 1.5 0.57     94.9   3.14e+0  5.34e+0  6.89e+2  2.16e+3  3.68e+3   5.19e-2  2.98e-2  6.89e+2  3.58e+1  2.05e+1
  38  16  92 1.5 0.57     90.0   3.61e+0  3.16e+0  6.58e+2  2.38e+3  2.08e+3   2.83e-2  6.65e-2  6.58e+2  1.86e+1  4.38e+1
  38  32 180 1.5 0.57    178.6   8.32e+0  7.11e+0  2.99e+2  2.49e+3  2.12e+3   7.38e-2  4.07e-2  2.99e+2  2.21e+1  1.22e+1
```

```
  38  28 240 1.5 0.57    238.5   2.53e+0  4.82e+0  2.02e+2  5.11e+2  9.76e+2   1.03e-1  5.02e-2  2.02e+2  2.09e+1  1.02e+1
  38  48 340 1.5 0.57    338.3   4.54e+0  7.65e+0  8.75e+1  3.98e+2  6.70e+2   2.06e-1  1.09e-1  8.75e+1  1.80e+1  9.53e+0
  38  44 370 1.5 0.57    368.3   3.93e+0  1.58e+1  1.02e+2  3.99e+2  1.60e+3   2.11e-1  1.70e-1  1.02e+2  2.14e+1  1.72e+1
  38  40 400 1.5 0.57    398.3   3.65e+0  6.10e+0  9.16e+1  3.34e+2  5.59e+2   1.37e-1  5.29e-2  9.16e+1  1.26e+1  4.85e+0
  40   8  62 1.5 0.57     67.1   3.18e+0  4.07e+0  1.10e+3  3.49e+3  4.47e+3   5.53e-2  3.29e-2  1.10e+3  6.07e+1  3.61e+1
  40   3  92 1.5 0.57     94.9   3.35e+0  5.60e+0  6.35e+2  2.12e+3  3.55e+3   5.36e-2  3.53e-2  6.35e+2  3.40e+1  2.24e+1
  40  16  92 1.5 0.57     90.0   3.57e+0  3.05e+0  7.20e+2  2.57e+3  2.20e+3   2.67e-2  6.21e-2  7.20e+2  1.92e+1  4.47e+1
  40  36 120 1.5 0.57    118.9   2.95e+0  2.84e+0  5.29e+2  1.56e+3  1.50e+3   3.94e-2  2.90e-2  5.29e+2  2.09e+1  1.54e+1
  40  32 180 1.5 0.57    178.6   8.23e+0  6.94e+0  3.07e+2  2.52e+3  2.13e+3   7.52e-2  3.80e-2  3.07e+2  2.31e+1  1.17e+1
  40  28 240 1.5 0.57    238.5   2.47e+0  4.71e+0  2.15e+2  5.32e+2  1.01e+3   9.35e-2  4.92e-2  2.15e+2  2.01e+1  1.06e+1
  40  48 340 1.5 0.57    338.3   4.35e+0  7.33e+0  9.61e+1  4.19e+2  7.05e+2   1.85e-1  8.88e-2  9.61e+1  1.78e+1  8.54e+0
  40  44 370 1.5 0.57    368.3   4.16e+0  1.72e+1  1.01e+2  4.19e+2  1.73e+3   2.44e-1  2.13e-1  1.01e+2  2.45e+1  2.14e+1
  40  40 400 1.5 0.57    398.3   3.47e+0  5.87e+0  8.97e+1  3.11e+2  5.27e+2   1.77e-1  6.24e-2  8.97e+1  1.59e+1  5.60e+0
  75   8  62 1.5 0.57     67.1   3.10e+0  4.04e+0  9.78e+2  3.04e+3  3.96e+3   6.09e-2  3.48e-2  9.78e+2  5.96e+1  3.41e+1
  75   3  92 1.5 0.57     94.9   3.17e+0  5.45e+0  6.54e+2  2.07e+3  3.56e+3   4.90e-2  2.73e-2  6.54e+2  3.20e+1  1.78e+1
  75  16  92 1.5 0.57     90.0   3.08e+0  2.48e+0  7.26e+2  2.24e+3  1.80e+3   2.70e-2  5.83e-2  7.26e+2  1.96e+1  4.24e+1
  75  36 120 1.5 0.57    118.9   2.78e+0  2.50e+0  4.71e+2  1.31e+3  1.18e+3   4.03e-2  2.20e-2  4.71e+2  1.90e+1  1.04e+1
  75  32 180 1.5 0.57    178.6   7.89e+0  6.56e+0  2.87e+2  2.26e+3  1.88e+3   7.97e-2  4.00e-2  2.87e+2  2.29e+1  1.15e+1
  75  28 240 1.5 0.57    238.5   2.32e+0  4.40e+0  1.96e+2  4.56e+2  8.64e+2   1.42e-1  6.09e-2  1.96e+2  2.78e+1  1.20e+1
  75  48 340 1.5 0.57    338.3   4.04e+0  6.72e+0  8.84e+1  3.57e+2  5.94e+2   1.97e-1  1.15e-1  8.84e+1  1.74e+1  1.02e+1
  75  44 370 1.5 0.57    368.3   4.03e+0  1.40e+1  9.61e+1  3.87e+2  1.35e+3   2.32e-1  1.82e-1  9.61e+1  2.23e+1  1.75e+1
  75  40 400 1.5 0.57    398.3   3.40e+0  5.43e+0  8.33e+1  2.83e+2  4.52e+2   1.71e-1  6.11e-2  8.33e+1  1.42e+1  5.08e+0
  77   8  62 1.5 0.57     67.1   3.08e+0  3.97e+0  1.12e+3  3.44e+3  4.44e+3   5.42e-2  3.51e-2  1.12e+3  6.06e+1  3.92e+1
  77   3  92 1.5 0.57     94.9   3.38e+0  6.07e+0  6.52e+2  2.20e+3  3.96e+3   5.12e-2  3.02e-2  6.52e+2  3.34e+1  1.97e+1
  77  16  92 1.5 0.57     90.0   3.08e+0  2.56e+0  7.74e+2  2.38e+3  1.98e+3   2.60e-2  5.55e-2  7.74e+2  2.01e+1  4.30e+1
  77  36 120 1.5 0.57    118.9   2.72e+0  2.49e+0  5.36e+2  1.45e+3  1.33e+3   3.54e-2  1.94e-2  5.36e+2  1.90e+1  1.04e+1
  77  32 180 1.5 0.57    178.6   7.80e+0  6.54e+0  3.23e+2  2.52e+3  2.11e+3   7.49e-2  3.64e-2  3.23e+2  2.42e+1  1.17e+1
  77  28 240 1.5 0.57    238.5   2.36e+0  4.23e+0  2.40e+2  5.66e+2  1.01e+3   8.95e-2  4.76e-2  2.40e+2  2.14e+1  1.14e+1
  77  48 340 1.5 0.57    338.3   3.98e+0  6.76e+0  1.07e+2  4.28e+2  7.26e+2   1.70e-1  8.31e-2  1.07e+2  1.83e+1  8.92e+0
  77  44 370 1.5 0.57    368.3   4.59e+0  1.82e+1  9.68e+1  4.44e+2  1.77e+3   2.38e-1  1.79e-1  9.68e+1  2.30e+1  1.73e+1
  77  40 400 1.5 0.57    398.3   3.49e+0  5.26e+0  1.03e+2  3.59e+2  5.41e+2   1.37e-1  4.90e-2  1.03e+2  1.41e+1  5.04e+0
  79   8  62 1.5 0.57     67.1   2.97e+0  3.72e+0  1.06e+3  3.15e+3  3.95e+3   5.54e-2  3.59e-2  1.06e+3  5.88e+1  3.81e+1
  79   3  92 1.5 0.57     94.9   3.06e+0  4.84e+0  7.04e+2  2.16e+3  3.41e+3   4.78e-2  2.89e-2  7.04e+2  3.37e+1  2.03e+1
  79  16  92 1.5 0.57     90.0   3.41e+0  2.63e+0  7.53e+2  2.57e+3  1.98e+3   3.11e-2  6.27e-2  7.53e+2  2.34e+1  4.72e+1
  79  36 120 1.5 0.57    118.9   3.07e+0  2.70e+0  4.67e+2  1.44e+3  1.26e+3   4.73e-2  2.72e-2  4.67e+2  2.21e+1  1.27e+1
  79  32 180 1.5 0.57    178.6   7.57e+0  6.69e+0  2.95e+2  2.23e+3  1.97e+3   9.37e-2  4.86e-2  2.95e+2  2.76e+1  1.43e+1
  79  28 240 1.5 0.57    238.5   2.28e+0  4.46e+0  2.07e+2  4.71e+2  9.22e+2   1.26e-1  6.86e-2  2.07e+2  2.61e+1  1.42e+1
  79  48 340 1.5 0.57    338.3   4.50e+0  7.30e+0  7.94e+1  3.57e+2  5.80e+2   2.91e-1  1.54e-1  7.94e+1  2.31e+1  1.22e+1
  79  44 370 1.5 0.57    368.3   3.82e+0  1.60e+1  8.44e+1  3.22e+2  1.35e+3   2.86e-1  2.25e-1  8.44e+1  2.41e+1  1.90e+1
  79  40 400 1.5 0.57    398.3   3.24e+0  5.76e+0  7.43e+1  2.41e+2  4.28e+2   2.21e-1  9.56e-2  7.43e+1  1.64e+1  7.11e+0
];
MD05Gravel05 = [...
  44   8  62 3.0 0.57     67.0   2.93e+0  4.72e+0  1.09e+3  3.21e+3  5.17e+3   4.56e-2  3.27e-2  1.09e+3  4.99e+1  3.58e+1
  44   3  92 3.0 0.57     97.0   2.22e+0  4.75e+0  6.27e+2  1.39e+3  2.98e+3   4.33e-2  3.18e-2  6.27e+2  2.72e+1  2.00e+1
  44  16  92 3.0 0.57    101.5   2.70e+0  2.32e+0  6.86e+2  1.85e+3  1.59e+3   1.74e-2  4.70e-2  6.86e+2  1.20e+1  3.22e+1
  44  36 120 3.0 0.57    125.9   2.67e+0  2.69e+0  4.52e+2  1.20e+3  1.22e+3   4.15e-2  2.32e-2  4.52e+2  1.87e+1  1.05e+1
  44  32 180 3.0 0.57    185.6   7.98e+0  6.01e+0  2.79e+2  2.23e+3  1.68e+3   6.66e-2  4.24e-2  2.79e+2  1.86e+1  1.18e+1
  44  28 240 3.0 0.57    245.5   2.39e+0  3.93e+0  1.72e+2  4.10e+2  6.75e+2   1.44e-1  7.73e-2  1.72e+2  2.47e+1  1.33e+1
  44  48 340 3.0 0.57    345.3   3.77e+0  6.03e+0  8.15e+1  3.07e+2  4.91e+2   2.73e-1  1.56e-1  8.15e+1  2.23e+1  1.28e+1
  44  44 370 3.0 0.57    375.3   3.34e+0  1.32e+1  9.36e+1  3.12e+2  1.23e+3   2.55e-1  2.25e-1  9.36e+1  2.39e+1  2.11e+1
  44  40 400 3.0 0.57    405.3   3.63e+0  4.91e+0  8.03e+1  2.92e+2  3.94e+2   1.50e-1  6.49e-2  8.03e+1  1.21e+1  5.22e+0
  46   8  62 3.0 0.57     67.0   2.90e+0  4.74e+0  9.27e+2  2.68e+3  4.39e+3   5.94e-2  4.24e-2  9.27e+2  5.51e+1  3.93e+1
  46   3  92 3.0 0.57     97.0   2.06e+0  4.85e+0  5.68e+2  1.17e+3  2.76e+3   5.36e-2  3.33e-2  5.68e+2  3.05e+1  1.89e+1
  46  16  92 3.0 0.57    101.5   2.74e+0  2.01e+0  5.58e+2  1.53e+3  1.12e+3   2.20e-2  6.03e-2  5.58e+2  1.23e+1  3.36e+1
  46  36 120 3.0 0.57    125.9   2.32e+0  2.42e+0  3.96e+2  9.19e+2  9.57e+2   5.25e-2  2.94e-2  3.96e+2  2.08e+1  1.16e+1
  46  32 180 3.0 0.57    185.6   7.47e+0  5.63e+0  2.48e+2  1.85e+3  1.39e+3   7.83e-2  4.77e-2  2.48e+2  1.94e+1  1.18e+1
  46  28 240 3.0 0.57    245.5   2.19e+0  3.42e+0  1.74e+2  3.83e+2  5.97e+2   1.54e-1  8.11e-2  1.74e+2  2.69e+1  1.41e+1
  46  48 340 3.0 0.57    345.3   3.42e+0  5.32e+0  7.61e+1  2.60e+2  4.05e+2   3.07e-1  1.67e-1  7.61e+1  2.33e+1  1.27e+1
  46  44 370 3.0 0.57    375.3   3.16e+0  1.21e+1  8.74e+1  2.76e+2  1.05e+3   2.82e-1  2.66e-1  8.74e+1  2.47e+1  2.32e+1
  46  40 400 3.0 0.57    405.3   3.39e+0  4.40e+0  7.99e+1  2.71e+2  3.51e+2   1.65e-1  6.80e-2  7.99e+1  1.32e+1  5.43e+0
  82   8  62 3.0 0.57     67.0   2.77e+0  4.46e+0  9.86e+2  2.73e+3  4.39e+3   6.11e-2  4.35e-2  9.86e+2  6.02e+1  4.29e+1
  82   3  92 3.0 0.57     97.0   2.27e+0  5.48e+0  5.73e+2  1.30e+3  3.14e+3   6.01e-2  3.66e-2  5.73e+2  3.44e+1  2.10e+1
  82  16  92 3.0 0.57    101.5   2.97e+0  2.72e+0  6.00e+2  1.78e+3  1.63e+3   2.26e-2  6.13e-2  6.00e+2  1.36e+1  3.68e+1
  82  36 120 3.0 0.57    125.9   2.53e+0  2.47e+0  4.44e+2  1.12e+3  1.10e+3   4.88e-2  2.86e-2  4.44e+2  2.17e+1  1.27e+1
  82  32 180 3.0 0.57    185.6   7.93e+0  6.06e+0  2.77e+2  2.20e+3  1.68e+3   7.70e-2  5.29e-2  2.77e+2  2.13e+1  1.47e+1
  82  28 240 3.0 0.57    245.5   2.35e+0  3.57e+0  2.05e+2  4.81e+2  7.33e+2   1.45e-1  7.46e-2  2.05e+2  2.97e+1  1.53e+1
  82  48 340 3.0 0.57    345.3   3.71e+0  5.79e+0  8.90e+1  3.30e+2  5.15e+2   2.90e-1  1.59e-1  8.90e+1  2.58e+1  1.42e+1
  82  44 370 3.0 0.57    375.3   3.42e+0  1.30e+1  9.95e+1  3.40e+2  1.29e+3   2.76e-1  2.62e-1  9.95e+1  2.75e+1  2.61e+1
  82  40 400 3.0 0.57    405.3   3.69e+0  4.71e+0  8.52e+1  3.14e+2  4.01e+2   1.69e-1  6.49e-2  8.52e+1  1.44e+1  5.53e+0
  84   8  62 3.0 0.57     67.0   2.91e+0  4.41e+0  8.59e+2  2.50e+3  3.79e+3   6.81e-2  4.50e-2  8.59e+2  5.85e+1  3.87e+1
  84   3  92 3.0 0.57     97.0   2.03e+0  4.58e+0  5.93e+2  1.21e+3  2.71e+3   5.63e-2  3.40e-2  5.93e+2  3.34e+1  2.02e+1
  84  20  62 3.0 0.57     73.4   1.77e+0  4.02e+0  1.03e+3  1.83e+3  4.16e+3   4.26e-2  3.59e-2  1.03e+3  4.40e+1  3.72e+1
  84  16  92 3.0 0.57    101.5   3.09e+0  2.95e+0  5.18e+2  1.60e+3  1.53e+3   2.53e-2  7.11e-2  5.18e+2  1.31e+1  3.68e+1
  84  36 120 3.0 0.57    125.9   2.67e+0  2.73e+0  3.45e+2  9.21e+2  9.40e+2   6.25e-2  3.36e-2  3.45e+2  2.16e+1  1.16e+1
  84  32 180 3.0 0.57    185.6   7.80e+0  6.50e+0  2.19e+2  1.71e+3  1.43e+3   1.02e-1  5.96e-2  2.19e+2  2.23e+1  1.31e+1
  84  28 240 3.0 0.57    245.5   2.27e+0  3.93e+0  1.52e+2  3.46e+2  5.97e+2   2.02e-1  1.13e-1  1.52e+2  3.06e+1  1.72e+1
  84  48 340 3.0 0.57    345.3   4.01e+0  6.49e+0  5.56e+1  2.23e+2  3.60e+2   4.31e-1  2.46e-1  5.56e+1  2.40e+1  1.37e+1
  84  44 370 3.0 0.57    375.3   3.32e+0  1.26e+1  6.35e+1  2.11e+2  8.00e+2   4.11e-1  3.63e-1  6.35e+1  2.61e+1  2.31e+1
  84  40 400 3.0 0.57    405.3   2.83e+0  4.56e+0  5.15e+1  1.46e+2  2.35e+2   2.68e-1  1.09e-1  5.15e+1  1.38e+1  5.63e+0
  86   8  62 3.0 0.57     67.0   2.78e+0  5.01e+0  8.02e+2  2.23e+3  4.02e+3   7.93e-2  4.82e-2  8.02e+2  6.36e+1  3.87e+1
  86   3  92 3.0 0.57     97.0   2.02e+0  3.60e+0  5.37e+2  1.09e+3  1.93e+3   6.70e-2  4.02e-2  5.37e+2  3.60e+1  2.16e+1
  86  20  62 3.0 0.57     73.4   2.29e+0  5.71e+0  6.22e+2  1.43e+3  3.55e+3   7.81e-2  5.89e-2  6.22e+2  4.86e+1  3.66e+1
  86  16  92 3.0 0.57    101.5   3.21e+0  2.39e+0  4.36e+2  1.40e+3  1.04e+3   4.62e-2  8.98e-2  4.36e+2  2.01e+1  3.91e+1
  86  32 180 3.0 0.57    185.6   7.10e+0  6.06e+0  2.17e+2  1.54e+3  1.32e+3   1.11e-1  6.67e-2  2.17e+2  2.42e+1  1.45e+1
  86  28 240 3.0 0.57    245.5   2.18e+0  3.78e+0  1.57e+2  3.42e+2  5.93e+2   1.89e-1  1.10e-1  1.57e+2  2.96e+1  1.72e+1
  86  48 340 3.0 0.57    345.3   3.51e+0  5.39e+0  6.55e+1  2.30e+2  3.53e+2   4.08e-1  2.09e-1  6.55e+1  2.67e+1  1.37e+1
  86  44 370 3.0 0.57    375.3   3.34e+0  1.18e+1  7.28e+1  2.43e+2  8.57e+2   3.55e-1  3.69e-1  7.28e+1  2.58e+1  2.68e+1
  86  40 400 3.0 0.57    405.3   3.21e+0  4.66e+0  6.22e+1  1.99e+2  2.90e+2   2.40e-1  1.03e-1  6.22e+1  1.49e+1  6.38e+0
  70   8  62 1.0 0.57     67.0   2.49e+0  4.58e+0  7.27e+2  1.81e+3  3.33e+3   9.15e-2  6.21e-2  7.27e+2  6.65e+1  4.52e+1
 % Rec Chan rx  sz size      Dist   Vratio   Hratio   Pmax     Vmax     Hmax      Vratio   Hratio   Pmax     Vmax     Hmax
  70   3  92 1.0 0.57     97.0   2.30e+0  5.20e+0  4.71e+2  1.08e+3  2.45e+3   7.53e-2  4.13e-2  4.71e+2  3.55e+1  1.94e+1
  70  16  92 1.0 0.57    101.5   3.06e+0  2.16e+0  5.25e+2  1.60e+3  1.13e+3   2.76e-2  6.89e-2  5.25e+2  1.45e+1  3.61e+1
  70  36 120 1.0 0.57    125.9   2.53e+0  2.65e+0  3.46e+2  8.76e+2  9.18e+2   7.02e-2  3.52e-2  3.46e+2  2.43e+1  1.22e+1
  70  32 180 1.0 0.57    185.6   7.87e+0  6.17e+0  2.28e+2  1.79e+3  1.41e+3   9.42e-2  5.75e-2  2.28e+2  2.14e+1  1.31e+1
  70  28 240 1.0 0.57    245.5   2.07e+0  3.81e+0  1.65e+2  3.42e+2  6.29e+2   1.85e-1  8.27e-2  1.65e+2  3.06e+1  1.37e+1
```

```
  70  48 340 1.0 0.57    345.3   3.65e+0  5.73e+0  7.53e+1  2.75e+2  4.31e+2   3.41e-1  1.85e-1  7.53e+1  2.56e+1  1.39e+1
  70  44 370 1.0 0.57    375.3   3.37e+0  1.19e+1  8.57e+1  2.89e+2  1.02e+3   3.17e-1  2.35e-1  8.57e+1  2.72e+1  2.02e+1
  70  40 400 1.0 0.57    405.3   3.32e+0  4.78e+0  7.30e+1  2.43e+2  3.49e+2   1.91e-1  7.78e-2  7.30e+1  1.40e+1  5.68e+0
  72   8  62 1.0 0.57     67.0   2.42e+0  4.26e+0  7.23e+2  1.75e+3  3.08e+3   9.67e-2  5.82e-2  7.23e+2  6.99e+1  4.20e+1
  72   3  92 1.0 0.57     97.0   2.54e+0  5.08e+0  4.39e+2  1.12e+3  2.23e+3   8.44e-2  4.28e-2  4.39e+2  3.71e+1  1.88e+1
  72  16  92 1.0 0.57    101.5   3.31e+0  2.42e+0  5.09e+2  1.68e+3  1.23e+3   2.85e-2  7.86e-2  5.09e+2  1.45e+1  4.01e+1
  72  36 120 1.0 0.57    125.9   2.61e+0  2.74e+0  3.42e+2  8.92e+2  9.38e+2   7.41e-2  3.41e-2  3.42e+2  2.53e+1  1.17e+1
  72  32 180 1.0 0.57    185.6   7.86e+0  6.51e+0  2.24e+2  1.76e+3  1.46e+3   1.03e-1  6.10e-2  2.24e+2  2.32e+1  1.37e+1
  72  28 240 1.0 0.57    245.5   2.03e+0  4.04e+0  1.52e+2  3.10e+2  6.15e+2   2.11e-1  1.08e-1  1.52e+2  3.21e+1  1.64e+1
  72  48 340 1.0 0.57    345.3   3.82e+0  5.83e+0  7.19e+1  2.74e+2  4.19e+2   3.72e-1  2.07e-1  7.19e+1  2.67e+1  1.49e+1
  72  44 370 1.0 0.57    375.3   3.36e+0  1.20e+1  8.06e+1  2.71e+2  9.69e+2   3.55e-1  2.69e-1  8.06e+1  2.87e+1  2.17e+1
  72  40 400 1.0 0.57    405.3   3.14e+0  4.70e+0  7.04e+1  2.21e+2  3.31e+2   2.10e-1  8.33e-2  7.04e+1  1.48e+1  5.87e+0
  74   8  62 1.5 0.57     67.0   2.53e+0  4.31e+0  7.80e+2  1.97e+3  3.36e+3   9.47e-2  6.16e-2  7.80e+2  7.39e+1  4.80e+1
  74   3  92 1.5 0.57     97.0   2.42e+0  4.96e+0  4.87e+2  1.18e+3  2.41e+3   7.78e-2  4.22e-2  4.87e+2  3.79e+1  2.05e+1
  74  16  92 1.5 0.57    101.5   3.12e+0  2.42e+0  5.44e+2  1.69e+3  1.32e+3   3.03e-2  7.33e-2  5.44e+2  1.65e+1  3.99e+1
  74  36 120 1.5 0.57    125.9   2.49e+0  2.73e+0  3.60e+2  8.97e+2  9.81e+2   7.31e-2  4.19e-2  3.60e+2  2.63e+1  1.51e+1
  74  32 180 1.5 0.57    185.6   7.69e+0  6.43e+0  2.26e+2  1.74e+3  1.45e+3   1.04e-1  6.24e-2  2.26e+2  2.35e+1  1.41e+1
  74  28 240 1.5 0.57    245.5   2.08e+0  3.86e+0  1.55e+2  3.23e+2  5.98e+2   2.07e-1  9.62e-2  1.55e+2  3.20e+1  1.49e+1
  74  48 340 1.5 0.57    345.3   3.78e+0  5.84e+0  6.83e+1  2.58e+2  3.99e+2   3.94e-1  2.10e-1  6.83e+1  2.69e+1  1.43e+1
  74  44 370 1.5 0.57    375.3   3.24e+0  1.19e+1  7.84e+1  2.54e+2  9.36e+2   3.56e-1  2.77e-1  7.84e+1  2.79e+1  2.17e+1
  74  40 400 1.5 0.57    405.3   3.27e+0  4.69e+0  6.67e+1  2.18e+2  3.13e+2   2.40e-1  9.45e-2  6.67e+1  1.60e+1  6.30e+0
  88   8  62 1.0 0.57     67.0   2.63e+0  4.19e+0  7.46e+2  1.96e+3  3.13e+3   9.28e-2  6.06e-2  7.46e+2  6.93e+1  4.53e+1
  88   3  92 1.0 0.57     97.0   2.24e+0  4.47e+0  4.99e+2  1.12e+3  2.23e+3   8.04e-2  3.93e-2  4.99e+2  4.01e+1  1.96e+1
  88  20  62 1.0 0.57     73.4   2.03e+0  4.05e+0  8.39e+2  1.70e+3  3.40e+3   6.28e-2  4.15e-2  8.39e+2  5.27e+1  3.48e+1
  88  16  92 1.0 0.57    101.5   3.19e+0  2.36e+0  5.00e+2  1.59e+3  1.18e+3   2.85e-2  7.87e-2  5.00e+2  1.43e+1  3.93e+1
  88  36 120 1.0 0.57    125.9   2.70e+0  2.94e+0  3.08e+2  8.30e+2  9.06e+2   8.49e-2  5.04e-2  3.08e+2  2.61e+1  1.55e+1
  88  32 180 1.0 0.57    185.6   7.33e+0  6.38e+0  1.93e+2  1.41e+3  1.23e+3   1.28e-1  6.69e-2  1.93e+2  2.46e+1  1.29e+1
  88  28 240 1.0 0.57    245.5   1.92e+0  4.00e+0  1.32e+2  2.54e+2  5.29e+2   2.44e-1  1.35e-1  1.32e+2  3.22e+1  1.78e+1
  88  48 340 1.0 0.57    345.3   3.90e+0  6.08e+0  5.61e+1  2.19e+2  3.42e+2   4.49e-1  2.47e-1  5.61e+1  2.52e+1  1.39e+1
  88  44 370 1.0 0.57    375.3   3.53e+0  1.26e+1  6.52e+1  2.30e+2  8.22e+2   4.25e-1  3.39e-1  6.52e+1  2.77e+1  2.21e+1
  88  40 400 1.0 0.57    405.3   2.92e+0  4.78e+0  5.65e+1  1.65e+2  2.70e+2   2.89e-1  1.01e-1  5.65e+1  1.63e+1  5.72e+0
  90   8  62 1.0 0.57     67.0   2.34e+0  4.14e+0  7.12e+2  1.66e+3  2.95e+3   1.02e-1  7.21e-2  7.12e+2  7.25e+1  5.14e+1
  90   3  92 1.0 0.57     97.0   2.08e+0  4.35e+0  4.90e+2  1.02e+3  2.13e+3   8.01e-2  4.22e-2  4.90e+2  3.92e+1  2.07e+1
  90  20  62 1.0 0.57     73.4   2.23e+0  3.67e+0  7.42e+2  1.65e+3  2.73e+3   7.36e-2  4.72e-2  7.42e+2  5.46e+1  3.50e+1
  90  16  92 1.0 0.57    101.5   3.72e+0  2.67e+0  4.02e+2  1.49e+3  1.07e+3   3.65e-2  1.04e-1  4.02e+2  1.47e+1  4.16e+1
  90  36 120 1.0 0.57    125.9   2.86e+0  3.25e+0  2.45e+2  7.02e+2  7.98e+2   1.07e-1  5.94e-2  2.45e+2  2.62e+1  1.46e+1
  90  32 180 1.0 0.57    185.6   6.69e+0  5.92e+0  2.01e+2  1.34e+3  1.19e+3   1.17e-1  7.14e-2  2.01e+2  2.35e+1  1.43e+1
  90  28 240 1.0 0.57    245.5   1.88e+0  3.62e+0  1.53e+2  2.88e+2  5.54e+2   2.26e-1  1.04e-1  1.53e+2  3.46e+1  1.60e+1
  90  48 340 1.0 0.57    345.3   3.91e+0  6.00e+0  6.25e+1  2.44e+2  3.75e+2   4.40e-1  2.73e-1  6.25e+1  2.75e+1  1.71e+1
  90  44 370 1.0 0.57    375.3   3.76e+0  1.25e+1  6.98e+1  2.63e+2  8.72e+2   4.09e-1  3.36e-1  6.98e+1  2.85e+1  2.35e+1
  90  40 400 1.0 0.57    405.3   3.32e+0  5.06e+0  6.09e+1  2.02e+2  3.08e+2   2.54e-1  1.08e-1  6.09e+1  1.55e+1  6.58e+0
  92   8  62 1.0 0.57     67.0   2.52e+0  4.20e+0  8.46e+2  2.13e+3  3.56e+3   8.72e-2  5.67e-2  8.46e+2  7.38e+1  4.80e+1
  92   3  92 1.0 0.57     97.0   2.54e+0  4.84e+0  5.07e+2  1.29e+3  2.45e+3   7.90e-2  4.06e-2  5.07e+2  4.01e+1  2.06e+1
  92  20  62 1.0 0.57     73.4   1.98e+0  3.70e+0  9.74e+2  1.93e+3  3.60e+3   5.90e-2  4.25e-2  9.74e+2  5.75e+1  4.14e+1
  92  16  92 1.0 0.57    101.5   2.92e+0  2.18e+0  6.20e+2  1.81e+3  1.35e+3   2.64e-2  6.83e-2  6.20e+2  1.63e+1  4.23e+1
  92  36 120 1.0 0.57    125.9   2.77e+0  3.12e+0  3.60e+2  9.97e+2  1.12e+3   7.52e-2  4.13e-2  3.60e+2  2.70e+1  1.49e+1
  92  32 180 1.0 0.57    185.6   7.82e+0  6.20e+0  2.58e+2  2.02e+3  1.60e+3   9.38e-2  5.09e-2  2.58e+2  2.42e+1  1.31e+1
  92  28 240 1.0 0.57    245.5   2.15e+0  3.82e+0  1.72e+2  3.69e+2  6.57e+2   2.02e-1  9.33e-2  1.72e+2  3.47e+1  1.60e+1
  92  48 340 1.0 0.57    345.3   4.21e+0  5.94e+0  7.73e+1  3.25e+2  4.59e+2   3.55e-1  1.87e-1  7.73e+1  2.74e+1  1.45e+1
  92  44 370 1.0 0.57    375.3   3.24e+0  1.26e+1  8.87e+1  2.87e+2  1.12e+3   3.44e-1  2.58e-1  8.87e+1  3.05e+1  2.28e+1
  92  40 400 1.0 0.57    405.3   3.26e+0  5.06e+0  7.77e+1  2.53e+2  3.93e+2   1.98e-1  7.27e-2  7.77e+1  1.54e+1  5.64e+0
];

MD05Gravel02 = [...
  39   8  62 1.5 0.57     60.0   3.29e+0  4.38e+0  1.37e+3  4.52e+3  6.02e+3   4.05e-2  4.14e-2  1.37e+3  5.57e+1  5.69e+1
  39   3  92 1.5 0.57     90.0   2.49e+0  5.74e+0  7.56e+2  1.88e+3  4.34e+3   4.00e-2  3.97e-2  7.56e+2  3.03e+1  3.00e+1
  39  16  92 1.5 0.57     94.9   3.41e+0  2.34e+0  8.00e+2  2.73e+3  1.87e+3   1.59e-2  3.51e-2  8.00e+2  1.27e+1  2.81e+1
  39  32 180 1.5 0.57    178.6   8.30e+0  6.45e+0  3.54e+2  2.94e+3  2.29e+3   4.30e-2  3.52e-2  3.54e+2  1.52e+1  1.25e+1
  39  28 240 1.5 0.57    238.5   2.44e+0  4.19e+0  2.39e+2  5.81e+2  9.99e+2   1.06e-1  5.27e-2  2.39e+2  2.54e+1  1.26e+1
  39  48 340 1.5 0.57    338.3   4.56e+0  7.35e+0  9.40e+1  4.28e+2  6.91e+2   2.12e-1  1.01e-1  9.40e+1  1.99e+1  9.50e+0
  39  44 370 1.5 0.57    368.3   3.80e+0  1.65e+1  1.02e+2  3.88e+2  1.68e+3   2.32e-1  1.83e-1  1.02e+2  2.37e+1  1.87e+1
  39  40 400 1.5 0.57    398.3   3.71e+0  5.54e+0  9.33e+1  3.46e+2  5.17e+2   1.20e-1  5.91e-2  9.33e+1  1.12e+1  5.51e+0
  76   8  62 1.5 0.57     60.0   2.80e+0  4.41e+0  1.28e+3  3.58e+3  5.65e+3   4.50e-2  4.62e-2  1.28e+3  5.75e+1  5.91e+1
  76   3  92 1.5 0.57     90.0   2.25e+0  4.91e+0  7.72e+2  1.74e+3  3.79e+3   4.06e-2  4.21e-2  7.72e+2  3.13e+1  3.25e+1
  76  16  92 1.5 0.57     94.9   3.11e+0  2.55e+0  6.70e+2  2.08e+3  1.71e+3   1.72e-2  4.03e-2  6.70e+2  1.15e+1  2.70e+1
  76  36 120 1.5 0.57    118.9   2.50e+0  2.57e+0  5.58e+2  1.40e+3  1.44e+3   3.13e-2  1.99e-2  5.58e+2  1.75e+1  1.11e+1
  76  32 180 1.5 0.57    178.6   8.12e+0  6.32e+0  3.43e+2  2.78e+3  2.17e+3   4.63e-2  3.08e-2  3.43e+2  1.59e+1  1.06e+1
  76  28 240 1.5 0.57    238.5   2.32e+0  4.17e+0  1.97e+2  4.57e+2  8.22e+2   1.13e-1  5.07e-2  1.97e+2  2.22e+1  1.00e+1
  76  48 340 1.5 0.57    338.3   3.89e+0  6.21e+0  8.85e+1  3.44e+2  5.49e+2   2.10e-1  1.10e-1  8.85e+1  1.86e+1  9.76e+0
  76  44 370 1.5 0.57    368.3   3.47e+0  1.29e+1  9.64e+1  3.35e+2  1.24e+3   2.16e-1  1.76e-1  9.64e+1  2.08e+1  1.70e+1
  76  40 400 1.5 0.57    398.3   3.51e+0  4.96e+0  9.08e+1  3.18e+2  4.50e+2   1.19e-1  5.59e-2  9.08e+1  1.08e+1  5.08e+0
  78   8  62 1.5 0.57     60.0   3.03e+0  4.19e+0  1.20e+3  3.66e+3  5.05e+3   4.99e-2  5.19e-2  1.20e+3  6.01e+1  6.26e+1
  78   3  92 1.5 0.57     90.0   2.54e+0  4.93e+0  7.21e+2  1.83e+3  3.56e+3   4.72e-2  4.60e-2  7.21e+2  3.41e+1  3.32e+1
  78  16  92 1.5 0.57     94.9   3.32e+0  2.49e+0  6.83e+2  2.26e+3  1.70e+3   1.72e-2  4.46e-2  6.83e+2  1.17e+1  3.05e+1
  78  36 120 1.5 0.57    118.9   2.49e+0  2.90e+0  5.00e+2  1.25e+3  1.45e+3   3.96e-2  2.17e-2  5.00e+2  1.98e+1  1.09e+1
  78  32 180 1.5 0.57    178.6   8.28e+0  6.37e+0  3.13e+2  2.59e+3  1.99e+3   6.14e-2  3.76e-2  3.13e+2  1.92e+1  1.18e+1
  78  28 240 1.5 0.57    238.5   2.13e+0  4.12e+0  2.11e+2  4.50e+2  8.70e+2   1.13e-1  4.71e-2  2.11e+2  2.38e+1  9.93e+0
  78  48 340 1.5 0.57    338.3   4.40e+0  7.22e+0  8.47e+1  3.72e+2  6.11e+2   2.18e-1  9.67e-2  8.47e+1  1.85e+1  8.18e+0
  78  44 370 1.5 0.57    368.3   3.53e+0  1.37e+1  9.63e+1  3.40e+2  1.32e+3   2.22e-1  1.78e-1  9.63e+1  2.13e+1  1.71e+1
  78  40 400 1.5 0.57    398.3   3.61e+0  5.68e+0  8.40e+1  3.03e+2  4.77e+2   1.30e-1  5.53e-2  8.40e+1  1.09e+1  4.64e+0
  80   8  62 1.5 0.57     60.0   2.71e+0  4.16e+0  1.20e+3  3.25e+3  5.00e+3   5.25e-2  5.39e-2  1.20e+3  6.30e+1  6.46e+1
  80   3  92 1.5 0.57     90.0   2.34e+0  4.94e+0  7.25e+2  1.69e+3  3.58e+3   4.37e-2  4.51e-2  7.25e+2  3.17e+1  3.27e+1
  80  16  92 1.5 0.57     94.9   3.63e+0  2.74e+0  5.63e+2  2.04e+3  1.54e+3   2.40e-2  5.05e-2  5.63e+2  1.35e+1  2.84e+1
  80  36 120 1.5 0.57    118.9   2.76e+0  2.95e+0  4.48e+2  1.24e+3  1.32e+3   4.22e-2  2.87e-2  4.48e+2  1.89e+1  1.28e+1
  80  32 180 1.5 0.57    178.6   8.08e+0  6.57e+0  3.21e+2  2.60e+3  2.11e+3   5.13e-2  3.27e-2  3.21e+2  1.65e+1  1.05e+1
  80  28 240 1.5 0.57    238.5   2.27e+0  3.89e+0  2.35e+2  5.33e+2  9.13e+2   1.04e-1  4.87e-2  2.35e+2  2.43e+1  1.14e+1
  80  48 340 1.5 0.57    338.3   3.84e+0  6.24e+0  9.13e+1  3.51e+2  5.70e+2   2.08e-1  1.09e-1  9.13e+1  1.90e+1  9.95e+0
  80  44 370 1.5 0.57    368.3   3.35e+0  1.25e+1  9.74e+1  3.26e+2  1.22e+3   2.39e-1  1.88e-1  9.74e+1  2.33e+1  1.83e+1
  80  40 400 1.5 0.57    398.3   3.45e+0  5.16e+0  7.98e+1  2.75e+2  4.12e+2   1.41e-1  6.09e-2  7.98e+1  1.12e+1  4.86e+0
];

%Test 4 - Tropical Vegetation -----------------------------
% Rec Chan rx  sz size      Dist   Vratio   Hratio   Pmax      Vmax      Hmax       Vratio   Hratio   Pmax      Vmax      Hmax
FL02brk8 = [...
 230   8  30 1.5 4.55      30.0   5.65e+0  5.40e+0  7.74e+3  4.37e+4  4.18e+4   8.28e-2  2.52e-2  7.74e+3  6.41e+2  1.95e+2
```

```
 230  13  60 1.5 4.55     60.0   1.41e+1  6.64e+0  3.05e+3  4.29e+4  2.02e+4   6.09e-2  2.19e-2  3.05e+3  1.86e+2  6.66e+1
 230  28  75 1.5 4.55     75.0   1.00e+1  7.38e+0  2.33e+3  2.33e+4  1.72e+4   1.10e-1  7.80e-2  2.33e+3  2.57e+2  1.82e+2
 230  17  90 1.5 4.55     90.0   6.88e+0  6.11e+0  1.96e+3  1.35e+4  1.20e+4   9.19e-2  6.45e-2  1.96e+3  1.80e+2  1.26e+2
 230  21 100 1.5 4.55    100.0   3.32e+0  3.20e+0  1.70e+3  5.65e+3  5.45e+3   1.44e-1  5.06e-2  1.70e+3  2.45e+2  8.62e+1
 232   8  30 0.0 4.55     30.0   7.22e+0  4.98e+0  6.05e+3  4.37e+4  3.01e+4   6.16e-2  2.51e-2  6.05e+3  3.73e+2  1.52e+2
 232  13  60 0.0 4.55     60.0   1.53e+1  6.51e+0  2.38e+3  3.64e+4  1.55e+4   7.87e-2  3.07e-2  2.38e+3  1.87e+2  7.30e+1
 232  28  75 0.0 4.55     75.0   1.07e+1  8.12e+0  1.78e+3  1.90e+4  1.44e+4   7.85e-2  7.32e-2  1.78e+3  1.39e+2  1.30e+2
 232  17  90 0.0 4.55     90.0   7.04e+0  6.52e+0  1.48e+3  1.04e+4  9.64e+3   8.76e-2  3.52e-2  1.48e+3  1.30e+2  5.20e+1
 232  21 100 0.0 4.55    100.0   3.20e+0  3.47e+0  1.27e+3  4.07e+3  4.41e+3   1.34e-1  4.81e-2  1.27e+3  1.71e+2  6.12e+1
 258   8  30 0.0 4.55     30.0   6.06e+0  4.97e+0  7.21e+3  4.37e+4  3.59e+4   5.54e-2  3.04e-2  7.21e+3  3.99e+2  2.19e+2
 258  13  60 0.0 4.55     60.0   1.44e+1  5.34e+0  2.85e+3  4.09e+4  1.52e+4   7.52e-2  3.00e-2  2.85e+3  2.14e+2  8.53e+1
 258  28  75 0.0 4.55     75.0   9.87e+0  7.14e+0  2.17e+3  2.14e+4  1.55e+4   9.00e-2  6.85e-2  2.17e+3  1.95e+2  1.49e+2
 258  17  90 0.0 4.55     90.0   6.77e+0  5.54e+0  1.77e+3  1.20e+4  9.82e+3   9.48e-2  4.00e-2  1.77e+3  1.68e+2  7.09e+1
 258  21 100 0.0 4.55    100.0   3.20e+0  2.88e+0  1.54e+3  4.91e+3  4.42e+3   1.40e-1  7.46e-2  1.54e+3  2.16e+2  1.15e+2
];
FL02brk4 = [...
 257   8  30 0.0 2.27     30.0   9.06e+0  5.31e+0  4.82e+3  4.37e+4  2.56e+4   5.95e-2  2.89e-2  4.82e+3  2.87e+2  1.39e+2
 257  13  60 0.0 2.27     60.0   1.56e+1  6.21e+0  2.00e+3  3.13e+4  1.24e+4   7.78e-2  2.54e-2  2.00e+3  1.56e+2  5.08e+1
 257  28  75 0.0 2.27     75.0   1.07e+1  8.96e+0  1.56e+3  1.67e+4  1.40e+4   7.53e-2  4.73e-2  1.56e+3  1.17e+2  7.37e+1
 257  17  90 0.0 2.27     90.0   7.09e+0  6.64e+0  1.29e+3  9.14e+3  8.56e+3   5.82e-2  3.45e-2  1.29e+3  7.51e+1  4.44e+1
 257  21 100 0.0 2.27    100.0   3.10e+0  3.13e+0  1.10e+3  3.40e+3  3.43e+3   1.32e-1  3.52e-2  1.10e+3  1.45e+2  3.86e+1
];
FL02brk1 = [...
 222   8  30 1.5 0.57     30.0   1.11e+1  6.22e+0  2.24e+3  2.49e+4  1.39e+4   7.14e-2  2.63e-2  2.24e+3  1.60e+2  5.89e+1
 222  13  60 1.5 0.57     60.0   1.94e+1  7.98e+0  8.32e+2  1.61e+4  6.63e+3   7.30e-2  3.09e-2  8.32e+2  6.08e+1  2.57e+1
 222  28  75 1.5 0.57     75.0   1.35e+1  9.97e+0  7.34e+2  9.91e+3  7.32e+3   9.66e-2  5.52e-2  7.34e+2  7.09e+1  4.05e+1
 222  17  90 1.5 0.57     90.0   7.71e+0  7.11e+0  6.13e+2  4.73e+3  4.36e+3   6.21e-2  3.49e-2  6.13e+2  3.81e+1  2.14e+1
 222  21 100 1.5 0.57    100.0   2.82e+0  2.97e+0  5.36e+2  1.51e+3  1.59e+3   1.20e-1  3.85e-2  5.36e+2  6.45e+1  2.06e+1
 225   8  30 1.5 0.57     30.0   1.09e+1  6.72e+0  2.53e+3  2.75e+4  1.70e+4   7.68e-2  2.78e-2  2.53e+3  1.94e+2  7.04e+1
 225  13  60 1.5 0.57     60.0   1.66e+1  7.13e+0  1.10e+3  1.82e+4  7.83e+3   6.42e-2  2.07e-2  1.10e+3  7.05e+1  2.27e+1
 225  28  75 1.5 0.57     75.0   1.31e+1  1.11e+1  7.91e+2  1.04e+4  8.75e+3   1.01e-1  4.60e-2  7.91e+2  7.99e+1  3.64e+1
 225  17  90 1.5 0.57     90.0   8.18e+0  7.54e+0  6.77e+2  5.54e+3  5.10e+3   6.45e-2  2.96e-2  6.77e+2  4.37e+1  2.01e+1
 225  21 100 1.5 0.57    100.0   2.93e+0  3.20e+0  5.91e+2  1.73e+3  1.89e+3   1.25e-1  2.77e-2  5.91e+2  7.37e+1  1.63e+1
 239   8  30 0.0 0.57     30.0   1.07e+1  5.12e+0  2.55e+3  2.74e+4  1.31e+4   5.20e-2  2.40e-2  2.55e+3  1.33e+2  6.12e+1
 239  13  60 0.0 0.57     60.0   1.78e+1  8.10e+0  1.01e+3  1.80e+4  8.18e+3   7.52e-2  1.75e-2  1.01e+3  7.60e+1  1.77e+1
 239  28  75 0.0 0.57     75.0   1.52e+1  1.05e+1  7.33e+2  1.11e+4  7.68e+3   1.02e-1  6.45e-2  7.33e+2  7.50e+1  4.72e+1
 239  17  90 0.0 0.57     90.0   9.14e+0  6.95e+0  6.36e+2  5.81e+3  4.42e+3   5.04e-2  2.86e-2  6.36e+2  3.21e+1  1.82e+1
 239  21 100 0.0 0.57    100.0   2.87e+0  3.06e+0  5.50e+2  1.58e+3  1.68e+3   1.22e-1  3.55e-2  5.50e+2  6.69e+1  1.95e+1
 246   8  30 0.0 0.57     30.0   1.27e+1  6.94e+0  1.91e+3  2.44e+4  1.33e+4   7.70e-2  2.67e-2  1.91e+3  1.47e+2  5.11e+1
 246  13  60 0.0 0.57     60.0   1.45e+1  6.26e+0  8.52e+2  1.24e+4  5.33e+3   7.00e-2  1.71e-2  8.52e+2  5.96e+1  1.46e+1
 246  28  75 0.0 0.57     75.0   1.61e+1  1.20e+1  6.59e+2  1.06e+4  7.92e+3   3.92e-2  1.29e-2  6.59e+2  2.59e+1  8.49e+0
 246  17  90 0.0 0.57     90.0   9.92e+0  8.08e+0  5.75e+2  5.71e+3  4.65e+3   3.22e-2  2.85e-2  5.75e+2  1.85e+1  1.64e+1
 246  21 100 0.0 0.57    100.0   3.00e+0  3.86e+0  4.97e+2  1.49e+3  1.92e+3   2.49e-2  2.10e-2  4.97e+2  1.24e+1  1.05e+1
 249   8  30 0.0 0.57     30.0   1.23e+1  6.69e+0  2.16e+3  2.67e+4  1.45e+4   6.30e-2  2.14e-2  2.16e+3  1.36e+2  4.64e+1
 249  13  60 0.0 0.57     60.0   1.73e+1  7.58e+0  9.29e+2  1.61e+4  7.04e+3   6.28e-2  1.85e-2  9.29e+2  5.83e+1  1.72e+1
 249  28  75 0.0 0.57     75.0   1.79e+1  1.32e+1  6.74e+2  1.21e+4  8.92e+3   8.97e-2  4.12e-2  6.74e+2  6.05e+1  2.77e+1
 249  17  90 0.0 0.57     90.0   1.05e+1  7.96e+0  5.90e+2  6.18e+3  4.70e+3   4.09e-2  2.77e-2  5.90e+2  2.41e+1  1.64e+1
 249  21 100 0.0 0.57    100.0   3.13e+0  4.05e+0  5.10e+2  1.60e+3  2.07e+3   1.07e-1  2.39e-2  5.10e+2  5.47e+1  1.22e+1
 250   8  30 0.0 0.57     30.0   1.23e+1  6.55e+0  1.78e+3  2.19e+4  1.17e+4   6.30e-2  2.32e-2  1.78e+3  1.12e+2  4.14e+1
 250  13  60 0.0 0.57     60.0   1.81e+1  8.07e+0  7.69e+2  1.39e+4  6.21e+3   6.08e-2  2.17e-2  7.69e+2  4.68e+1  1.67e+1
 250  28  75 0.0 0.57     75.0   1.77e+1  1.25e+1  5.57e+2  9.85e+3  6.94e+3   9.29e-2  4.43e-2  5.57e+2  5.17e+1  2.47e+1
 250  17  90 0.0 0.57     90.0   1.09e+1  7.87e+0  4.83e+2  5.29e+3  3.80e+3   3.70e-2  3.68e-2  4.83e+2  1.78e+1  1.78e+1
 250  21 100 0.0 0.57    100.0   3.40e+0  3.88e+0  4.14e+2  1.41e+3  1.61e+3   1.08e-1  2.88e-2  4.14e+2  4.47e+1  1.19e+1
 251   8  30 0.0 0.57     30.0   1.24e+1  6.82e+0  2.22e+3  2.74e+4  1.51e+4   6.46e-2  2.02e-2  2.22e+3  1.43e+2  4.47e+1
 251  13  60 0.0 0.57     60.0   1.82e+1  7.71e+0  9.66e+2  1.76e+4  7.45e+3   5.84e-2  1.87e-2  9.66e+2  5.64e+1  1.81e+1
 251  28  75 0.0 0.57     75.0   1.65e+1  1.23e+1  7.03e+2  1.16e+4  8.61e+3   8.31e-2  4.04e-2  7.03e+2  5.84e+1  2.84e+1
 251  17  90 0.0 0.57     90.0   1.05e+1  7.87e+0  6.00e+2  6.33e+3  4.72e+3   3.98e-2  2.90e-2  6.00e+2  2.39e+1  1.74e+1
 251  21 100 0.0 0.57    100.0   3.09e+0  3.89e+0  5.14e+2  1.59e+3  2.00e+3   9.61e-2  2.08e-2  5.14e+2  4.94e+1  1.07e+1
 252   8  30 0.0 0.57     30.0   1.16e+1  5.93e+0  1.81e+3  2.11e+4  1.08e+4   6.00e-2  2.37e-2  1.81e+3  1.09e+2  4.30e+1
 252  13  60 0.0 0.57     60.0   1.75e+1  6.65e+0  7.87e+2  1.38e+4  5.23e+3   7.96e-2  2.33e-2  7.87e+2  6.26e+1  1.83e+1
 252  28  75 0.0 0.57     75.0   1.48e+1  1.06e+1  5.98e+2  8.84e+3  6.36e+3   8.58e-2  4.93e-2  5.98e+2  5.13e+1  2.95e+1
 252  17  90 0.0 0.57     90.0   8.53e+0  6.89e+0  5.14e+2  4.38e+3  3.54e+3   4.92e-2  4.03e-2  5.14e+2  2.53e+1  2.07e+1
 252  21 100 0.0 0.57    100.0   2.97e+0  3.17e+0  4.38e+2  1.30e+3  1.39e+3   1.17e-1  2.85e-2  4.38e+2  5.14e+1  1.25e+1
 253   8  30 0.0 0.57     30.0   1.21e+1  6.89e+0  1.87e+3  2.27e+4  1.29e+4   6.51e-2  2.69e-2  1.87e+3  1.21e+2  5.01e+1
 253  13  60 0.0 0.57     60.0   1.74e+1  8.05e+0  8.28e+2  1.44e+4  6.67e+3   6.43e-2  1.99e-2  8.28e+2  5.32e+1  1.65e+1
 253  28  75 0.0 0.57     75.0   1.46e+1  1.23e+1  6.25e+2  9.11e+3  7.68e+3   1.06e-1  5.07e-2  6.25e+2  6.61e+1  3.16e+1
 253  17  90 0.0 0.57     90.0   9.78e+0  7.57e+0  5.51e+2  5.38e+3  4.17e+3   6.02e-2  2.89e-2  5.51e+2  3.32e+1  1.59e+1
 253  21 100 0.0 0.57    100.0   2.97e+0  3.61e+0  4.80e+2  1.43e+3  1.73e+3   1.21e-1  2.42e-2  4.80e+2  5.82e+1  1.16e+1
 256   8  30 0.0 0.57     30.0   1.20e+1  9.29e+0  2.26e+3  2.71e+4  2.09e+4   6.43e-2  2.34e-2  2.26e+3  1.45e+2  5.28e+1
 256  13  60 0.0 0.57     60.0   1.85e+1  8.86e+0  9.71e+2  1.80e+4  8.60e+3   5.59e-2  1.24e-2  9.71e+2  5.43e+1  1.20e+1
 256  28  75 0.0 0.57     75.0   1.80e+1  1.25e+1  6.98e+2  1.26e+4  8.71e+3   8.87e-2  3.80e-2  6.98e+2  6.19e+1  2.65e+1
 256  17  90 0.0 0.57     90.0   1.10e+1  7.85e+0  6.07e+2  6.66e+3  4.76e+3   3.46e-2  2.68e-2  6.07e+2  2.10e+1  1.63e+1
 256  21 100 0.0 0.57    100.0   3.47e+0  4.27e+0  4.81e+2  1.67e+3  2.05e+3   3.69e-2  2.85e-2  4.81e+2  1.77e+1  1.37e+1
 210   8  30 1.5 0.57     30.0   1.04e+1  5.49e+0  2.43e+3  2.54e+4  1.33e+4   6.58e-2  2.61e-2  2.43e+3  1.60e+2  6.35e+1
 210  13  60 1.5 0.57     60.0   1.67e+1  6.16e+0  9.76e+2  1.63e+4  6.02e+3   6.68e-2  2.45e-2  9.76e+2  6.52e+1  2.39e+1
 210  28  75 1.5 0.57     75.0   1.24e+1  9.41e+0  7.58e+2  9.38e+3  7.13e+3   8.91e-2  5.38e-2  7.58e+2  6.75e+1  4.08e+1
 210  17  90 1.5 0.57     90.0   7.04e+0  6.83e+0  6.40e+2  4.51e+3  4.38e+3   6.24e-2  3.05e-2  6.40e+2  4.00e+1  1.95e+1
 210  21 100 1.5 0.57    100.0   2.95e+0  3.00e+0  5.47e+2  1.61e+3  1.64e+3   1.24e-1  2.45e-2  5.47e+2  6.76e+1  1.34e+1
 211   8  30 1.5 0.57     30.0   9.23e+0  4.24e+0  2.52e+3  2.33e+4  1.07e+4   6.44e-2  2.65e-2  2.52e+3  1.63e+2  6.68e+1
 211  13  60 1.5 0.57     60.0   1.55e+1  6.53e+0  1.02e+3  1.58e+4  6.65e+3   6.03e-2  2.14e-2  1.02e+3  6.15e+1  2.18e+1
 211  28  75 1.5 0.57     75.0   1.10e+1  9.74e+0  7.63e+2  8.42e+3  7.43e+3   9.43e-2  5.35e-2  7.63e+2  7.20e+1  4.08e+1
 211  17  90 1.5 0.57     90.0   6.44e+0  6.99e+0  6.20e+2  3.99e+3  4.34e+3   5.16e-2  3.71e-2  6.20e+2  3.20e+1  2.30e+1
 211  21 100 1.5 0.57    100.0   2.97e+0  2.99e+0  5.44e+2  1.62e+3  1.63e+3   1.19e-1  2.64e-2  5.44e+2  6.46e+1  1.44e+1
];
% Rec Chan rx  sz size     Dist   Vratio   Hratio   Pmax     Vmax     Hmax      Vratio   Hratio   Pmax     Vmax     Hmax
FL02brk05 = [...
 223   8  30 1.5 0.28     30.0   1.14e+1  5.41e+0  1.68e+3  1.90e+4  9.08e+3   7.58e-2  2.38e-2  1.68e+3  1.27e+2  4.00e+1
 223  13  60 1.5 0.28     60.0   1.82e+1  8.05e+0  7.30e+2  1.33e+4  5.87e+3   5.26e-2  2.51e-2  7.30e+2  3.84e+1  1.83e+1
 223  28  75 1.5 0.28     75.0   1.51e+1  1.24e+1  5.42e+2  8.17e+3  6.71e+3   8.56e-2  3.00e-2  5.42e+2  4.63e+1  1.62e+1
 223  17  90 1.5 0.28     90.0   9.36e+0  7.92e+0  4.54e+2  4.25e+3  3.60e+3   4.91e-2  3.54e-2  4.54e+2  2.23e+1  1.61e+1
 223  21 100 1.5 0.28    100.0   3.21e+0  3.45e+0  3.90e+2  1.25e+3  1.35e+3   1.05e-1  2.75e-2  3.90e+2  4.09e+1  1.07e+1
 224   8  30 1.5 0.28     30.0   1.14e+1  5.66e+0  2.02e+3  2.30e+4  1.14e+4   7.03e-2  2.11e-2  2.02e+3  1.42e+2  4.26e+1
 224  13  60 1.5 0.28     60.0   1.84e+1  8.35e+0  8.37e+2  1.54e+4  6.99e+3   4.28e-2  2.41e-2  8.37e+2  3.59e+1  2.01e+1
 224  28  75 1.5 0.28     75.0   1.62e+1  1.24e+1  6.11e+2  9.92e+3  7.58e+3   8.95e-2  3.24e-2  6.11e+2  5.47e+1  1.98e+1
 224  17  90 1.5 0.28     90.0   1.00e+1  8.11e+0  5.14e+2  5.14e+3  4.17e+3   4.20e-2  3.15e-2  5.14e+2  2.16e+1  1.62e+1
```

```
 224  21 100 1.5 0.28    100.0   3.30e+0  3.65e+0  4.42e+2  1.46e+3  1.62e+3   1.05e-1  2.24e-2  4.42e+2  4.62e+1  9.88e+0
 244   8  30 0.0 0.28     30.0   1.38e+1  6.20e+0  1.52e+3  2.10e+4  9.44e+3   6.89e-2  1.86e-2  1.52e+3  1.05e+2  2.83e+1
 244  13  60 0.0 0.28     60.0   1.63e+1  7.10e+0  6.66e+2  1.09e+4  4.73e+3   5.07e-2  1.87e-2  6.66e+2  3.38e+1  1.24e+1
 244  28  75 0.0 0.28     75.0   1.81e+1  1.17e+1  4.89e+2  8.83e+3  5.73e+3   3.05e-3  3.71e-3  4.89e+2  1.49e+0  1.81e+0
 244  17  90 0.0 0.28     90.0   1.05e+1  7.78e+0  4.20e+2  4.41e+3  3.27e+3   2.46e-2  1.11e-2  4.20e+2  1.03e+1  4.64e+0
 244  21 100 0.0 0.28    100.0   3.50e+0  3.94e+0  3.54e+2  1.24e+3  1.39e+3   1.91e-2  5.21e-3  3.54e+2  6.76e+0  1.85e+0
 245   8  30 0.0 0.28     30.0   1.36e+1  6.01e+0  1.41e+3  1.91e+4  8.46e+3   6.38e-2  1.92e-2  1.41e+3  8.98e+1  2.71e+1
 245  13  60 0.0 0.28     60.0   1.66e+1  6.67e+0  6.02e+2  1.00e+4  4.02e+3   5.24e-2  1.79e-2  6.02e+2  3.15e+1  1.08e+1
 245  28  75 0.0 0.28     75.0   1.81e+1  1.21e+1  4.41e+2  7.99e+3  5.36e+3   3.21e-2  1.31e-2  4.41e+2  1.42e+1  5.80e+0
 245  17  90 0.0 0.28     90.0   1.04e+1  7.68e+0  3.84e+2  4.01e+3  2.95e+3   2.82e-2  2.28e-2  3.84e+2  1.08e+1  8.76e+0
 245  21 100 0.0 0.28    100.0   3.65e+0  3.89e+0  3.29e+2  1.20e+3  1.28e+3   2.37e-2  2.09e-2  3.29e+2  7.82e+0  6.90e+0
 247   8  30 0.0 0.28     30.0   1.28e+1  5.75e+0  1.44e+3  1.85e+4  8.31e+3   5.69e-2  1.62e-2  1.44e+3  8.21e+1  2.34e+1
 247  13  60 0.0 0.28     60.0   2.09e+1  8.27e+0  5.39e+2  1.13e+4  4.45e+3   4.05e-2  2.51e-2  5.39e+2  2.18e+1  1.35e+1
 247  28  75 0.0 0.28     75.0   1.93e+1  1.36e+1  4.31e+2  8.34e+3  5.88e+3   2.53e-2  1.47e-2  4.31e+2  1.09e+1  6.34e+0
 247  17  90 0.0 0.28     90.0   1.09e+1  7.62e+0  3.84e+2  4.18e+3  2.93e+3   3.79e-2  2.76e-2  3.84e+2  1.46e+1  1.06e+1
 247  21 100 0.0 0.28    100.0   3.81e+0  3.90e+0  3.28e+2  1.25e+3  1.28e+3   1.99e-2  2.41e-2  3.28e+2  6.54e+0  7.90e+0
 248   8  30 0.0 0.28     30.0   1.26e+1  5.84e+0  1.55e+3  1.95e+4  9.03e+3   6.10e-2  1.83e-2  1.55e+3  9.42e+1  2.82e+1
 248  13  60 0.0 0.28     60.0   1.86e+1  7.42e+0  6.55e+2  1.22e+4  4.86e+3   4.82e-2  2.10e-2  6.55e+2  3.15e+1  1.38e+1
 248  28  75 0.0 0.28     75.0   1.87e+1  1.32e+1  4.66e+2  8.71e+3  6.13e+3   7.40e-2  2.89e-2  4.66e+2  3.45e+1  1.34e+1
 248  17  90 0.0 0.28     90.0   1.07e+1  7.51e+0  4.12e+2  4.42e+3  3.09e+3   3.96e-2  3.00e-2  4.12e+2  1.63e+1  1.24e+1
 248  21 100 0.0 0.28    100.0   3.68e+0  3.79e+0  3.50e+2  1.29e+3  1.33e+3   8.26e-2  1.86e-2  3.50e+2  2.89e+1  6.49e+0
];

%Test 5 - Light snow cover --------------------------------
% Rec Chan rx  sz size      Dist   Vratio   Hratio   Pmax      Vmax      Hmax       Vratio   Hratio   Pmax      Vmax      Hmax
MN02brk1 = [...
  35   4  30 1.5 0.57     30.0   6.47e-1  2.82e-1  2.73e+3  1.76e+3  7.69e+2   3.87e-2  1.77e-2  2.73e+3  1.06e+2  4.83e+1
  35  14  60 1.5 0.57     60.0   9.74e-1  2.44e-1  1.08e+3  1.06e+3  2.64e+2   5.47e-2  4.48e-2  1.08e+3  5.93e+1  4.86e+1
  35  17  90 1.5 0.57     90.0   9.77e-1  3.02e-1  6.86e+2  6.70e+2  2.07e+2   3.38e-2  2.95e-2  6.86e+2  2.32e+1  2.02e+1
  35  22 100 1.5 0.57    100.0   1.26e+0  2.59e-1  6.40e+2  8.06e+2  1.66e+2   3.55e-2  1.64e-2  6.40e+2  2.27e+1  1.05e+1
  36   4  30 1.5 0.57     30.0   6.49e-1  3.57e-1  3.02e+3  1.96e+3  1.08e+3   4.14e-2  1.46e-2  3.02e+3  1.25e+2  4.39e+1
  36  14  60 1.5 0.57     60.0   7.76e-1  2.29e-1  1.31e+3  1.01e+3  2.99e+2   3.90e-2  4.06e-2  1.31e+3  5.09e+1  5.30e+1
  36  17  90 1.5 0.57     90.0   9.45e-1  2.44e-1  7.92e+2  7.49e+2  1.94e+2   2.90e-2  2.62e-2  7.92e+2  2.30e+1  2.07e+1
  36  22 100 1.5 0.57    100.0   1.28e+0  2.29e-1  7.00e+2  8.98e+2  1.60e+2   3.17e-2  1.57e-2  7.00e+2  2.22e+1  1.10e+1
  37   4  30 1.5 0.57     30.0   7.79e-1  3.32e-1  2.52e+3  1.96e+3  8.36e+2   4.21e-2  1.67e-2  2.52e+3  1.06e+2  4.20e+1
  37  14  60 1.5 0.57     60.0   1.03e+0  2.39e-1  9.95e+2  1.03e+3  2.38e+2   5.70e-2  5.07e-2  9.95e+2  5.67e+1  5.04e+1
  37  17  90 1.5 0.57     90.0   1.08e+0  2.68e-1  6.40e+2  6.88e+2  1.71e+2   3.70e-2  3.33e-2  6.40e+2  2.37e+1  2.13e+1
  37  22 100 1.5 0.57    100.0   1.42e+0  2.64e-1  6.00e+2  8.53e+2  1.58e+2   3.78e-2  1.74e-2  6.00e+2  2.27e+1  1.04e+1
  70   4  30 1.5 0.57     30.0   7.99e-1  3.13e-1  2.60e+3  2.07e+3  8.12e+2   4.87e-2  1.63e-2  2.60e+3  1.27e+2  4.24e+1
  70  14  60 1.5 0.57     60.0   7.96e-1  2.40e-1  1.15e+3  9.16e+2  2.76e+2   4.71e-2  4.22e-2  1.15e+3  5.42e+1  4.85e+1
  70  22 100 1.5 0.57    100.0   1.27e+0  2.78e-1  6.71e+2  8.52e+2  1.86e+2   3.65e-2  1.69e-2  6.71e+2  2.45e+1  1.13e+1
  71   4  30 1.5 0.57     30.0   7.63e-1  2.87e-1  2.71e+3  2.07e+3  7.78e+2   4.54e-2  1.55e-2  2.71e+3  1.23e+2  4.19e+1
  71  14  60 1.5 0.57     60.0   8.68e-1  2.28e-1  1.13e+3  9.83e+2  2.58e+2   4.52e-2  4.16e-2  1.13e+3  5.12e+1  4.71e+1
  71  17  90 1.5 0.57     90.0   1.11e+0  2.26e-1  7.01e+2  7.79e+2  1.58e+2   3.77e-2  2.84e-2  7.01e+2  2.64e+1  1.99e+1
  71  22 100 1.5 0.57    100.0   1.25e+0  2.34e-1  6.64e+2  8.32e+2  1.56e+2   3.76e-2  1.64e-2  6.64e+2  2.49e+1  1.09e+1
 103   4  30 1.5 0.57     30.0   7.58e-1  2.92e-1  2.91e+3  2.20e+3  8.50e+2   4.99e-2  2.00e-2  2.91e+3  1.45e+2  5.83e+1
 103  14  60 1.5 0.57     60.0   7.12e-1  3.18e-1  1.27e+3  9.06e+2  4.05e+2   5.06e-2  3.76e-2  1.27e+3  6.43e+1  4.79e+1
 103  17  90 1.5 0.57     90.0   1.06e+0  2.17e-1  7.98e+2  8.48e+2  1.74e+2   3.47e-2  2.43e-2  7.98e+2  2.77e+1  1.94e+1
 103  22 100 1.5 0.57    100.0   1.02e+0  2.16e-1  7.86e+2  8.05e+2  1.70e+2   3.10e-2  1.42e-2  7.86e+2  2.44e+1  1.12e+1
 104   4  30 1.5 0.57     30.0   6.82e-1  3.03e-1  3.00e+3  2.04e+3  9.09e+2   4.52e-2  1.74e-2  3.00e+3  1.35e+2  5.21e+1
 104  14  60 1.5 0.57     60.0   7.62e-1  3.37e-1  1.17e+3  8.88e+2  3.93e+2   6.56e-2  4.61e-2  1.17e+3  7.64e+1  5.37e+1
 104  17  90 1.5 0.57     90.0   1.09e+0  2.51e-1  7.47e+2  8.17e+2  1.87e+2   3.60e-2  2.62e-2  7.47e+2  2.69e+1  1.95e+1
 104  22 100 1.5 0.57    100.0   1.12e+0  2.74e-1  7.12e+2  7.94e+2  1.95e+2   3.49e-2  1.54e-2  7.12e+2  2.49e+1  1.10e+1
 162   4  30 1.5 0.57     30.0   9.24e-1  2.74e-1  2.19e+3  2.02e+3  5.99e+2   5.94e-2  2.86e-2  2.19e+3  1.30e+2  6.27e+1
 162  14  60 1.5 0.57     60.0   9.05e-1  2.32e-1  9.50e+2  8.59e+2  2.20e+2   4.97e-2  4.66e-2  9.50e+2  4.73e+1  4.42e+1
 162  17  90 1.5 0.57     90.0   1.15e+0  2.48e-1  6.10e+2  7.00e+2  1.51e+2   4.49e-2  3.13e-2  6.10e+2  2.74e+1  1.91e+1
 162  22 100 1.5 0.57    100.0   1.45e+0  2.95e-1  5.30e+2  7.71e+2  1.57e+2   4.30e-2  1.88e-2  5.30e+2  2.28e+1  9.97e+0
 163   4  30 1.5 0.57     30.0   8.54e-1  2.50e-1  2.47e+3  2.11e+3  6.16e+2   5.47e-2  2.62e-2  2.47e+3  1.35e+2  6.47e+1
 163  14  60 1.5 0.57     60.0   8.88e-1  2.24e-1  1.00e+3  8.91e+2  2.24e+2   4.39e-2  4.40e-2  1.00e+3  4.41e+1  4.41e+1
 163  17  90 1.5 0.57     90.0   1.22e+0  2.44e-1  5.83e+2  7.10e+2  1.42e+2   4.79e-2  3.31e-2  5.83e+2  2.79e+1  1.93e+1
 163  22 100 1.5 0.57    100.0   1.43e+0  2.34e-1  5.31e+2  7.57e+2  1.24e+2   4.45e-2  2.00e-2  5.31e+2  2.37e+1  1.06e+1
  42   4  30 0.0 0.57     30.0   5.46e-1  3.35e-1  2.93e+3  1.60e+3  9.81e+2   3.71e-2  1.31e-1  2.93e+3  1.09e+2  3.84e+2
  42  14  60 0.0 0.57     60.0   6.38e-1  2.38e-1  1.21e+3  7.73e+2  2.88e+2   5.86e-2  2.86e-2  1.21e+3  7.10e+1  3.46e+1
  42  17  90 0.0 0.57     90.0   7.65e-1  2.54e-1  7.60e+2  5.82e+2  1.93e+2   2.48e-2  2.37e-2  7.60e+2  1.89e+1  1.80e+1
  42  22 100 0.0 0.57    100.0   1.27e+0  3.75e-1  6.83e+2  8.65e+2  2.56e+2   2.53e-2  1.42e-2  6.83e+2  1.73e+1  9.70e+0
  43   4  30 0.0 0.57     30.0   6.10e-1  2.97e-1  2.32e+3  1.42e+3  6.89e+2   3.42e-2  1.67e-1  2.32e+3  7.93e+1  3.87e+2
  43  14  60 0.0 0.57     60.0   6.63e-1  2.59e-1  1.01e+3  6.70e+2  2.62e+2   5.06e-2  2.77e-2  1.01e+3  5.11e+1  2.80e+1
  43  17  90 0.0 0.57     90.0   7.43e-1  2.99e-1  6.27e+2  4.66e+2  1.87e+2   2.91e-2  2.54e-2  6.27e+2  1.82e+1  1.60e+1
  43  22 100 0.0 0.57    100.0   1.32e+0  3.40e-1  5.67e+2  7.50e+2  1.93e+2   2.89e-2  1.56e-2  5.67e+2  1.64e+1  8.86e+0
  44   4  30 0.0 0.57     30.0   6.92e-1  2.97e-1  1.98e+3  1.37e+3  5.89e+2   3.08e-2  2.93e-1  1.98e+3  6.11e+1  5.80e+2
  44  14  60 0.0 0.57     60.0   6.06e-1  2.46e-1  9.57e+2  5.80e+2  2.35e+2   4.77e-2  4.07e-2  9.57e+2  4.57e+1  3.89e+1
  44  17  90 0.0 0.57     90.0   7.47e-1  3.09e-1  5.34e+2  3.99e+2  1.65e+2   3.45e-2  3.19e-2  5.34e+2  1.84e+1  1.70e+1
  44  22 100 0.0 0.57    100.0   1.37e+0  3.34e-1  4.99e+2  6.84e+2  1.67e+2   3.33e-2  1.75e-2  4.99e+2  1.66e+1  8.74e+0
  81   4  30 0.0 0.57     31.1   6.50e-1  2.87e-1  2.57e+3  1.67e+3  7.36e+2   4.19e-2  1.26e-1  2.57e+3  1.07e+2  3.23e+2
  81  14  60 0.0 0.57     61.0   7.24e-1  3.07e-1  1.06e+3  7.68e+2  3.26e+2   5.44e-2  2.71e-2  1.06e+3  5.78e+1  2.88e+1
  81  17  90 0.0 0.57     91.0   9.06e-1  2.21e-1  6.48e+2  5.87e+2  1.43e+2   2.72e-2  2.12e-2  6.48e+2  1.76e+1  1.37e+1
  81  22 100 0.0 0.57    101.0   1.49e+0  2.96e-1  5.84e+2  8.69e+2  1.73e+2   2.54e-2  1.36e-2  5.84e+2  1.48e+1  7.95e+0
  82   4  30 0.0 0.57     31.1   7.59e-1  3.02e-1  2.64e+3  2.00e+3  7.96e+2   4.51e-2  1.66e-1  2.64e+3  1.19e+2  4.37e+2
  82  14  60 0.0 0.57     61.0   7.47e-1  3.04e-1  1.06e+3  7.92e+2  3.23e+2   5.15e-2  2.78e-2  1.06e+3  5.46e+1  2.96e+1
  82  17  90 0.0 0.57     91.0   9.38e-1  2.30e-1  6.98e+2  6.55e+2  1.61e+2   2.64e-2  2.12e-2  6.98e+2  1.85e+1  1.48e+1
  82  22 100 0.0 0.57    101.0   1.39e+0  2.91e-1  6.39e+2  8.85e+2  1.86e+2   2.45e-2  1.34e-2  6.39e+2  1.56e+1  8.54e+0
 115   4  30 0.0 0.57     30.1   6.67e-1  3.41e-1  3.09e+3  2.06e+3  1.05e+3   4.88e-2  1.59e-1  3.09e+3  1.50e+2  4.90e+2
 115  14  60 0.0 0.57     60.0   7.04e-1  3.40e-1  1.23e+3  8.63e+2  4.17e+2   6.93e-2  3.72e-2  1.23e+3  8.50e+1  4.57e+1
 115  17  90 0.0 0.57     90.0   9.73e-1  2.83e-1  7.79e+2  7.58e+2  2.20e+2   2.24e-2  2.06e-2  7.79e+2  1.74e+1  1.61e+1
% Rec Chan rx  sz size      Dist   Vratio   Hratio   Pmax      Vmax      Hmax       Vratio   Hratio   Pmax      Vmax      Hmax
 115  22 100 0.0 0.57    100.0   1.40e+0  3.66e-1  7.12e+2  1.00e+3  2.61e+2   2.14e-2  1.11e-2  7.12e+2  1.53e+1  7.94e+0
 116   4  30 0.0 0.57     30.1   6.86e-1  3.00e-1  3.01e+3  2.07e+3  9.04e+2   5.00e-2  2.56e-1  3.01e+3  1.51e+2  7.69e+2
 116  14  60 0.0 0.57     60.0   6.72e-1  3.34e-1  1.22e+3  8.19e+2  4.07e+2   7.15e-2  4.11e-2  1.22e+3  8.71e+1  5.01e+1
 116  17  90 0.0 0.57     90.0   9.86e-1  2.85e-1  7.85e+2  7.74e+2  2.24e+2   2.28e-2  2.07e-2  7.85e+2  1.79e+1  1.63e+1
 116  22 100 0.0 0.57    100.0   1.36e+0  3.28e-1  7.24e+2  9.86e+2  2.38e+2   2.16e-2  1.17e-2  7.24e+2  1.56e+1  8.45e+0
 171   4  30 0.0 0.57     30.0   5.78e-1  2.11e-1  2.61e+3  1.51e+3  5.50e+2   5.03e-2  2.11e-1  2.61e+3  1.31e+2  5.50e+2
 171  14  60 0.0 0.57     60.0   5.75e-1  2.77e-1  9.86e+2  5.67e+2  2.73e+2   4.55e-2  3.96e-2  9.86e+2  4.49e+1  3.91e+1
 171  17  90 0.0 0.57     90.0   1.20e+0  3.97e-1  4.88e+2  5.83e+2  1.94e+2   3.32e-2  2.75e-2  4.88e+2  1.62e+1  1.34e+1
 171  22 100 0.0 0.57    100.0   1.45e+0  3.47e-1  5.48e+2  7.95e+2  1.90e+2   2.48e-2  1.46e-2  5.48e+2  1.36e+1  8.00e+0
 172   4  30 0.0 0.57     30.0   5.90e-1  2.65e-1  2.51e+3  1.48e+3  6.66e+2   5.26e-2  2.65e-1  2.51e+3  1.32e+2  6.66e+2
```

```
 172  14  60 0.0 0.57     60.0   6.03e-1  2.59e-1  1.02e+3  6.13e+2  2.63e+2   4.85e-2  4.62e-2  1.02e+3  4.93e+1  4.70e+1
 172  17  90 0.0 0.57     90.0   1.14e+0  3.50e-1  5.01e+2  5.72e+2  1.76e+2   3.33e-2  2.97e-2  5.01e+2  1.67e+1  1.49e+1
 172  22 100 0.0 0.57    100.0   1.58e+0  3.66e-1  5.23e+2  8.28e+2  1.91e+2   2.70e-2  1.47e-2  5.23e+2  1.41e+1  7.70e+0
];
MN02brk05 = [...
  38   4  30 1.5 0.28     30.0   6.95e-1  3.21e-1  1.71e+3  1.19e+3  5.51e+2   4.28e-2  1.59e-2  1.71e+3  7.34e+1  2.73e+1
  38  14  60 1.5 0.28     60.0   1.02e+0  2.83e-1  6.63e+2  6.75e+2  1.88e+2   6.09e-2  4.70e-2  6.63e+2  4.04e+1  3.12e+1
  38  17  90 1.5 0.28     90.0   9.17e-1  6.08e-1  4.21e+2  3.85e+2  2.56e+2   3.14e-2  2.97e-2  4.21e+2  1.32e+1  1.25e+1
  38  22 100 1.5 0.28    100.0   1.51e+0  4.75e-1  4.11e+2  6.21e+2  1.95e+2   3.13e-2  1.72e-2  4.11e+2  1.29e+1  7.05e+0
  39   4  30 1.5 0.28     30.0   5.73e-1  3.38e-1  1.94e+3  1.11e+3  6.56e+2   3.92e-2  1.50e-2  1.94e+3  7.61e+1  2.92e+1
  39  14  60 1.5 0.28     60.0   5.98e-1  1.91e-1  1.09e+3  6.50e+2  2.08e+2   3.46e-2  2.56e-2  1.09e+3  3.76e+1  2.78e+1
  39  17  90 1.5 0.28     90.0   7.81e-1  2.17e-1  5.53e+2  4.32e+2  1.20e+2   2.36e-2  2.30e-2  5.53e+2  1.31e+1  1.27e+1
  39  22 100 1.5 0.28    100.0   1.37e+0  2.44e-1  4.75e+2  6.49e+2  1.16e+2   2.63e-2  1.48e-2  4.75e+2  1.25e+1  7.01e+0
  72   4  30 1.5 0.28     30.0   6.51e-1  2.99e-1  1.86e+3  1.21e+3  5.55e+2   5.03e-2  1.78e-2  1.86e+3  9.34e+1  3.31e+1
  72  14  60 1.5 0.28     60.0   6.98e-1  2.52e-1  8.25e+2  5.75e+2  2.08e+2   4.25e-2  3.36e-2  8.25e+2  3.51e+1  2.77e+1
  72  17  90 1.5 0.28     90.0   9.85e-1  2.54e-1  4.85e+2  4.77e+2  1.23e+2   2.87e-2  2.34e-2  4.85e+2  1.39e+1  1.13e+1
  72  22 100 1.5 0.28    100.0   1.37e+0  2.97e-1  4.61e+2  6.34e+2  1.37e+2   2.72e-2  1.29e-2  4.61e+2  1.26e+1  5.96e+0
  73   4  30 1.5 0.28     30.0   7.46e-1  2.95e-1  1.74e+3  1.30e+3  5.13e+2   4.93e-2  2.20e-2  1.74e+3  8.57e+1  3.83e+1
  73  14  60 1.5 0.28     60.0   8.70e-1  2.65e-1  7.26e+2  6.31e+2  1.92e+2   4.83e-2  4.05e-2  7.26e+2  3.51e+1  2.94e+1
  73  17  90 1.5 0.28     90.0   1.05e+0  2.61e-1  4.51e+2  4.75e+2  1.18e+2   3.46e-2  2.72e-2  4.51e+2  1.56e+1  1.23e+1
  73  22 100 1.5 0.28    100.0   1.43e+0  2.75e-1  4.42e+2  6.32e+2  1.22e+2   3.22e-2  1.59e-2  4.42e+2  1.42e+1  7.04e+0
 105   4  30 1.5 0.28     30.0   6.59e-1  2.78e-1  1.94e+3  1.28e+3  5.38e+2   4.63e-2  2.09e-2  1.94e+3  8.96e+1  4.04e+1
 105  14  60 1.5 0.28     60.0   7.10e-1  3.18e-1  7.76e+2  5.52e+2  2.47e+2   3.28e-2  3.42e-2  7.76e+2  2.55e+1  2.66e+1
 105  17  90 1.5 0.28     90.0   1.14e+0  3.00e-1  4.59e+2  5.26e+2  1.38e+2   3.05e-2  2.35e-2  4.59e+2  1.40e+1  1.08e+1
 105  22 100 1.5 0.28    100.0   1.19e+0  2.76e-1  4.88e+2  5.81e+2  1.35e+2   2.60e-2  1.13e-2  4.88e+2  1.27e+1  5.51e+0
 106   4  30 1.5 0.28     30.0   6.37e-1  2.42e-1  2.04e+3  1.30e+3  4.95e+2   4.56e-2  1.82e-2  2.04e+3  9.32e+1  3.73e+1
 106  14  60 1.5 0.28     60.0   6.45e-1  1.97e-1  8.58e+2  5.53e+2  1.69e+2   3.22e-2  2.95e-2  8.58e+2  2.76e+1  2.53e+1
 106  17  90 1.5 0.28     90.0   1.01e+0  2.50e-1  5.29e+2  5.33e+2  1.32e+2   2.74e-2  2.01e-2  5.29e+2  1.45e+1  1.07e+1
 106  22 100 1.5 0.28    100.0   1.23e+0  2.38e-1  4.88e+2  6.01e+2  1.16e+2   2.74e-2  1.26e-2  4.88e+2  1.34e+1  6.16e+0
 107   4  30 1.5 0.28     30.0   6.23e-1  2.37e-1  1.97e+3  1.22e+3  4.66e+2   4.43e-2  1.84e-2  1.97e+3  8.70e+1  3.63e+1
 107  14  60 1.5 0.28     60.0   6.39e-1  2.85e-1  8.17e+2  5.22e+2  2.33e+2   3.45e-2  2.93e-2  8.17e+2  2.82e+1  2.39e+1
 107  17  90 1.5 0.28     90.0   1.01e+0  2.18e-1  5.01e+2  5.08e+2  1.09e+2   2.72e-2  2.05e-2  5.01e+2  1.37e+1  1.03e+1
 107  22 100 1.5 0.28    100.0   1.31e+0  3.21e-1  4.43e+2  5.80e+2  1.42e+2   2.80e-2  1.40e-2  4.43e+2  1.24e+1  6.18e+0
 108   4  30 0.0 0.28     30.1   5.16e-1  2.90e-1  1.97e+3  1.02e+3  5.71e+2   4.74e-2  2.90e-1  1.97e+3  9.34e+1  5.71e+2
 108  14  60 0.0 0.28     60.0   7.37e-1  3.74e-1  7.91e+2  5.83e+2  2.96e+2   4.32e-2  4.60e-2  7.91e+2  3.42e+1  3.64e+1
 108  17  90 0.0 0.28     90.0   9.25e-1  2.89e-1  5.07e+2  4.69e+2  1.46e+2   2.02e-2  2.03e-2  5.07e+2  1.02e+1  1.03e+1
 108  22 100 0.0 0.28    100.0   1.53e+0  3.27e-1  4.32e+2  6.61e+2  1.42e+2   1.94e-2  1.27e-2  4.32e+2  8.37e+0  5.49e+0
 109   4  30 0.0 0.28     30.1   5.22e-1  2.42e-1  1.85e+3  9.68e+2  4.48e+2   4.79e-2  2.31e-1  1.85e+3  8.88e+1  4.28e+2
 109  14  60 0.0 0.28     60.0   7.52e-1  3.74e-1  7.06e+2  5.31e+2  2.64e+2   4.53e-2  3.75e-2  7.06e+2  3.20e+1  2.65e+1
 109  17  90 0.0 0.28     90.0   9.58e-1  2.99e-1  4.62e+2  4.43e+2  1.38e+2   2.03e-2  2.02e-2  4.62e+2  9.38e+0  9.32e+0
 109  22 100 0.0 0.28    100.0   1.52e+0  3.30e-1  4.28e+2  6.52e+2  1.41e+2   1.81e-2  1.04e-2  4.28e+2  7.77e+0  4.47e+0
 110   4  30 0.0 0.28     30.1   4.93e-1  2.35e-1  1.72e+3  8.47e+2  4.04e+2   4.37e-2  8.50e-2  1.72e+3  7.51e+1  1.46e+2
 110  14  60 0.0 0.28     60.0   6.53e-1  3.39e-1  7.01e+2  4.58e+2  2.38e+2   2.95e-2  2.38e-2  7.01e+2  2.07e+1  1.67e+1
 110  17  90 0.0 0.28     90.0   9.05e-1  2.63e-1  4.48e+2  4.05e+2  1.18e+2   2.05e-2  1.86e-2  4.48e+2  9.19e+0  8.34e+0
 110  22 100 0.0 0.28    100.0   1.39e+0  3.37e-1  3.78e+2  5.24e+2  1.27e+2   2.14e-2  1.11e-2  3.78e+2  8.08e+0  4.18e+0
];
MN02brk4 = [...
  40   4  30 1.5 2.27     30.0   7.56e-1  3.67e-1  6.66e+3  5.04e+3  2.44e+3   3.35e-2  1.49e-2  6.66e+3  2.23e+2  9.96e+1
  40  14  60 1.5 2.27     60.0   9.07e-1  2.16e-1  2.74e+3  2.49e+3  5.91e+2   7.18e-2  7.72e-2  2.74e+3  1.97e+2  2.12e+2
  40  17  90 1.5 2.27     90.0   1.33e+0  4.15e-1  1.72e+3  2.29e+3  7.15e+2   5.02e-2  4.62e-2  1.72e+3  8.66e+1  7.97e+1
  40  22 100 1.5 2.27    100.0   1.07e+0  4.18e-1  1.58e+3  1.70e+3  6.61e+2   5.27e-2  2.57e-2  1.58e+3  8.34e+1  4.06e+1
  41   4  30 1.5 2.27     30.0   7.60e-1  3.71e-1  6.93e+3  5.27e+3  2.57e+3   3.34e-2  1.70e-2  6.93e+3  2.32e+2  1.18e+2
  41  14  60 1.5 2.27     60.0   7.85e-1  2.22e-1  2.79e+3  2.19e+3  6.20e+2   8.78e-2  7.67e-2  2.79e+3  2.45e+2  2.14e+2
  41  17  90 1.5 2.27     90.0   1.15e+0  4.83e-1  1.80e+3  2.08e+3  8.72e+2   4.58e-2  4.20e-2  1.80e+3  8.26e+1  7.58e+1
  41  22 100 1.5 2.27    100.0   1.06e+0  4.01e-1  1.59e+3  1.69e+3  6.37e+2   4.97e-2  2.42e-2  1.59e+3  7.90e+1  3.85e+1
 168   4  30 1.5 2.27     30.0   8.13e-1  3.16e-1  5.48e+3  4.45e+3  1.73e+3   1.13e-1  3.19e-2  5.48e+3  6.20e+2  1.75e+2
 168  14  60 1.5 2.27     60.0   1.23e+0  2.77e-1  2.42e+3  2.97e+3  6.71e+2   9.46e-2  7.31e-2  2.42e+3  2.29e+2  1.77e+2
 168  17  90 1.5 2.27     90.0   1.36e+0  3.13e-1  1.64e+3  2.23e+3  5.13e+2   6.58e-2  5.13e-2  1.64e+3  1.08e+2  8.40e+1
 168  22 100 1.5 2.27    100.0   1.08e+0  3.25e-1  1.54e+3  1.66e+3  5.00e+2   5.80e-2  2.94e-2  1.54e+3  8.93e+1  4.53e+1
 169   4  30 1.5 2.27     30.0   8.06e-1  3.35e-1  5.53e+3  4.45e+3  1.85e+3   1.10e-1  3.17e-2  5.53e+3  6.08e+2  1.75e+2
 169  14  60 1.5 2.27     60.0   1.30e+0  3.05e-1  2.38e+3  3.11e+3  7.28e+2   1.05e-1  7.63e-2  2.38e+3  2.49e+2  1.82e+2
 169  17  90 1.5 2.27     90.0   1.64e+0  3.88e-1  1.33e+3  2.19e+3  5.17e+2   8.18e-2  6.39e-2  1.33e+3  1.09e+2  8.51e+1
 169  22 100 1.5 2.27    100.0   1.12e+0  2.79e-1  1.50e+3  1.68e+3  4.19e+2   6.03e-2  3.03e-2  1.50e+3  9.05e+1  4.55e+1
];
MN02brk8 = [...
  48   4  30 1.5 4.55     30.0   7.93e-1  3.48e-1  9.29e+3  7.36e+3  3.23e+3   4.64e-2  3.64e-2  9.29e+3  4.31e+2  3.38e+2
  48  14  60 1.5 4.55     60.0   1.07e+0  2.69e-1  3.87e+3  4.14e+3  1.04e+3   1.09e-1  8.53e-2  3.87e+3  4.22e+2  3.30e+2
  48  17  90 1.5 4.55     90.0   1.25e+0  4.76e-1  2.49e+3  3.11e+3  1.18e+3   6.01e-2  5.42e-2  2.49e+3  1.49e+2  1.35e+2
  48  22 100 1.5 4.55    100.0   9.95e-1  3.60e-1  2.21e+3  2.20e+3  7.96e+2   6.40e-2  3.14e-2  2.21e+3  1.42e+2  6.94e+1
 170   4  30 1.5 4.55     30.0   9.71e-1  3.71e-1  9.67e+3  9.39e+3  3.59e+3   1.10e-1  4.32e-2  9.67e+3  1.06e+3  4.18e+2
 170  14  60 1.5 4.55     60.0   1.39e+0  2.81e-1  4.11e+3  5.72e+3  1.15e+3   1.11e-1  6.88e-2  4.11e+3  4.55e+2  2.82e+2
 170  17  90 1.5 4.55     90.0   1.26e+0  2.76e-1  2.44e+3  3.08e+3  6.73e+2   8.29e-2  6.20e-2  2.44e+3  2.02e+2  1.51e+2
 170  22 100 1.5 4.55    100.0   1.00e+0  3.28e-1  2.30e+3  2.31e+3  7.54e+2   7.04e-2  3.53e-2  2.30e+3  1.62e+2  8.11e+1
  49   4  30 0.0 4.55     30.0   1.29e+0  4.04e-1  5.94e+3  7.64e+3  2.40e+3   5.34e-2  4.04e-1  5.94e+3  3.17e+2  2.40e+3
  49  14  60 0.0 4.55     60.0   1.02e+0  2.40e-1  2.89e+3  2.95e+3  6.95e+2   1.07e-1  8.40e-2  2.89e+3  3.08e+2  2.43e+2
  49  17  90 0.0 4.55     90.0   1.25e+0  5.13e-1  1.97e+3  2.47e+3  1.01e+3   6.45e-2  5.71e-2  1.97e+3  1.27e+2  1.13e+2
  49  22 100 0.0 4.55    100.0   1.15e+0  4.86e-1  1.79e+3  2.06e+3  8.69e+2   6.92e-2  3.31e-2  1.79e+3  1.24e+2  5.93e+1
 173   4  30 0.0 4.55     30.0   9.04e-1  3.37e-1  8.35e+3  7.56e+3  2.82e+3   7.50e-2  2.37e-1  8.35e+3  6.26e+2  1.98e+3
 173  14  60 0.0 4.55     60.0   1.08e+0  2.12e-1  3.59e+3  3.86e+3  7.59e+2   1.03e-1  6.11e-2  3.59e+3  3.70e+2  2.19e+2
 173  17  90 0.0 4.55     90.0   1.44e+0  3.20e-1  1.85e+3  2.66e+3  5.93e+2   6.35e-2  5.54e-2  1.85e+3  1.18e+2  1.03e+2
 173  22 100 0.0 4.55    100.0   1.03e+0  2.77e-1  2.02e+3  2.08e+3  5.59e+2   5.06e-2  2.93e-2  2.02e+3  1.02e+2  5.91e+1
];

%Test 6 - Snow cover ----------------------------------------
% Rec Chan rx  sz size     Dist   Vratio   Hratio   Pmax     Vmax     Hmax      Vratio   Hratio   Pmax     Vmax     Hmax
NY04brk1 = [...
 399   9  60 1.5 0.57     60.0   2.01e-2  2.39e-2  7.23e+2  1.46e+1  1.73e+1   1.75e-4  4.48e-4  7.23e+2  1.26e-1  3.24e-1
 406   9  60 1.5 0.57     60.0   1.86e-2  1.82e-2  6.80e+2  1.27e+1  1.23e+1   2.03e-4  4.70e-4  6.80e+2  1.38e-1  3.19e-1
 406  15 150 1.5 0.57    150.0   2.10e-2  2.70e-2  2.06e+2  4.32e+0  5.55e+0   3.27e-4  5.88e-4  2.06e+2  6.73e-2  1.21e-1
 407   9  60 1.5 0.57     60.0   2.42e-2  2.25e-2  7.14e+2  1.73e+1  1.61e+1   1.75e-4  4.40e-4  7.14e+2  1.25e-1  3.14e-1
 407  15 150 1.5 0.57    150.0   2.71e-2  3.28e-2  2.03e+2  5.50e+0  6.64e+0   3.99e-4  7.06e-4  2.03e+2  8.08e-2  1.43e-1
 412   9  60 0.0 0.57     60.0   2.52e-2  2.61e-2  3.90e+2  9.82e+0  1.02e+1   2.91e-4  5.55e-4  3.90e+2  1.14e-1  2.17e-1
 412  15 150 0.0 0.57    150.0   2.50e-2  3.68e-2  1.21e+2  3.04e+0  4.47e+0   5.86e-4  7.78e-4  1.21e+2  7.11e-2  9.44e-2
 413   9  60 0.0 0.57     60.0   2.16e-2  2.40e-2  5.99e+2  1.30e+1  1.44e+1   2.27e-4  3.74e-4  5.99e+2  1.36e-1  2.24e-1
 413  15 150 0.0 0.57    150.0   2.50e-2  3.91e-2  1.40e+2  3.50e+0  5.47e+0   5.46e-4  7.50e-4  1.40e+2  7.64e-2  1.05e-1
```

```
 414   9  60 0.0 0.57     60.0   2.58e-2  2.89e-2  4.26e+2  1.10e+1  1.23e+1   3.66e-4  4.53e-4  4.26e+2  1.56e-1  1.93e-1
 414  15 150 0.0 0.57    150.0   2.48e-2  3.81e-2  1.21e+2  3.00e+0  4.60e+0   7.53e-4  1.04e-3  1.21e+2  9.10e-2  1.25e-1
 415   9  60 0.0 0.57     60.0   2.84e-2  3.09e-2  3.04e+2  8.61e+0  9.39e+0   6.07e-4  8.04e-4  3.04e+2  1.84e-1  2.44e-1
 415  15 150 0.0 0.57    150.0   2.78e-2  4.01e-2  9.79e+1  2.72e+0  3.92e+0   1.35e-3  1.58e-3  9.79e+1  1.32e-1  1.55e-1
];
NY04brk05 = [...
 400   9  60 1.5 0.28     60.0   1.76e-2  2.09e-2  6.37e+2  1.12e+1  1.33e+1   1.48e-4  3.56e-4  6.37e+2  9.42e-2  2.27e-1
 400  15 150 1.5 0.28    150.0   1.60e-2  2.88e-2  2.19e+2  3.49e+0  6.29e+0   1.65e-4  3.55e-4  2.19e+2  3.60e-2  7.75e-2
 403   9  60 1.5 0.28     60.0   1.73e-2  2.27e-2  4.78e+2  8.26e+0  1.08e+1   1.64e-4  4.69e-4  4.78e+2  7.86e-2  2.24e-1
 403  15 150 1.5 0.28    150.0   1.91e-2  3.35e-2  1.60e+2  3.06e+0  5.37e+0   2.27e-4  4.58e-4  1.60e+2  3.63e-2  7.34e-2
 408   9  60 0.0 0.28     60.0   2.33e-2  2.41e-2  3.50e+2  8.16e+0  8.42e+0   2.92e-4  4.03e-4  3.50e+2  1.02e-1  1.41e-1
 408  15 150 0.0 0.28    150.0   2.27e-2  3.59e-2  8.81e+1  2.00e+0  3.17e+0   4.41e-4  5.67e-4  8.81e+1  3.89e-2  5.00e-2
 411   9  60 0.0 0.28     60.0   2.37e-2  2.62e-2  2.96e+2  7.03e+0  7.76e+0   3.13e-4  4.90e-4  2.96e+2  9.27e-2  1.45e-1
 411  15 150 0.0 0.28    150.0   2.58e-2  4.37e-2  6.85e+1  1.77e+0  2.99e+0   6.49e-4  7.72e-4  6.85e+1  4.45e-2  5.29e-2
];
NY04brk4 = [...
 404   9  60 1.5 2.27     60.0   1.72e-2  2.64e-2  1.80e+3  3.09e+1  4.74e+1   1.68e-4  5.20e-4  1.80e+3  3.02e-1  9.34e-1
 404  15 150 1.5 2.27    150.0   8.87e-3  2.71e-2  6.62e+2  5.87e+0  1.79e+1   3.64e-4  6.25e-4  6.62e+2  2.41e-1  4.13e-1
 405   9  60 1.5 2.27     60.0   1.49e-2  2.48e-2  1.65e+3  2.46e+1  4.09e+1   1.71e-4  4.47e-4  1.65e+3  2.82e-1  7.37e-1
 405  15 150 1.5 2.27    150.0   7.86e-3  2.77e-2  5.97e+2  4.69e+0  1.65e+1   3.62e-4  6.58e-4  5.97e+2  2.16e-1  3.93e-1
 418   9  60 0.0 2.27     61.3   3.12e-2  2.63e-2  1.01e+3  3.15e+1  2.65e+1   3.06e-4  5.98e-4  1.01e+3  3.09e-1  6.03e-1
 418  15 150 0.0 2.27    151.3   2.59e-2  2.66e-2  3.46e+2  8.95e+0  9.22e+0   6.50e-4  7.69e-4  3.46e+2  2.25e-1  2.66e-1
 419   9  60 0.0 2.27     61.3   2.49e-2  1.86e-2  1.15e+3  2.85e+1  2.13e+1   3.02e-4  5.28e-4  1.15e+3  3.47e-1  6.06e-1
 419  15 150 0.0 2.27    151.3   2.75e-2  2.65e-2  3.44e+2  9.48e+0  9.13e+0   6.84e-4  8.17e-4  3.44e+2  2.35e-1  2.81e-1
];
NY04brk8 = [...
 416   9  60 1.5 4.55     60.0   2.58e-2  1.64e-2  1.92e+3  4.97e+1  3.16e+1   1.66e-4  5.38e-4  1.92e+3  3.19e-1  1.03e+0
 416  15 150 1.5 4.55    150.0   2.19e-2  2.34e-2  6.82e+2  1.49e+1  1.59e+1   3.55e-4  7.93e-4  6.82e+2  2.42e-1  5.40e-1
 417   9  60 1.5 4.55     60.5   2.91e-2  1.88e-2  2.10e+3  6.11e+1  3.94e+1   6.04e-4  9.50e-4  2.10e+3  1.27e+0  1.99e+0
 417  15 150 1.5 4.55    150.5   2.24e-2  2.33e-2  6.96e+2  1.56e+1  1.62e+1   2.91e-4  7.25e-4  6.96e+2  2.03e-1  5.05e-1
];
%Test 7 - Conifer forest ----------------------------------
% Rec Chan rx  sz size     Dist   Vratio   Hratio   Pmax     Vmax     Hmax      Vratio   Hratio   Pmax     Vmax     Hmax
TX02brk1 = [...
  41   4  30 3.8 0.57     90.5   2.31e+0  4.73e+0  5.65e+2  1.30e+3  2.67e+3   4.71e-2  7.54e-2  5.65e+2  2.66e+1  4.26e+1
  41  12  90 3.8 0.57    150.5   2.69e+0  4.46e+0  3.20e+2  8.61e+2  1.43e+3   3.64e-2  6.39e-2  3.20e+2  1.16e+1  2.05e+1
  41  16 120 3.8 0.57    180.5   3.30e+0  4.01e+0  2.50e+2  8.25e+2  1.00e+3   2.92e-2  3.66e-2  2.50e+2  7.31e+0  9.16e+0
  41  20 150 3.8 0.57    210.5   4.26e+0  3.14e+0  2.31e+2  9.84e+2  7.25e+2   2.86e-2  3.72e-2  2.31e+2  6.61e+0  8.58e+0
  42   4  30 3.8 0.57     90.5   2.85e+0  5.59e+0  4.92e+2  1.40e+3  2.75e+3   6.07e-2  1.01e-1  4.92e+2  2.99e+1  4.99e+1
  42  12  90 3.8 0.57    150.5   3.02e+0  4.61e+0  3.03e+2  9.16e+2  1.40e+3   4.48e-2  8.13e-2  3.03e+2  1.36e+1  2.47e+1
  42  16 120 3.8 0.57    180.5   3.30e+0  4.09e+0  2.35e+2  7.76e+2  9.61e+2   3.30e-2  4.59e-2  2.35e+2  7.75e+0  1.08e+1
  42  20 150 3.8 0.57    210.5   4.51e+0  3.62e+0  2.01e+2  9.05e+2  7.27e+2   3.18e-2  4.50e-2  2.01e+2  6.39e+0  9.04e+0
  61   4  30 1.9 0.57    444.7   2.32e+0  2.81e+0  8.68e+1  2.01e+2  2.44e+2   1.06e-1  8.77e-2  8.68e+1  9.18e+0  7.61e+0
  61  12  90 1.9 0.57    504.7   2.19e+0  4.31e+0  9.00e+1  1.97e+2  3.88e+2   1.98e-2  2.78e-2  9.00e+1  1.78e+0  2.50e+0
  61  16 120 1.9 0.57    534.7   3.42e+0  3.79e+0  6.90e+1  2.36e+2  2.61e+2   2.33e-2  4.59e-2  6.90e+1  1.60e+0  3.17e+0
  61  20 150 1.9 0.57    564.7   4.54e+0  4.23e+0  6.71e+1  3.05e+2  2.84e+2   2.65e-2  3.98e-2  6.71e+1  1.78e+0  2.67e+0
  62   4  30 1.9 0.57     90.5   3.01e+0  5.62e+0  4.55e+2  1.37e+3  2.56e+3   8.67e-2  1.50e-1  4.55e+2  3.95e+1  6.85e+1
  62  12  90 1.9 0.57    150.5   2.59e+0  4.62e+0  3.38e+2  8.75e+2  1.56e+3   4.62e-2  8.18e-2  3.38e+2  1.56e+1  2.77e+1
  62  16 120 1.9 0.57    180.5   3.41e+0  4.24e+0  2.48e+2  8.46e+2  1.05e+3   3.89e-2  4.97e-2  2.48e+2  9.65e+0  1.23e+1
  62  20 150 1.9 0.57    210.5   4.48e+0  3.77e+0  2.09e+2  9.33e+2  7.87e+2   4.16e-2  4.96e-2  2.09e+2  8.68e+0  1.04e+1
  64  12  90 1.9 0.57    221.0   3.08e+0  5.86e+0  2.37e+2  7.28e+2  1.39e+3   8.95e-3  1.59e-2  2.37e+2  2.12e+0  3.77e+0
  64  16 120 1.9 0.57    191.0   2.41e+0  4.58e+0  2.63e+2  6.33e+2  1.20e+3   1.05e-2  1.84e-2  2.63e+2  2.76e+0  4.83e+0
  64  20 150 1.9 0.57    161.0   3.18e+0  3.34e+0  3.54e+2  1.13e+3  1.18e+3   1.70e-2  2.19e-2  3.54e+2  6.00e+0  7.76e+0
  65   4  30 1.9 0.57    444.7   2.20e+0  2.91e+0  7.38e+1  1.63e+2  2.15e+2   2.35e-2  4.68e-2  7.38e+1  1.74e+0  3.45e+0
  65  12  90 1.9 0.57    504.7   2.07e+0  4.07e+0  7.48e+1  1.55e+2  3.04e+2   2.78e-2  4.68e-2  7.48e+1  2.08e+0  3.50e+0
  65  16 120 1.9 0.57    534.7   2.65e+0  3.13e+0  6.95e+1  1.85e+2  2.18e+2   3.05e-2  3.47e-2  6.95e+1  2.12e+0  2.41e+0
  65  20 150 1.9 0.57    564.7   4.62e+0  4.15e+0  5.13e+1  2.37e+2  2.13e+2   3.26e-2  4.72e-2  5.13e+1  1.68e+0  2.42e+0
  66   4  30 1.9 0.57     90.5   2.93e+0  5.45e+0  4.39e+2  1.29e+3  2.39e+3   9.22e-2  1.58e-1  4.39e+2  4.05e+1  6.95e+1
  66  12  90 1.9 0.57    150.5   2.64e+0  4.69e+0  3.17e+2  8.35e+2  1.48e+3   4.93e-2  8.50e-2  3.17e+2  1.56e+1  2.69e+1
  66  16 120 1.9 0.57    180.5   3.35e+0  4.40e+0  2.24e+2  7.52e+2  9.87e+2   4.48e-2  5.72e-2  2.24e+2  1.01e+1  1.28e+1
  66  20 150 1.9 0.57    210.5   4.31e+0  3.63e+0  1.94e+2  8.35e+2  7.03e+2   4.41e-2  5.11e-2  1.94e+2  8.54e+0  9.90e+0
  67  12  90 1.9 0.57     90.0   4.25e+0  5.35e+0  6.50e+2  2.76e+3  3.48e+3   3.20e-2  5.86e-2  6.50e+2  2.08e+1  3.80e+1
  67  16 120 1.9 0.57    120.0   2.97e+0  5.07e+0  4.03e+2  1.20e+3  2.04e+3   2.40e-2  3.46e-2  4.03e+2  9.67e+0  1.40e+1
  67  20 150 1.9 0.57    150.0   4.45e+0  3.19e+0  3.18e+2  1.42e+3  1.01e+3   1.96e-2  2.79e-2  3.18e+2  6.23e+0  8.89e+0
  68  12  90 1.9 0.57    221.0   3.02e+0  6.02e+0  2.53e+2  7.65e+2  1.52e+3   1.00e-2  2.26e-2  2.53e+2  2.54e+0  5.72e+0
  68  16 120 1.9 0.57    191.0   2.39e+0  4.49e+0  2.73e+2  6.52e+2  1.23e+3   1.12e-2  2.12e-2  2.73e+2  3.06e+0  5.79e+0
  68  20 150 1.9 0.57    161.0   3.13e+0  3.30e+0  3.70e+2  1.16e+3  1.22e+3   1.89e-2  2.38e-2  3.70e+2  6.97e+0  8.80e+0
  70   4  30 3.8 0.57     90.5   2.89e+0  5.48e+0  4.30e+2  1.24e+3  2.36e+3   7.72e-2  1.36e-1  4.30e+2  3.32e+1  5.87e+1
  70  12  90 3.8 0.57    150.5   2.41e+0  4.63e+0  3.14e+2  7.57e+2  1.45e+3   4.32e-2  7.31e-2  3.14e+2  1.36e+1  2.29e+1
  70  16 120 3.8 0.57    180.5   3.77e+0  4.62e+0  2.13e+2  8.04e+2  9.85e+2   4.10e-2  4.96e-2  2.13e+2  8.73e+0  1.06e+1
  70  20 150 3.8 0.57    210.5   4.33e+0  3.60e+0  1.88e+2  8.13e+2  6.76e+2   4.16e-2  5.09e-2  1.88e+2  7.80e+0  9.56e+0
  71   4  30 3.8 0.57     90.5   3.07e+0  5.72e+0  4.62e+2  1.42e+3  2.64e+3   8.03e-2  1.35e-1  4.62e+2  3.71e+1  6.21e+1
  71  12  90 3.8 0.57    150.5   2.69e+0  4.80e+0  3.32e+2  8.95e+2  1.59e+3   4.46e-2  7.73e-2  3.32e+2  1.48e+1  2.57e+1
  71  16 120 3.8 0.57    180.5   3.77e+0  4.66e+0  2.33e+2  8.76e+2  1.08e+3   4.04e-2  5.46e-2  2.33e+2  9.39e+0  1.27e+1
  71  20 150 3.8 0.57    210.5   4.30e+0  3.65e+0  1.95e+2  8.39e+2  7.13e+2   3.82e-2  4.84e-2  1.95e+2  7.46e+0  9.46e+0
  72   4  30 3.0 0.57     90.5   2.91e+0  4.98e+0  5.72e+2  1.67e+3  2.85e+3   8.12e-2  1.25e-1  5.72e+2  4.65e+1  7.15e+1
  72  12  90 3.0 0.57    150.5   2.61e+0  4.73e+0  3.57e+2  9.30e+2  1.69e+3   4.35e-2  7.61e-2  3.57e+2  1.55e+1  2.71e+1
  72  16 120 3.0 0.57    180.5   3.71e+0  4.53e+0  2.56e+2  9.47e+2  1.16e+3   4.05e-2  5.19e-2  2.56e+2  1.04e+1  1.33e+1
  72  20 150 3.0 0.57    210.5   4.29e+0  3.50e+0  2.22e+2  9.53e+2  7.78e+2   3.89e-2  4.45e-2  2.22e+2  8.63e+0  9.89e+0
  73   4  30 1.2 0.57     90.5   2.76e+0  4.68e+0  5.09e+2  1.40e+3  2.38e+3   7.96e-2  1.24e-1  5.09e+2  4.05e+1  6.34e+1
  73  12  90 1.2 0.57    150.5   2.57e+0  4.83e+0  3.11e+2  7.99e+2  1.50e+3   4.25e-2  7.79e-2  3.11e+2  1.32e+1  2.42e+1
  73  16 120 1.2 0.57    180.5   3.44e+0  4.48e+0  2.23e+2  7.69e+2  1.00e+3   4.16e-2  5.25e-2  2.23e+2  9.29e+0  1.17e+1
  73  20 150 1.2 0.57    210.5   4.09e+0  3.52e+0  1.92e+2  7.83e+2  6.74e+2   3.87e-2  4.61e-2  1.92e+2  7.42e+0  8.84e+0
  % Rec Chan rx  sz size     Dist   Vratio   Hratio   Pmax     Vmax     Hmax      Vratio   Hratio   Pmax     Vmax     Hmax
  74   4  30 0.3 0.57     90.5   2.96e+0  4.70e+0  4.63e+2  1.37e+3  2.18e+3   9.12e-2  1.40e-1  4.63e+2  4.22e+1  6.51e+1
  74  12  90 0.3 0.57    150.5   2.62e+0  4.80e+0  2.81e+2  7.37e+2  1.35e+3   4.91e-2  8.76e-2  2.81e+2  1.38e+1  2.46e+1
  74  16 120 0.3 0.57    180.5   3.44e+0  4.42e+0  2.04e+2  7.01e+2  8.99e+2   4.58e-2  5.68e-2  2.04e+2  9.33e+0  1.16e+1
  74  20 150 0.3 0.57    210.5   4.20e+0  3.73e+0  1.69e+2  7.09e+2  6.30e+2   4.39e-2  5.41e-2  1.69e+2  7.42e+0  9.14e+0
  93   4  30 1.9 0.57    444.7   1.91e+0  2.70e+0  7.57e+1  1.45e+2  2.04e+2   2.47e-2  3.22e-2  7.57e+1  1.87e+0  2.44e+0
  93  12  90 1.9 0.57    504.7   1.78e+0  3.88e+0  6.75e+1  1.20e+2  2.62e+2   2.73e-2  5.15e-2  6.75e+1  1.84e+0  3.47e+0
  93  16 120 1.9 0.57    534.7   2.68e+0  3.22e+0  5.47e+1  1.47e+2  1.76e+2   3.38e-2  4.85e-2  5.47e+1  1.85e+0  2.65e+0
  93  20 150 1.9 0.57    564.7   4.36e+0  4.56e+0  4.36e+1  1.90e+2  1.99e+2   3.84e-2  6.22e-2  4.36e+1  1.67e+0  2.71e+0
  94   4  30 1.9 0.57     90.5   2.85e+0  5.06e+0  5.01e+2  1.43e+3  2.54e+3   8.72e-2  1.30e-1  5.01e+2  4.37e+1  6.52e+1
  94  12  90 1.9 0.57    150.5   2.65e+0  4.61e+0  2.94e+2  7.81e+2  1.36e+3   4.83e-2  8.74e-2  2.94e+2  1.42e+1  2.57e+1
  94  16 120 1.9 0.57    180.5   3.26e+0  4.20e+0  2.05e+2  6.68e+2  8.62e+2   4.53e-2  5.98e-2  2.05e+2  9.29e+0  1.23e+1
```

```
  94  20 150 1.9 0.57    210.5   4.16e+0  3.67e+0  1.69e+2  7.03e+2  6.21e+2   4.26e-2  5.62e-2  1.69e+2  7.20e+0  9.50e+0
  95  12  90 1.9 0.57    221.0   2.99e+0  6.01e+0  2.42e+2  7.23e+2  1.45e+3   1.09e-2  2.20e-2  2.42e+2  2.63e+0  5.32e+0
  95  16 120 1.9 0.57    191.0   2.31e+0  4.36e+0  2.68e+2  6.19e+2  1.17e+3   1.45e-2  2.69e-2  2.68e+2  3.90e+0  7.23e+0
  95  20 150 1.9 0.57    161.0   3.04e+0  3.03e+0  3.68e+2  1.12e+3  1.11e+3   1.76e-2  2.06e-2  3.68e+2  6.50e+0  7.60e+0
];
% Rec Chan rx  sz size     Dist   Vratio   Hratio   Pmax     Vmax     Hmax      Vratio   Hratio   Pmax     Vmax     Hmax
TX02brk4 = [...
  40   4  30 1.9 2.27     90.5   3.11e+0  4.58e+0  1.13e+3  3.50e+3  5.15e+3   6.35e-2  1.08e-1  1.13e+3  7.15e+1  1.22e+2
  40  12  90 1.9 2.27    150.5   2.71e+0  4.01e+0  6.81e+2  1.85e+3  2.73e+3   3.58e-2  6.90e-2  6.81e+2  2.44e+1  4.70e+1
  40  16 120 1.9 2.27    180.5   2.76e+0  3.77e+0  5.40e+2  1.49e+3  2.03e+3   3.12e-2  4.04e-2  5.40e+2  1.69e+1  2.18e+1
  40  20 150 1.9 2.27    210.5   3.65e+0  3.38e+0  5.04e+2  1.84e+3  1.70e+3   2.66e-2  3.72e-2  5.04e+2  1.34e+1  1.88e+1
  96   4  30 1.9 2.27    444.7   1.92e+0  2.48e+0  1.71e+2  3.28e+2  4.23e+2   3.39e-2  4.95e-2  1.71e+2  5.79e+0  8.44e+0
  96  12  90 1.9 2.27    504.7   1.78e+0  3.21e+0  1.48e+2  2.63e+2  4.75e+2   4.23e-2  5.69e-2  1.48e+2  6.26e+0  8.42e+0
  96  16 120 1.9 2.27    534.7   2.34e+0  2.74e+0  1.19e+2  2.78e+2  3.25e+2   4.27e-2  5.29e-2  1.19e+2  5.08e+0  6.29e+0
  96  20 150 1.9 2.27    564.7   3.19e+0  3.04e+0  1.13e+2  3.62e+2  3.44e+2   3.87e-2  5.27e-2  1.13e+2  4.39e+0  5.98e+0
  97   4  30 1.9 2.27     90.5   3.25e+0  5.06e+0  1.06e+3  3.46e+3  5.38e+3   9.18e-2  1.36e-1  1.06e+3  9.76e+1  1.45e+2
  97  12  90 1.9 2.27    150.5   2.79e+0  3.96e+0  6.61e+2  1.84e+3  2.62e+3   4.57e-2  8.13e-2  6.61e+2  3.02e+1  5.38e+1
  97  16 120 1.9 2.27    180.5   3.01e+0  3.98e+0  4.65e+2  1.40e+3  1.85e+3   4.35e-2  5.47e-2  4.65e+2  2.03e+1  2.55e+1
  97  20 150 1.9 2.27    210.5   3.79e+0  3.64e+0  3.86e+2  1.46e+3  1.41e+3   4.12e-2  5.11e-2  3.86e+2  1.59e+1  1.97e+1
  98  12  90 1.9 2.27     90.0   3.86e+0  4.88e+0  1.47e+3  5.67e+3  7.18e+3   3.26e-2  5.29e-2  1.47e+3  4.80e+1  7.78e+1
  98  16 120 1.9 2.27    120.0   3.06e+0  3.92e+0  9.39e+2  2.87e+3  3.68e+3   2.40e-2  2.77e-2  9.39e+2  2.25e+1  2.60e+1
  98  20 150 1.9 2.27    150.0   3.96e+0  3.48e+0  7.20e+2  2.85e+3  2.50e+3   2.86e-2  4.58e-2  7.20e+2  2.06e+1  3.30e+1
  99   4  30 1.9 2.27    281.0   2.07e+0  3.30e+0  3.96e+2  8.20e+2  1.31e+3   1.57e-2  2.30e-2  3.96e+2  6.22e+0  9.09e+0
  99  12  90 1.9 2.27    221.0   2.62e+0  5.01e+0  5.27e+2  1.38e+3  2.64e+3   1.91e-2  3.15e-2  5.27e+2  1.01e+1  1.66e+1
  99  16 120 1.9 2.27    191.0   2.15e+0  3.80e+0  6.18e+2  1.33e+3  2.35e+3   1.60e-2  3.83e-2  6.18e+2  9.91e+0  2.37e+1
  99  20 150 1.9 2.27    161.0   2.43e+0  3.49e+0  8.32e+2  2.02e+3  2.90e+3   2.75e-2  3.57e-2  8.32e+2  2.29e+1  2.97e+1
 100   4  30 1.9 2.27    444.7   1.95e+0  2.59e+0  1.76e+2  3.44e+2  4.56e+2   4.13e-2  4.39e-2  1.76e+2  7.27e+0  7.74e+0
 100  12  90 1.9 2.27    504.7   1.75e+0  3.48e+0  1.55e+2  2.72e+2  5.39e+2   4.17e-2  6.77e-2  1.55e+2  6.46e+0  1.05e+1
 100  16 120 1.9 2.27    534.7   2.12e+0  2.79e+0  1.22e+2  2.57e+2  3.40e+2   4.15e-2  5.72e-2  1.22e+2  5.05e+0  6.96e+0
 100  20 150 1.9 2.27    564.7   3.12e+0  3.29e+0  1.07e+2  3.32e+2  3.51e+2   5.25e-2  5.59e-2  1.07e+2  5.59e+0  5.95e+0
 101   4  30 1.9 2.27     90.5   3.32e+0  4.96e+0  1.05e+3  3.48e+3  5.21e+3   9.01e-2  1.37e-1  1.05e+3  9.46e+1  1.44e+2
 101  12  90 1.9 2.27    150.5   2.54e+0  3.79e+0  6.17e+2  1.57e+3  2.34e+3   4.84e-2  9.38e-2  6.17e+2  2.99e+1  5.79e+1
 101  16 120 1.9 2.27    180.5   2.90e+0  4.01e+0  4.42e+2  1.28e+3  1.77e+3   4.70e-2  6.16e-2  4.42e+2  2.08e+1  2.73e+1
 101  20 150 1.9 2.27    210.5   3.77e+0  3.76e+0  3.57e+2  1.35e+3  1.34e+3   4.58e-2  5.96e-2  3.57e+2  1.64e+1  2.13e+1
 102   4  30 1.9 2.27     30.0   5.97e+0  4.53e+0  4.44e+3  2.65e+4  2.01e+4   6.50e-3  9.62e-4  4.44e+3  2.89e+1  4.27e+0
 102  12  90 1.9 2.27     90.0   3.94e+0  5.00e+0  1.38e+3  5.41e+3  6.88e+3   4.22e-2  6.28e-2  1.38e+3  5.80e+1  8.64e+1
 102  16 120 1.9 2.27    120.0   3.05e+0  3.73e+0  8.85e+2  2.70e+3  3.30e+3   3.14e-2  3.17e-2  8.85e+2  2.78e+1  2.81e+1
 102  20 150 1.9 2.27    150.0   4.03e+0  3.41e+0  6.71e+2  2.70e+3  2.29e+3   3.37e-2  4.66e-2  6.71e+2  2.26e+1  3.13e+1
 103   4  30 1.9 2.27    281.0   2.10e+0  3.35e+0  4.20e+2  8.83e+2  1.40e+3   1.70e-2  1.65e-2  4.20e+2  7.13e+0  6.94e+0
 103  12  90 1.9 2.27    221.0   2.48e+0  5.08e+0  5.46e+2  1.35e+3  2.77e+3   1.86e-2  3.48e-2  5.46e+2  1.02e+1  1.90e+1
 103  16 120 1.9 2.27    191.0   2.14e+0  3.74e+0  6.20e+2  1.33e+3  2.32e+3   1.97e-2  4.44e-2  6.20e+2  1.22e+1  2.75e+1
 103  20 150 1.9 2.27    161.0   2.40e+0  3.49e+0  8.29e+2  1.99e+3  2.89e+3   3.16e-2  3.90e-2  8.29e+2  2.62e+1  3.23e+1
 104   4  30 1.9 2.27    444.7   1.97e+0  2.53e+0  1.51e+2  2.97e+2  3.81e+2   5.00e-2  5.62e-2  1.51e+2  7.54e+0  8.46e+0
 104  12  90 1.9 2.27    504.7   1.77e+0  3.48e+0  1.37e+2  2.43e+2  4.77e+2   4.68e-2  7.50e-2  1.37e+2  6.43e+0  1.03e+1
 104  16 120 1.9 2.27    534.7   2.34e+0  2.83e+0  1.09e+2  2.55e+2  3.08e+2   5.07e-2  6.45e-2  1.09e+2  5.51e+0  7.01e+0
 104  20 150 1.9 2.27    564.7   3.19e+0  3.38e+0  9.28e+1  2.96e+2  3.14e+2   5.85e-2  6.54e-2  9.28e+1  5.43e+0  6.07e+0
 105   4  30 1.9 2.27     90.5   3.34e+0  5.22e+0  1.03e+3  3.46e+3  5.40e+3   9.41e-2  1.42e-1  1.03e+3  9.73e+1  1.47e+2
 105  12  90 1.9 2.27    150.5   2.67e+0  3.75e+0  6.45e+2  1.72e+3  2.42e+3   4.86e-2  9.19e-2  6.45e+2  3.13e+1  5.93e+1
 105  16 120 1.9 2.27    180.5   3.08e+0  3.99e+0  4.56e+2  1.40e+3  1.82e+3   4.70e-2  6.09e-2  4.56e+2  2.14e+1  2.78e+1
 105  20 150 1.9 2.27    210.5   3.72e+0  3.63e+0  3.84e+2  1.43e+3  1.39e+3   4.33e-2  5.66e-2  3.84e+2  1.66e+1  2.17e+1
 106  12  90 1.9 2.27     90.0   3.98e+0  5.06e+0  1.45e+3  5.77e+3  7.33e+3   4.80e-2  6.21e-2  1.45e+3  6.96e+1  9.00e+1
 106  16 120 1.9 2.27    120.0   2.94e+0  3.59e+0  9.35e+2  2.74e+3  3.36e+3   3.55e-2  3.27e-2  9.35e+2  3.31e+1  3.06e+1
 106  20 150 1.9 2.27    150.0   3.80e+0  3.21e+0  6.93e+2  2.63e+3  2.23e+3   3.75e-2  4.55e-2  6.93e+2  2.60e+1  3.15e+1
 107   4  30 1.9 2.27    281.0   2.15e+0  3.42e+0  4.04e+2  8.68e+2  1.38e+3   1.62e-2  1.80e-2  4.04e+2  6.54e+0  7.29e+0
 107  12  90 1.9 2.27    221.0   2.51e+0  4.93e+0  5.23e+2  1.31e+3  2.58e+3   1.98e-2  3.93e-2  5.23e+2  1.03e+1  2.05e+1
 107  16 120 1.9 2.27    191.0   2.10e+0  3.70e+0  6.19e+2  1.30e+3  2.29e+3   2.04e-2  4.35e-2  6.19e+2  1.26e+1  2.69e+1
 107  20 150 1.9 2.27    161.0   2.37e+0  3.46e+0  8.09e+2  1.91e+3  2.80e+3   3.32e-2  4.02e-2  8.09e+2  2.69e+1  3.25e+1
 108   4  30 1.9 2.27     90.5   3.13e+0  5.18e+0  1.04e+3  3.26e+3  5.38e+3   9.43e-2  1.45e-1  1.04e+3  9.80e+1  1.51e+2
 108  12  90 1.9 2.27    150.5   2.79e+0  3.76e+0  6.43e+2  1.80e+3  2.42e+3   4.72e-2  9.40e-2  6.43e+2  3.04e+1  6.05e+1
 108  16 120 1.9 2.27    180.5   2.98e+0  3.73e+0  4.75e+2  1.42e+3  1.77e+3   4.12e-2  6.00e-2  4.75e+2  1.96e+1  2.85e+1
 108  20 150 1.9 2.27    210.5   3.74e+0  3.60e+0  3.87e+2  1.45e+3  1.40e+3   4.38e-2  5.89e-2  3.87e+2  1.69e+1  2.28e+1
 109   4  30 3.8 2.27     90.5   3.18e+0  5.47e+0  1.07e+3  3.41e+3  5.88e+3   8.93e-2  1.32e-1  1.07e+3  9.60e+1  1.42e+2
 109  12  90 3.8 2.27    150.5   2.68e+0  3.82e+0  6.64e+2  1.78e+3  2.54e+3   4.72e-2  8.99e-2  6.64e+2  3.13e+1  5.97e+1
 109  16 120 3.8 2.27    180.5   2.89e+0  3.73e+0  4.82e+2  1.39e+3  1.80e+3   4.50e-2  5.80e-2  4.82e+2  2.17e+1  2.79e+1
 109  20 150 3.8 2.27    210.5   3.74e+0  3.49e+0  4.04e+2  1.51e+3  1.41e+3   4.50e-2  5.40e-2  4.04e+2  1.82e+1  2.18e+1
 110   4  30 3.8 2.27     90.5   3.26e+0  5.54e+0  1.10e+3  3.57e+3  6.08e+3   9.15e-2  1.34e-1  1.10e+3  1.00e+2  1.47e+2
 110  12  90 3.8 2.27    150.5   2.59e+0  3.95e+0  6.61e+2  1.71e+3  2.61e+3   4.90e-2  9.14e-2  6.61e+2  3.23e+1  6.04e+1
 110  16 120 3.8 2.27    180.5   2.82e+0  3.81e+0  4.86e+2  1.37e+3  1.85e+3   4.64e-2  5.89e-2  4.86e+2  2.26e+1  2.87e+1
 110  20 150 3.8 2.27    210.5   3.70e+0  3.43e+0  4.23e+2  1.57e+3  1.45e+3   3.94e-2  5.21e-2  4.23e+2  1.67e+1  2.21e+1
 111   4  30 3.0 2.27     90.5   2.85e+0  5.28e+0  9.41e+2  2.68e+3  4.97e+3   9.53e-2  1.42e-1  9.41e+2  8.97e+1  1.33e+2
 111  12  90 3.0 2.27    150.5   2.59e+0  3.91e+0  5.99e+2  1.55e+3  2.34e+3   4.72e-2  9.27e-2  5.99e+2  2.83e+1  5.55e+1
 111  16 120 3.0 2.27    180.5   2.85e+0  3.81e+0  4.41e+2  1.25e+3  1.68e+3   4.59e-2  6.31e-2  4.41e+2  2.02e+1  2.78e+1
 111  20 150 3.0 2.27    210.5   3.82e+0  3.61e+0  3.61e+2  1.38e+3  1.30e+3   4.29e-2  6.08e-2  3.61e+2  1.55e+1  2.20e+1
 112   4  30 1.2 2.27     90.5   3.18e+0  5.34e+0  9.02e+2  2.87e+3  4.82e+3   9.53e-2  1.43e-1  9.02e+2  8.60e+1  1.29e+2
 112  12  90 1.2 2.27    150.5   2.55e+0  3.82e+0  5.64e+2  1.44e+3  2.16e+3   4.78e-2  9.41e-2  5.64e+2  2.70e+1  5.31e+1
 112  16 120 1.2 2.27    180.5   2.78e+0  3.85e+0  4.09e+2  1.14e+3  1.57e+3   4.61e-2  6.18e-2  4.09e+2  1.88e+1  2.53e+1
 112  20 150 1.2 2.27    210.5   3.60e+0  3.45e+0  3.58e+2  1.29e+3  1.24e+3   4.22e-2  5.52e-2  3.58e+2  1.51e+1  1.98e+1
 113   4  30 0.3 2.27     90.5   2.86e+0  4.39e+0  8.43e+2  2.41e+3  3.70e+3   1.00e-1  1.49e-1  8.43e+2  8.45e+1  1.26e+2
 113  12  90 0.3 2.27    150.5   2.67e+0  3.82e+0  5.02e+2  1.34e+3  1.92e+3   5.39e-2  1.04e-1  5.02e+2  2.71e+1  5.23e+1
 113  16 120 0.3 2.27    180.5   2.78e+0  3.99e+0  3.58e+2  9.96e+2  1.43e+3   5.32e-2  6.93e-2  3.58e+2  1.90e+1  2.48e+1
 113  20 150 0.3 2.27    210.5   3.69e+0  3.33e+0  3.17e+2  1.17e+3  1.06e+3   4.65e-2  6.17e-2  3.17e+2  1.47e+1  1.96e+1
];
```

Appendix B: List of Technical Publications

1. Peer-reviewed publications (in print, accepted, or submitted)

In the planning stage, subject to Corps of Engineers funding.

2. Technical reports (in print, accepted, or submitted)

Boulanger, P. and K. Attenborough, Prediction of ground vibration from explosions, Final Report for Contract Number N62588-05-P-0247, University of Hull, Hull, UK (2005a).

Boulanger, P. and K. Attenborough, Supplement to Final Report: Prediction of ground vibration from explosions, University of Hull, Hull, UK (2005b).

A version of this final report will be published as an ERDC-CRREL Technical Report.

3. Conference or Other Referenced Papers

Some of the work reported in the following paper was supported by this SERDP project:

Attenborough, K., P. Boulanger, and Q. Qin, "Models of the ground for predicting linear and nonlinear acoustic-to-seismic coupling, Proceedings SAPEM (Symposium on the Acoustics of Poro-Elastic Materials), December 2005, Lyon, France.

4. Published technical abstracts

Attenborough, K., P. Boulanger, "On the prediction of ground vibrations resulting from outdoor explosions, Invited Paper, Institute of Acoustics (UK) Spring Meeting, 2006.

Albert, Donald G., K. Attenborough, and P. Boulanger, Measurements of acoustic and seismic pulses from outdoor explosions, Journal of the Acoustical Society of America 119, 3264-3265 (2006). Paper presented at the 151st Meeting of the Acoustical Society of America, June 2006.

Attenborough, K., P. Boulanger, and D. G. Albert, Predicting acoustic and seismic pulses from outdoor explosions, Journal of the Acoustical Society of America 119, 3385 (2006). Paper presented at the 151st Meeting of the Acoustical Society of America, June 2006.

5. Published text books or book chapters

None.

REPORT DOCUMENTATION PAGE

Form Approved
OMB No. 0704-0188

Public reporting burden for this collection of information is estimated to average 1 hour per response, including the time for reviewing instructions, searching existing data sources, gathering and maintaining the data needed, and completing and reviewing this collection of information. Send comments regarding this burden estimate or any other aspect of this collection of information, including suggestions for reducing this burden to Department of Defense, Washington Headquarters Services, Directorate for Information Operations and Reports (0704-0188), 1215 Jefferson Davis Highway, Suite 1204, Arlington, VA 22202-4302. Respondents should be aware that notwithstanding any other provision of law, no person shall be subject to any penalty for failing to comply with a collection of information if it does not display a currently valid OMB control number. **PLEASE DO NOT RETURN YOUR FORM TO THE ABOVE ADDRESS.**

1. REPORT DATE *(DD-MM-YYYY)*
August 2006

2. REPORT TYPE

3. DATES COVERED *(From - To)*

4. TITLE AND SUBTITLE

Evaluation of Ground Vibrations Induced by Military Noise Sources
Final Report for SERDP SEED Project SI-1410

5a. CONTRACT NUMBER

5b. GRANT NUMBER

5c. PROGRAM ELEMENT NUMBER

6. AUTHOR(S)

Donald G. Albert, Patrice Boulanger, Keith Attenborough
and Michael J. White

5d. PROJECT NUMBER
SI-1410

5e. TASK NUMBER

5f. WORK UNIT NUMBER

7. PERFORMING ORGANIZATION NAME(S) AND ADDRESS(ES)

U.S. Army Engineer Research and Development Center
72 Lyme Road
Hanover, NH 03755-1290

8. PERFORMING ORGANIZATION REPORT NUMBER

ERDC TR-06-5

9. SPONSORING / MONITORING AGENCY NAME(S) AND ADDRESS(ES)

Strategic Environmental Research and Development Program

10. SPONSOR/MONITOR'S ACRONYM(S)

11. SPONSOR/MONITOR'S REPORT NUMBER(S)

12. DISTRIBUTION / AVAILABILITY STATEMENT

Approved for public release; distribution is unlimited.

13. SUPPLEMENTARY NOTES

14. ABSTRACT

Measurements from locations with a variety of ground types were analyzed to determine the mechanisms and levels of the ground vibrations produced by airborne detonations of C4. The measurements show that an early seismic arrival from an underground path is always much smaller than the vibration induced by the air blast arrival. The acoustic-to-seismic coupling ratio for the atmospheric wave is a constant with respect to distance and peak pressure at a given location, but varies from site to site, and is usually between 1 and 13 (μm/s)/Pa. A numerically intense computational method to predict the air pressure spectrum above ground and the waveform shape of the vertical component of solid particle velocity near the ground surface compares tolerably well with measurements at short range (60 m) in grass and snow covered ground. A conservative empirical equation to predicts that the commonly used vibrational damage criteria of 12 or 25 mm/s will be exceeded when the peak positive pressure exceeds 480 Pa or 1 kPa, respectively. Either of these levels is much higher than the Army overpressure damage criterion of 159 Pa (138 dB). Thus, in most situations damage from blast overpressure will occur long before damaging levels of ground vibration are reached.

15. SUBJECT TERMS
Army training
Damage
Explosions
Ground vibrations

16. SECURITY CLASSIFICATION OF:			**17. LIMITATION OF ABSTRACT**	**18. NUMBER OF PAGES**	**19a. NAME OF RESPONSIBLE PERSON**
a. REPORT	**b. ABSTRACT**	**c. THIS PAGE**			**19b. TELEPHONE NUMBER** *(include area code)*
U	U	U	U	73	

Standard Form 298 (Rev. 8-98)
Prescribed by ANSI Std. 239.18